AD-A135 963 VISCOELASTIC ANALYSIS OF ADHESIVE STRESSES IN BONDED JOINTS(U) VIRGINIA POLYTECHNIC INST AND STATE UNIV BLACKSBURG DEPT OF E.. L R BOTHA ET AL. MAY 83 1/2

UNCLASSIFIED VPI-E-83-17 N00014-82-K-0185 F/G 11/1 NL

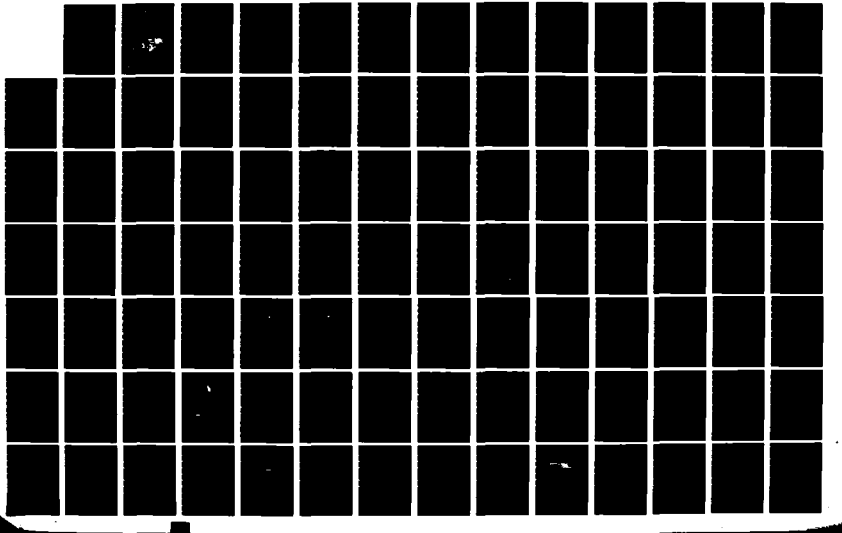

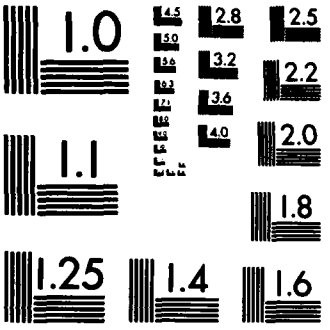

(1)

Center for Adhesion Science

VPI-E-83-17 May, 1983

VISCOELASTIC ANALYSIS OF ADHESIVE STRESSES IN BONDED JOINTS

Louis R. Botha*, Graduate Assistant
R. M. Jones*, Professor
H. F. Brinson*, Professor

Virginia Polytechnic Institute and State University

Blacksburg, Virginia 24061

College of Engineering
Virginia Polytechnic Institute and State University
Blacksburg, VA 24061

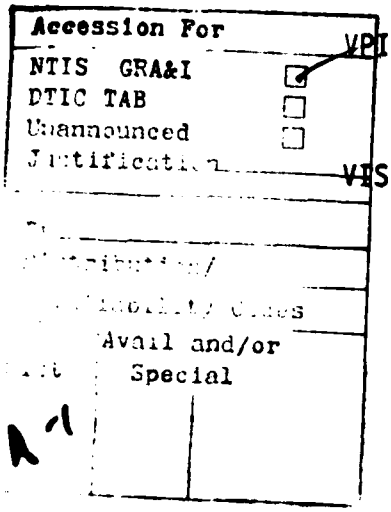

VPI-E-83-17 May, 1983

VISCOELASTIC ANALYSIS OF ADHESIVE STRESSES IN BONDED JOINTS

Louis R. Botha*, Graduate Assistant
R. M. Jones*, Professor
H. F. Brinson*, Professor

A Joint Project in: The Center for Adhesion Science
and
The Department of Engineering Science and Mechanics
Virginia Polytechnic Institute and State University
Blacksburg, VA 24061

This report was partially sponsored by:

C. A. du Toit and Partners
Cape Town
South Africa

Office of Naval Research
800 N. Quincy St.
Arlington, VA 22217

National Aeronautics
and Space Administratio
Langley Research Center
Hampton, VA 23665

*Graduate assistant and professors, respectively, in the Department of Engineering Science and Mechanics.

BIBLIOGRAPHIC DATA SHEET	1. Report No. VPI-E-83-17	2.	3. Recipient's Accession No.

4. Title and Subtitle
VISCOELASTIC STRESS ANALYSIS OF ADHESIVELY BONDED JOINTS

5. Report Date

6.

7. Author(s)
Louis R. Botha, Robert M. Jones, H. F. Brinson

8. Performing Organization Rept. No.

9. Performing Organization Name and Address
Engineering Science and Mechanics
225 Norris Hall, VPI&SU
Blacksburg, VA 24061

10. Project/Task/Work Unit No.

11. Contract/Grant No.
ONR N00014-82-K-0185
NASA NAG-1-227

12. Sponsoring Organization Name and Address
ONR, 800 N. Quincy St., Arlington, VA 22217
NASA-Langley, Hampton, VA 23665

13. Type of Report & Period Covered
Final

14.

15. Supplementary Notes

16. Abstracts Existing closed form solutions for the stress analysis of the single lap joint were studied intensively, and methods of analysis and assumptions between the analyses of Goland and Reissner, Hart-Smith and Delale and Erdogan were compared. The existing SAAS3V finite element program was modified to accommodate additional mesh generation and plotting capabilities. The modified version, SAAS3VP, was used for performing linear elastic and viscoelastic analyses on the single lap joint, and a non-linear viscoelastic analysis on the thick adherend specimen. Metlbond 1113 and Araldite adhesive properties were used in the linear elastic and viscoelastic analyses, respectively FM-73 adhesive properties were used in the non-linear viscoelastic analysis. Time-dependent shear moduli were calculated from the results of the latter analysis and compared with the experimentally obtained shear modulus of Krieger. Interface layers were defined in both the single lap and thick adherend analyses and the influence of changing the interface layer stiffness on adhesive stresses was also investigated.

17. Key Words and Document Analysis. 17a. Descriptors

Bonded joints, stress analysis, finite element, viscoelasticity

17b. Identifiers/Open-Ended Terms

17c. COSATI Field/Group

18 Availability Statement	19. Security Class (This Report)	21. No. of Pages
Distribution unlimited	UNCLASSIFIED	
	20. Security Class (This Page) UNCLASSIFIED	22. Price

ABSTRACT

Existing closed form solutions for the stress analysis of the single lap joint were studied intensively, and methods of analysis and assumptions between the analyses of Goland and Reissner, Hart-Smith and Delale and Erdogan were compared. The existing SAAS3V finite element program was modified to accommodate additional mesh generation and plotting capabilities. The modified version, SAAS3VP, was used for performing linear elastic and viscoelastic analyses on the single lap joint, and a non-linear viscoelastic analysis on the thick adherend specimen. Metlbond 1113 and Araldite adhesive properties were used in the linear elastic and viscoelastic analyses, respectively. FM-73 adhesive properties were used in the non-linear viscoelastic analysis. Time-dependent shear moduli were calculated from the results of the latter analysis and compared with the experimentally obtained shear modulus of Krieger. Interface layers were defined in both the single lap and thick adherend analyses and the influence of changing the interface layer stiffness on adhesive stresses was also investigated.

ACKNOWLEDGEMENTS

The authors are deeply indebted to the cooperation of many individuals who have helped make this work possible. Financial support for this project was provided by three groups. First, the financial support of Louis Botha was provided by his employer, C. A. du Toit and Partners, Cape Town, South Africa. Partial financial support for Robert M. Jones was provided by VPI&SU through a cost-sharing agreement on ONR Project N00014-82-K-0185, Arlington, VA 22217. The support of Hal F. Brinson was provided by both Office of Naval Research, Arlington, VA 22217, through contract N00014-82-K-0185 and by NASA-Langley through grant number NAG-1-227. Project monitors for the ONR and NASA-Langley contracts were Dr. Larry H. Peebles, Jr., and Dr. W. Steve Johnson, respectively. Their many helpful suggestions and discussions are greatly appreciated.

The authors are especially indebted to Mrs. Peggy Epperly for her excellent typing through numerous stages of this work.

TABLE OF CONTENTS

LIST OF FIGURES

LIST OF TABLES

Chapter 1

INTRODUCTION

The analysis of stresses in adhesively bonded joints is not only necessary for structural design purposes, but also for the determination of adhesive properties. When adhesive materials are characterized experimentally, different material properties are obtained when measured in structural joints than when they are measured in bulk. A possible reason is that the adherends act as constraints such that the bonded adhesive material is not as free to deform as in the "neat", "bulk" or unbonded state. Such constraints would likely lead to a greater stiffness and hence a brittle response. Another possible reason is that the interfacial region between the adhesive and the adherends, which is not present in the unbonded form, leads to greater ductility. For these reasons it is often preferred to measure adhesive properties in the form of structural joints similar to the manner that adhesives are applied in practice. As a result, a thorough understanding of the stresses in joints is required for property measurement as well as for design purposes and each represents the objective of the present study.

Two types of joints were considered during the course of this study, viz. the single lap joint and the thick adherend specimen. Interest in the single lap joint as a tool for characterizing adhesives is drawn from its simplicity in geometry and ease in manufacture. In this simple structure, however, closed form analytical solutions for stresses in the adhesive layer become extremely complex due to the

eccentricity in the load path and due to the non-linear behavior of the adhesive material. For example, consider the single lap joint of Figure 1.1. Bending moments are present upon loading in tension, which, at any point along the neutral axis of the structure, are proportional to the distance, from the neutral axis, perpendicular to the load path. Upon application of a load, however, the joint deforms in a manner as shown in Figure 1.1(b) and the deformation is accompanied by a change in the position of the neutral axis, which in turn influences the induced bending moment. The deformation, therefore, changes non-linearly with respect to the tensile loading. If this non-linearity is to be accounted for in closed-form analyses, many

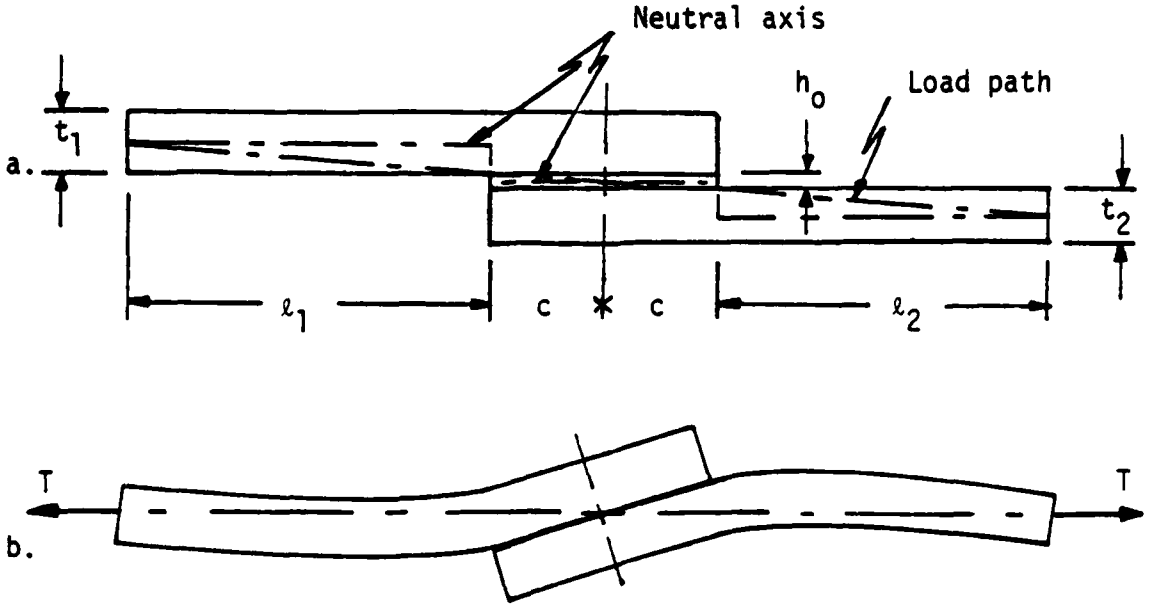

Figure 1.1 (a) Geometry and (b) Deformation of a Single Lap Joint Under Tension

simplifying assumptions have to be made. In most finite element codes for approximating stresses, strains and displacements, however, this non-linearity is automatically taken into account without needing many of the simplifying assumptions.

What is actually referred to as the geometric non-linearity, in the material description of motion, is the influence of the second order terms in the Lagrangian strain tensor

$$L_{ij} = \frac{1}{2}\left[\frac{\partial u_i}{\partial a_j} + \frac{\partial u_j}{\partial a_i} + \frac{\partial u_r}{\partial a_i}\frac{\partial u_r}{\partial a_j}\right]$$

where u_i and a_i are components of the displacement and vector position of a point in the structure. The second order terms are usually neglected but when derivatives of displacement become large, as is possibly the case with adhesives and other polymeric materials, the geometric non-linearity terms have to be included to avoid substantial errors in the calculation of strains, and hence also of stresses. Such geometric non-linearities are often not included in standard finite element codes due to the resulting complexity.

A feature often incorporated in finite element programs, however, for which a number of different methods may be used, is that of representing material non-linearities, i.e., materials which exhibit non-linear stress-strain curves. In the SAAS3VP program [1], used for the analyses of the present study, the deformation plasticity approach is followed in which, through a recursive iteration procedure and application of the von Mises yield criterion, the resulting stresses and strains are consistent with the appropriate secant modulus description

of a bi-linear effective stress-effective strain relationship [1]. Methods which are possibly more often employed in finite element codes are those in which the non-linear stress-strain curve is described by a Ramberg-Osgood or power law equation. A second approach, viz. the flow theory, or incremental strain theory of plasticity, may also be followed but this theory is more difficult to implement than the deformation theory of plasticity.

Adhesive materials generally exhibit viscoelastic behavior. In adhesive joints, the viscoelastic effect produces a more even stress distribution throughout the adhesive layer with increasing time. Peak stresses are lowered with increasing time under constant load but peak strains increase simultaneously which may in return lead to failure in time. Analytic viscoelastic solutions are usually obtained by first removing the time variable by a transform operation, leading to an equivalent problem in the theory of elasticity, called the associated elastic problem in terms of the transform parameter. The boundary conditions for the associated elastic problem must be in the form of transforms of the original time-dependent conditions. The inverse transformation of the solution to the associated elastic problem into the time domain is then the solution to the original viscoelastic problem. The Laplace transform is generally accepted as the most suitable method for removing the time variable, even though the exact inverse transformation into the time domain is often very difficult, if not impossible, to obtain. Various approximate methods for Laplace transform inversion may be used, however, such as Schapery's direct or quasi-elastic methods or by numerical integration of the

complex inversion integral for the Laplace transform. Schapery's approximate methods are discussed in more detail in Chapter 5.

Due to the chemical bonding between molecules of the adhesive and those of the adherend, it is suspected that the mechanical properties of the thin layer between the adhesive layer and the adherend, called the interface layer, may be quite different from the properties of both the two adjoining materials. As far as is known, no estimate as to what these properties might be has been proposed. In this study the mechanical properties were arbitrarily assumed and varied in order to establish what influence the interface layer has on the stress distributions in the adhesive.

The SAAS3V finite element stress analysis program for axisymmetric and plane solids was chosen for the purpose of this study because of its generality in application and since it had already been implemented in the local computer system network. Included in the program are a mesh generator and plotting capabilities for the generated mesh, deformed grid and stress contours. Various modifications were made to the SAAS3V program which improved its input and output capabilities. With the new version, SAAS3VP, stresses, strains or displacements may be plotted at any location within the structure which is being analyzed.

The thick adherend specimen, shown in Figure 1.2, is presently more popular than the single lap joint for characterizing adhesives since it is expected that shear stresses are more evenly distributed over the area of the overlap region of the former. Viscoelastic analyses in this joint configuration and in the single lap joint are

performed in the present study.

The crack lap specimen of Figure 1.3, also referred to as the skin doubler concept, is sometimes chosen as a device for studying the fracture behavior of adhesives. With this configuration, the onset of fracture is limited to one joint edge, and bending stresses in the adherends are small.

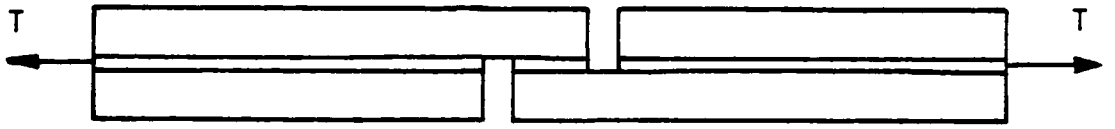

Figure 1.2 The thick adherend specimen

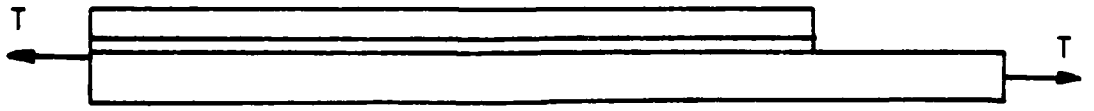

Figure 1.3 The crack lap specimen

Chapter 2

LITERATURE REVIEW

The first analysis of adhesive stresses in bonded joints which includes the effects of load eccentricity was performed by Goland and Reissner [2] in 1944. Their analysis of the single lap joint assumes linear elasticity, plane strain and cylindrical bending of the adherends. Two different approaches to the problem were considered: In the first case the adhesive layer was assumed to be either negligibly thin, or its stiffness to be such, that the flexibility of the joint is assumed to be unaffected by the presence of the adhesive layer. In the second approach, the flexibility of the joint was assumed to be mainly due to that of the adhesive layer. A further discussion of this paper is provided in Section 2.1.

In 1971 Erdogan and Ratwani [6] developed amodel for calculating stresses in stepped lap joints in which either plane strain or generalized plane stress was assumed. One adherend was assumed to consist of an isotropic material and the second of an orthotropic material. Linear elastic conditions for the materials were assumed. The thickness variation of the stresses in both the adherends and in the adhesive was neglected. All normal or peel stresses were thus also neglected.

Hart-Smith [3] discussed the work of Goland and Reissner in 1973 and improved upon their second approach by considering a third free body diagram for the adherend outside the joint in addition to

the two free body diagrams from each of the upper and lower halves of the joint. With three separate sections to consider, three relations between displacements and bending moments were obtained. Additional boundary conditions involving displacements and their first derivatives, not considered by Goland and Reissner, were imposed in order to solve for the additional unknowns. A further discussion of this paper is provided in Section 2.2.

In addition to the improvement on the analysis of Goland and Reissner, Hart-Smith [3] also established the quantitative influence of adhesive plasticity in shear. The elastic-plastic theory used by Hart-Smith predicts an increase in joint strength and was shown to be capable of explaining premature failure predictions found when using linear elastic analyses. The quantitative effects of stiffness imbalance were also accounted for.

The existence of stress gradients through the thickness of the adhesive layer, close to the joint edges, was acknowledged by Adams and Peppiatt [20] in 1974. They subsequently performed a linear elastic finite element analysis on adhesively bonded lap joints employing more than one element through the thickness of the adhesive layer, close to the joint edges. In 1977 Humphreys [5] presented a non-linear analysis of single and double lap joints using the finite element method. The non-linear stress-strain response was represented by a Ramberg-Osgood approximation. Mechanical and thermal loadings were considered but only one element through the thickness of the adhesive layer was used.

In 1977 Allman [10] presented an elastic stress analysis based on the strain energy density of any particular joint. The effects of bending, stretching and shearing of the adherends were included, and the shearing and tearing action in the adhesive was accounted for. All conditions of stress equilibrium in the joint and stress-free surface conditions were satisfied. It was assumed, however, that the axial stress varies linearly through the adherend thicknesses and that the shear stress is constant through the adhesive thickness. Allman obtained solutions for the single lap joint, although the method also appears to be applicable to other joint configurations. He found that the average shear stress concentration is 11% higher than that of Goland and Reissner's first analysis, while the average peel stress at the joint edge is 67% lower. Compared with the second analysis of Goland and Reissner, Allman's method yielded a shear stress concentration of 15% and 31% less for metal and composite adherends, respectively, while the average peel stress at the joint edge was 27% higher and 36% lower for the same types of adherends, respectively.

Phenomenological considerations were discussed in 1978 by Hart-Smith [11] which greatly improve our understanding of the sources of non-uniform load transfer, viz., adherend extensivity, stiffness imbalance and thermal mismatch. He also explained how the lightly loaded central area of the joint, away from the joint edges, restricts cumulative creep damage, and suggests that this region is vital for long term durability. The amount of lightly loaded central area is a function of the overlap length.

In 1980 Yuceoglu and Updike [12] presented a numerical method for solving peel and shear stresses in the adhesive of double lap, double strap and stiffner plate joints. Bending and transverse shear was included in the analytical model. Shear stresses were not required to drop to zero at the joint edges after reaching peak values close to the edges. Yuceoglu and Updike maintained that an analytical model which would allow the shear stresses to drop to zero at the joint edges would give approximately the same or slightly lower peak values of shear and peel stresses. Their method also reveals that adherend bending has a significant effect on both adhesive shear and peel stresses, especially the latter.

Also in 1980, Delale and Erdogan [4] performed an analysis on the single lap joint assuming linear elastic adherends and a linear viscoelastic adhesive. Separate stress distributions were calculated for membrane loading, bending, and for transverse shear loading. This paper is discussed in more detail in Section 2.3. Delale and Erdogan [13] further extended their viscoelastic analysis of the single lap joint to include time-dependent temperature variations approximated by a piecewise constant function.

The application of creep and viscoelasticity in conjunction with the finite element method of stress analysis has long been established for the design of nuclear reactor pressure vessels and for solid propellant rocket motors. White [14] presented such a stress analysis method for solid rocket propellant motors in 1968. Linear viscoelasticity in shear with a hereditary integral stress-strain relation, a constant bulk modulus and a reduced time hypothesis was assumed.

A transient, non-homogeneous temperature distribution was also included. In 1974 Zudans et al. [15] solved the problem of non-isothermal elastic-plastic creep in large structures using the finite element method. Material non-linearities were treated by the tangent stiffness method while geometric non-linearities were considered by updating the geometry after each increment of loading. An incremental finite element formulation involving non-isothermal elastic-plastic-creep-large strain analysis was developed for nuclear reactor pressure vessels in 1979 by Haisler and Sanders [16]. Apparently, none of these "advanced" methods of stress analysis have been applied to adhesive joint analyses.

Gali and Ishai [17], in 1978, performed a finite element analysis on a symmetric doubler model with linear elastic adherends and the adhesive obeying a non-linear effective-stress-strain relationship. The effective-stress-strain relationship was derived from stress-strain curves obtained by tensile and shear test data, and based on the von Mises deviatoric energy yield criterion. An iteration procedure was applied to the linearly elastic finite element problem using a specific secant modulus for each element separately. The secant modulus was found from the corresponding effective strain of the previous solution and the corresponding effective stress was found from the experimental stress-strain curves. This method is similar in nature to that used in the SAAS3V program which was used in the present study.

Gali and Ishai analyzed their symmetric doubler model using both plane stress and plane strain and found that the latter solutions converged faster and yielded less conservative results, i.e., lower

stresses, than the plane stress solutions. Non-linear solutions were also found to be considerably lower than the linear solutions, the difference being more pronounced in the plane stress case. The problem was also solved with the adhesive following an elastic-perfectly-plastic effective-stress-strain law. The difference between these results and those of the continuous non-linear effective-stress-strain case, was found to be very small.

In 1979 Nagaraja and Alwar [18] analyzed a tubular lap joint with the finite element method assuming linear elastic adherends and Kauderer's non-linear bi-axial stress-strain law in the adhesive. The constants appearing in Kauderer's law were obtained from uniaxial tension test data. The stress-strain relationship, however, was assumed to be time-independent. Nagaraja and Alwar demonstrated that for low stress levels, of the order of 12% of the fracture stress, the non-linear stresses were as much as 15% lower in shear and 8% lower in peel than the linear stresses. In 1980 Nagaraja and Alwar [19] performed a finite element analysis on a single lap joint, treating the adherends as linear elastic materials but the adhesive as a linear viscoelastic material. The relaxation modulus was assumed to be equal to the inverse of the creep compliance, the latter being obtained experimentally. Schapery's collocation method was used to represent the relaxation modulus by a Prony series. The advantage of the Prony series is that its Laplace transform is easily obtained. The transformed relaxation modulus was substituted for the adhesive modulus in the associated elastic solution. Schapery's direct method of inversion was applied to the solution in order to obtain the overall behavior of

the time-dependent adhesive quantities. This method is discussed in more detail in Chapter 5.

In 1980 Sen and Jones [8] performed a finite element analysis on a double lap joint bonded with a viscoelastic adhesive. They followed the same procedure as Nagaraja and Alwar, but in addition to Schapery's direct method, they also used Schapery's quasi-elastic method. The maximum difference in results from these two methods were found to be less than 0.2% for both the shear and peel stresses. The errors in the theoretical analysis was estimated by a graphical method suggested by Schapery and were found to be 0.85%, 0.77% and 0.21% in shear, peel and axial stresses, respectively.

The effect of joint geometry on the lap shear strength of joints was discussed by Bryant and Dukes [21] in 1965. They acknowledged that single lap shear strength cannot be measured independently of joint design. They indicated that bonded screw threads and cylindrical butt joints in torsion, however, gave failing stresses independent of specimen dimensions (the adhesive thicknesses excluded). In 1978 Amijima [22] investigated the effect of joint width on the shear stress distribution in the adhesive layer. This was done by a 2-dimensional finite element analysis in the shear plane, so that the thickness variation of all stresses necessarily had to be neglected. The shear stress was found to vary greatly through the width, with peak values along the sides of the joint. As can be expected, the shear stress at the corners of the joint, i.e., where the joint ends and sides meet, was more than twice the maximum values at the center of the joint ends or the joint sides. The overall shear stress was also found to be greatly

influenced by the width of the joint.

A greater interest in experimental methods in the field of adhesive joints has been observed in recent years. Brinson et al. [50] studied the strain-rate and creep properties of bulk adhesives under tension and of lap shear geometries in 1975. The modified Bingham model was used in conjunction with a delayed failure theory of Crocket to predict creep ruptures of the bulk adhesive and lap shear samples. Stress-strain responses were also fitted with Ramberg-Osgood approximations. A similar analysis to that of Brinson et al. was conducted by Cartner and Brinson [51] using Schapery's non-linear viscoelastic model.

Ishai, Peretz and Gali [23], in 1977, used a symmetrical doubler model as a method for direct measurement of normal (peel) and shear displacements and stresses along the adhesive layer, averaged through the adhesive thickness. Shear stresses and strains were obtained by measuring differential displacements of the adherend surfaces and peel stresses by measuring lateral displacements. Good agreement between the experimental results and analytical solutions were obtained. Elastic moduli for the adhesive had to be known for the analytical calculations. Renton [45] and Sancaktar [46] investigated a symmetric single lap shear specimen in 1978 in which the loads are not eccentric. Due to the nature of the joint, however, bending still occurs [46]. When joint elongation is used for the calculation of strains, measured shear properties are often in error. Small gauge length extensometers which measure deformation only over a small portion of the joint were developed for this reason. Sancaktar also studied strain-rate and

creep properties in bulk adhesives under tension and in lap shear geometries. Shear deformation from the lap shear joints was much larger than those that would be predicted from the bulk tensile samples and attempts to relate properties from the two were met with little success.

Krieger [24] developed the KGR-1 extensometer to give an experimental shear stress-strain curve for a glue-line in a thick adherend joint. Shear stress was averaged over the entire overlap area and assumed to be constant through the adhesive thickness, while shear strain was measured at a point one-quarter of the overlap length away from the joint edge. Extension of the adherends was accounted for so that the shear strain represents the adhesive strain at that point of measurement, assumed to be constant through the adhesive thickness. Although the frame of the KGR-1 gauge is made of aluminum, it is relatively heavy and expensive to manufacture. Presently, the use of a so-called ring gauge [47] is being investigated. The ring gauge is not only lighter but also simpler in construction. There is no apparent reason why these gauges may not also be used on other joint configurations. Sancaktar and Schenck [25] recently (1983) employed a simple and general method for characterizing structural adhesives using the single lap joint. This method involved a gauge which clips onto each adherend outside the joint area. Adherend extensions were calculated and subtracted from the extension measured by the clip-on gauge to give the total adhesive shear deformation. This value was divided by the average bond line thickness to obtain the average adhesive shear strain. Shear stress was also averaged along the entire

overlap area.

Peretz and Weitsman [29], in 1980, investigated experimentally the creep and recovery of neat FM-73 U adhesive (the U designates "unscrimmed"). The resulting data was reduced to analytical expressions for a non-linear viscoelastic model. Good agreement between the model predictions and test data for two-step loading as well as for constant stress-rate loading and unloading was obtained. Also in 1980, Romanko and Knauss [27] examined the time sensitivity of Poisson's ratio for FM-73 M adhesive. Holographic interferometry was employed, and for times in the glassy-to-rubbery range, Poisson's ratio remained constant, in spite of a measurable creep occurring in the same time domain.

In 1981, Hart-Smith [28] addressed the difference in adhesive behavior in test coupons and in structural joints. He showed that typical test coupons fail by a different mechanism than in structural joints, due to the absence of resistance to creep accumulation in the adhesive of test coupons. He also summarized behavior of adhesive bonds as a function of overlap length for joints with thin, moderate and thick adherends.

The quality of the interfacial bond is recognized as a prime ingredient to joint strength and, for this reason, non-destructive examination techniques are needed to evaluate bond quality prior to loading and under service conditions. Sancaktar et al. [52] recently conducted research using neutron radiography as a non-destructive technique for detecting defects in adhesively bonded joints. Other non-destructive examination techniques are C-scan and X-radiography.

Although the fracture aspects of adhesive joints are not included in this study, such aspects are important for developing any sort of failure criterion, which is the next logical step in a study of this nature. For this reason the work of some authors in the field of fracture and failure criteria of adhesive joints is briefly reviewed.

Arin and Erdogan [31] derived an equation for the stress intensity factor for a penny-shaped crack in an elastic adhesive layer between two dissimilar half spaces. Their results were applied to the simple butt joint by Hilton and Gupta [32]. Explicit equations for the stress intensity factor applicable to adhesive joints in general, however, are not available.

The fracture energy, or critical strain energy release rate, and the critical crack opening displacement are critical conditions for the onset of fracture. Neither the fracture energy nor the critical crack opening displacement, however, are true material constants, especially for adhesives. Bascom, Cottington and Timmons [33] found the fracture energy for adhesives to be strongly dependent on temperature. Mijovic [34] found the fracture energy of Epon 825 resin to be heavily dependent on the post-cure time, but that this dependence (as well as the level of fracture energy) was decreased by increasing the percentage of reinforcing particles. The increase in fracture energy with post-cure time was ascribed to additional cross-linking reactions. Several authors [33,35,36,37] investigated the dependence of adhesive layer thickness on the fracture energy. Bascom et al. [33], for example, found that the mode I as well as the combined mode I and II fracture energy increased to a maximum with increasing adhesive

thickness, then decreased slightly and leveled out to a constant value. Bascom et al. [33] also investigated the difference in fracture energy when measured in a structural joint and as bulk material. The difference was found to be dependent on the type of curing agent used for the epoxy adhesive. The same authors found the crack tip deformation zone diameter to increase steadily with increasing adhesive layer thickness. The effect of the location of the crack tip, i.e., at the center of the bond or at the interface, was investigated for mixed mode loading by Tratina [38], using finite elements. Analytical solutions for the fracture energy are available for simple geometries only [39]. For mode I loading, the fracture energy was obtained experimentally by Ripling, Mostovoy and Patric [40] and by Mostovoy and Ripling [41], using the double tapered cantilever beam. Ripling et al. [40,42] also designed a test specimen for measuring the fracture energy for the pure shear, mode II loading. Tratina [38] determined the mixed mode fracture energy using the so-called mixed mode test specimen, through the use of a finite element stress analysis. Anderson, de Vries and Williams [43] also demonstrated the use of finite element codes in fracture analyses. O'Connor and Brinson [54] performed a critical study of the sensitivity of the strain energy release rate to specimen preparation. The fracture surfaces were also studied using scanning electron microscopy to determine the mechanisms of failure. Dwight, Counts and Wightman [55] studied surface chemistry and interfacial effects on adhesive bonding and Dwight, Sancaktar and Brinson [56] studied the failure characteristics of an adhesive, and applied fracture mechanics to their analysis.

Mulville, Houston and Mast [53] developed a method of experimental failure criteria under complex loading using a strain energy release rate formulation and illustrated its application to the design of adhesively bonded structural components. For adhesive joints involving the absence of load or material symmetry, Sih [44] maintained that it is more convenient to apply the strain energy density criterion, or S-criterion, than the fracture energy or the strain energy release rate concept. Apparently, however, not much work has been done using the strain energy density criterion.

Only recently work involving the time dependent fracture characteristics of adhesively bonded joints has been under way. A program by Francis et al. [30] is to quantify the influence of the viscoelastic adhesive layer, geometry, fracture mode mix, mechanical load history, environmental history and processing variations on the fracture processes of adhesively bonded joints. Also of interest are the orthotropic properties of the adhesive, geometric non-linear behavior, fatigue fracture and the applicability of the developed methodology to bonded joints [30]. Johnson et al. [47] of NASA-Langley have performed cyclic de-bond research on the crack lap specimen and performed analyses with a finite element program.

2.1 Discussion of the Goland and Reissner Analysis

Goland and Reissner [2] considered the problem of the single lap joint to consist of two parts: First, the joint edge loads M_o, V_o and T_o, as shown in Figure 2.1, were determined and second, the joint stresses resulting from these loads were determined.

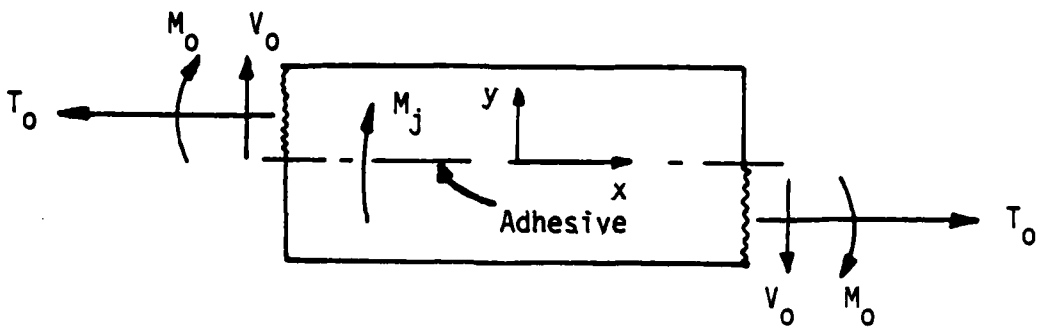

Figure 2.1 Joint Edge Loads in a Single Lap Joint Resulting from a Tensile Load T Applied to the Ends of the Adherends.

In order to account for the geometric non-linearity mentioned on page 1, the transverse displacement was calculated using cylindrically bent plate theory. The bending moments, M_j and M_i, in the joint section and in the adherends outside the joint, respectively, were determined purely from geometric considerations. It was assumed that the adhesive peel stress σ_o and shear stress τ_o are constant through the thickness of the adhesive layer. The peel and shear stresses in the adherends were assumed to decrease linearly and parabolically to zero through the thickness of the adherends respectively, as shown in Figure 2.2. It was also assumed that $\ell >> c >> t$, (ℓ, c and t are defined in Figure 2.4), and the adhesive layer thickness h_o was neglected when compared to the adherend thickness t.

In determining the joint stresses resulting from the joint edge loads, Goland and Reissner followed two distinct approaches. In the first, the effect of the adhesive on the flexibility of the joint was neglected and the joint was considered to be one homogeneous piece of

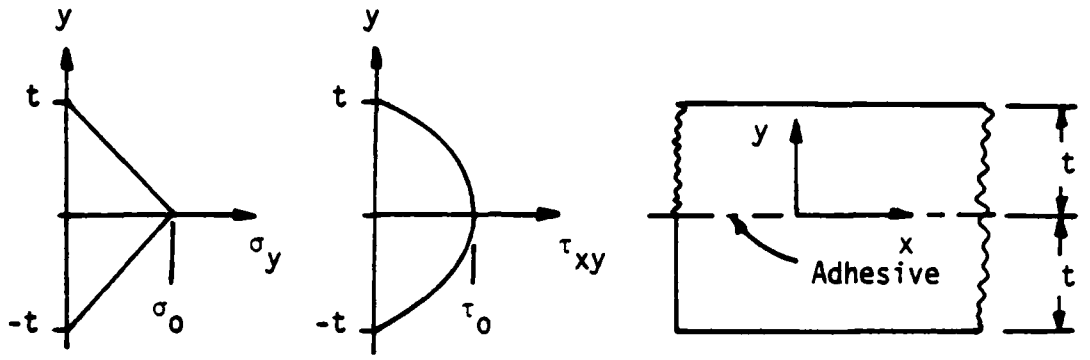

Figure 2.2 Variation of Peel Stress σ_y and Shear Stress τ_{xy} Through the Thickness of the Single Lap Adhesive Joint with Maximum Values σ_o and τ_o in the Adhesive Layer Respectively.

material and treated as a plane elasticity stress type boundary value elasticity problem. The shear load V_o was neglected. In the second approach, it was assumed that the joint flexibility is mainly due to the presence of the adhesive. The adhesive layer was thus necessarily taken into account and an element of length dx may be taken from each of the upper and lower halves of the joint to be treated as two adjoining free body diagrams, as shown in Figure 2.3. Equilibrium of moments and forces, stress-strain and strain-displacement relations and the necessary boundary conditions give rise to Goland and Reissner's constitutive equations for stresses in the adhesive layer.

Hart-Smith discussed the method of Goland and Reissner in his report on the single lap joint [3] of 1973 and noted that a deficiency in the determination of the bending moment by the latter causes a serious overestimate of the adhesive stresses at high tensile loadings. This deficiency is that M_j, which is used to calculate M_o (see Fig. 2.1),

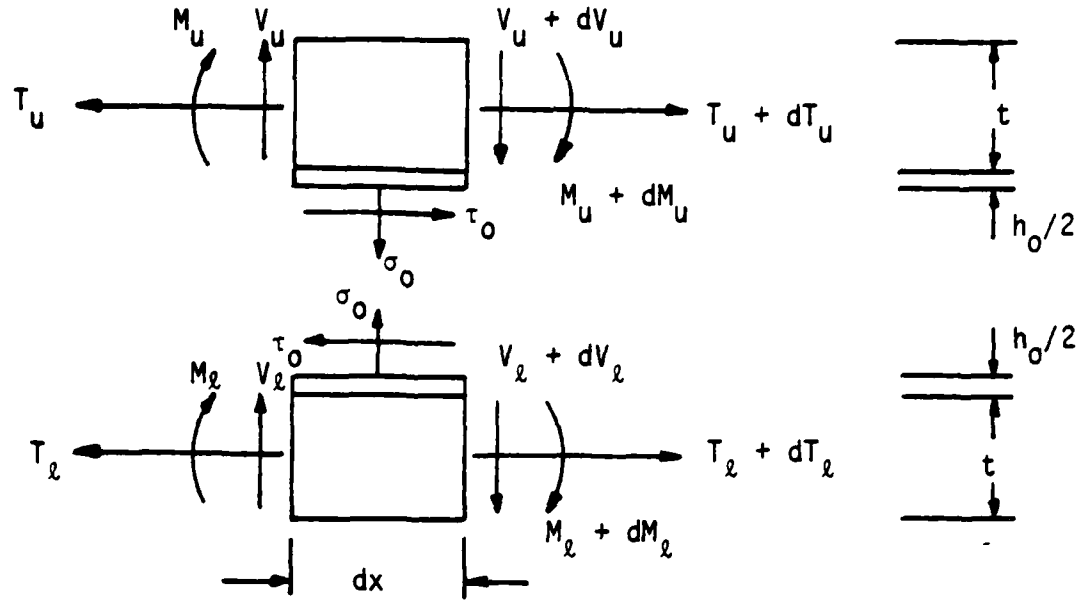

Figure 2.3 Differential elements of length dx from upper and lower joint halves, treated as free body diagrams for moment and force equilibrium.

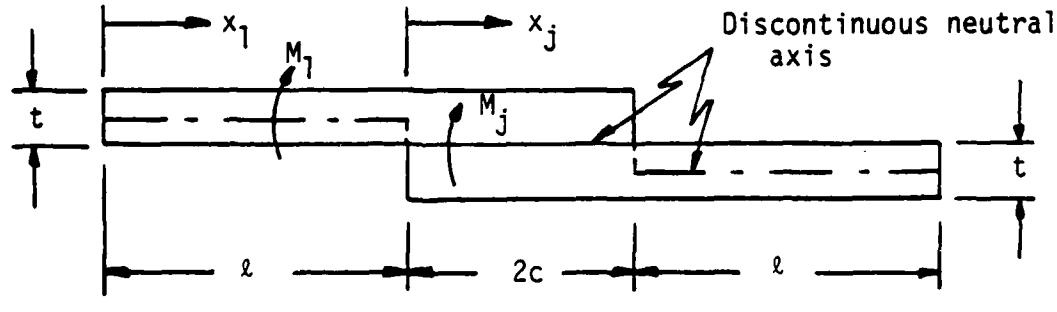

Figure 2.4 Single lap joint showing geometry and two separate coordinate systems x_1 and x_j.

does not accurately represent the boundary stresses at $x_j = 0$ or $2c$ (see Figure 2.4). Hart-Smith overcame this deficiency in a manner which is described in Section 2.2.

This deficiency of M_j not accurately representing the stresses at the joint edges is possibly not as serious as it is pointed out to be by Hart-Smith. Goland and Rissner merely used M_j to set up a differential equation for the transverse displacement w in the joint section by the equation

$$\frac{M}{EI} = -\frac{d^2w}{dx^2}$$

which was in turn used to enforce continuity of w at the joint edge $x_j = 0$ or $x_1 = \ell$. At $x_j = 0$, M_j was not required to equal either M_0 or M_1 at $x_1 = \ell$ (see Figure 2.4) as alleged by Hart-Smith, since the neutral axis of the joint section and of the adherend outside the joint are not continuous. This may also be seen from Goland and Reissner's equations (8), reference [2]. Joint edge stresses were not calculated from M_j but from solving the pure boundary value elasticity problem mentioned earlier.

Hart-Smith also indicated that the adhesive peel stress of Goland and Reissner is overestimated by a factor of nearly two for high loads or long overlap lengths. This conclusion was based on the ratio between maximum and average stresses. The latter, however, is not necessarily the same for the two analyses, even for fixed geometry, loading and material properties. The two analyses yield different stress distributions which, most likely, yield different values for σ_{ave}.

2.2 Discussion of Hart-Smith's Analysis

The deficiency in the determination of the bending moment by Goland and Reissner, as pointed out by Hart-Smith, was discussed in the previous section. This deficiency, being that M_j (see Figure 2.4) does not accurately represent the boundary stresses at $x_j = 0$, was overcome in the analysis of Hart-Smith by first considering M_o as an unknown and then following the second approach of Goland and Reissner for calculating the joint stresses, i.e., considering separate bending moments M_u and M_ℓ in the upper and lower halves of the joint, respectively. The sum of M_u and M_ℓ at any position x_j in the joint equals the single bending moment M_j of Goland and Reissner. Since M_u and M_ℓ are independent, they could be made to satisfy the boundary stresses at $x_j = 0$ or $x_j = 2c$ exactly. The bending moments M_i in the adherends outside the joint were determined in the same manner as by Goland and Reissner, i.e., from purely geometric considerations; the only difference is that Hart-Smith did not neglect the adhesive layer thickness h_o, as did Goland and Reissner.

Hart-Smith also established the quantitative influence of adhesive plasticity in shear which leads to a much better understanding of actual joint behavior. The influence of adhesive plasticity permits explanation of the premature failure predictions made when performing linearly elastic analysis.

2.3 Discussion of the Analysis of Delale and Erdogan

Delale and Erdogan [4] performed a viscoelastic analysis on the single lap joint in which they considered the adherends to be linearly

elastic and treated the adhesive as a linear viscoelastic solid. Plane strain and cylindrical bending of the adherends was assumed. By considering equilibrium of moments and forces on two differential elements from the upper and lower halves of the joint and combining the stress-strain and strain-displacement relations, Delale and Erdogan arrived at twelve simultaneous equations, but with fourteen unknowns. The fourteen unknowns being six adherend loads, six adherend displacements and two adhesive stresses. The two additional equations required to complete the formulation of the problem are the constitutive equations for the adhesive. Three equations for adhesive strains were obtained from two displacement vectors at points on the interfaces between the adhesive layer and the adherends. The adhesive stress and strain tensors were then decomposed into their hydrostatic and deviatoric components. The differential operator approach on the hydrostatic and deviatoric components was used and substitution of the three equations for adhesive strains led to the two constitutive equations for the adhesive.

The adhesive behavior was assumed to be represented by that of a three-parameter viscoelastic solid model and equations for the differential operators were obtained from the governing differential equation for this model. These operator equations were substituted into the constitutive equations for the adhesive, and differentiation with respect to time resulted in two uncoupled differential equations involving normal and shear adhesive stresses, each a function of position and time. The Laplace transform of these differential equations were taken and reduced to two ordinary differential equations which were

easily solved directly. The resulting constants of integration were determined by the application of the boundary conditions.

Exact inversion of the Laplace transforms of the adhesive stresses apparently became very complicated, and the method employed by Delale and Erdogan was to use the complex inversion integral equation for the Laplace transform. The integrals were solved numerically in conjunction with the residue theory. Material properties and geometric dimensions had to be assumed during the numerical integration.

It was shown that there is a redistribution of stresses with time. Not only was the normal stress in the adhesive found to be higher than the corresponding shear stress but it was also found to decay more slowly.

Chapter 3

FINITE ELEMENT CONSIDERATIONS

It is evident from the discussions in Chapter 2 that well-recognized closed form analytical solutions are not without questions as to how well they represent the true stress fields in adhesive joints. With present-day expertise, the finite element method is, no doubt, an efficient tool for approximating stresses in complex structures such as the two problems analyzed in this study. For this purpose the SAAS3VP finite element program, a modified version of the existing SAAS3V program [1], was used. Four-noded composite type elements are used by the SAAS3V programs in which the element stiffness matrices are obtained by superposing those of four constant strain triangular elements with two degrees of freedom per node.

As was found during the initial stages of modeling the single lap joint, high stress gradients in the adhesive layer, close to the joint edges, are not only present along the length of the layer but even more so across its thickness. It is, therefore, necessary to model the adhesive layer with more than one element through its thickness.

In both the single lap and thick adherend joints, the adherends undergo a fair amount of bending, and in various analytical studies, for example, Goland and Reissner [2], it was established that adherend bending severely influences adhesive stress distributions. For this reason it is imperative that the finite element discretization

accurately represents bending. The tendency is to model bonded joints such that the elements decrease in size transversely towards the adhesive layer, where stress gradients are highest. This was done by Sen and Jones [8] and Francis et al. [30], for example. However, if this is done, the adherends effectively have a greater stiffness on the side with the larger elements and bending may consequently not be represented accurately. In this study, elements are spaced evenly through the thickness of the adherends, which is possibly the best method to represent the bending effects.

In the axial direction of the joints, however, elements may decrease in size towards the joint edges where stress gradients in this direction are highest. In the present study, elements were generated such that they decrease exponentially in size in the axial direction towards the joint edges. The mathematical law according to which the elements change in size is given in Section 4.2 and allows high effectiveness in the use of elements and computer time.

The purpose of defining an interface layer between the adhesive and each adherend was explained in Chapter 1. Throughout this study, each interface layer was chosen to be 0.0003 inches thick, corresponding to one tenth the thickness of the adhesive layer used in the single lap analysis of Humphreys [5], whose results were used for comparison (Section 6.1).

To establish an efficient finite element discretization, first the aspect ratio of the smallest elements, which lie lengthwise in the interface layers adjacent to the joint edges, was chosen to be 3.0. This aspect ratio was considered suitable due to the stress gradients

which are higher in the transverse direction than in the axial direction. Only one element through the thickness of the interface layer was considered. The number of elements in different sections of the single lap joint was then increased in one section at a time, keeping the number of elements in other sections low (to save on computing costs) and constant, as well as keeping the aspect ratio of the smallest elements in the interface layers constant. The increase in number of elements was continued progressively in each section, and stresses compared accordingly, until any further increase was considered to be unjustified. Experience obtained in this manner enabled efficient finite element discretizations to be chosen for the final analysis of both the single lap and the thick adherend joints.

Chapter 4

MODIFICATION TO THE SAAS3V PROGRAM

The SAAS3V program is very general in application and could possibly have been used for the purpose of this study without any significant modifications being made. Certain improvements and additions were made, however, to facilitate the input and output capabilities, which would at least make the analysis more efficient, not only in the present analysis, but also for future use of the program.

Changes to the SAAS3V program were made using the program MUTATE, written by J. Mook, Virginia Polytechnic Institute and State University, which replaces, deletes or inserts records, and creates a new source program without changing or deleting the original version. The changes made during the course of the present study, however, were not intended to be temporary only, but were made from a general point of view in order that they would be beneficial in the future to the solving of a wide range of problems. The MUTATE program is especially helpful if the same features need to be incorporated in some other version of SAAS3V which was modified independently for some other purpose. The new modified version is named SAAS3VP and signifies that many of the improvements were made with regards to its plotting capabilities.

The major changes and additions incurred on SAAS3V are discussed under separate headings in this chapter. Most of the minor modifications in many subroutines, however, merely form part of the implementation of those discussed and are not mentioned. These changes

can easily be traced in Appendix B by searching for the record name SCAL in columns 73 to 76. SCAL signifies that the first addition to the program was that of subroutine SCALEM which is discussed in Section 4.3.

Although the main program of SAAS3V was reorganized, all the original facilities or options are retained. It was, however, necessary to change the order of data input, and for this purpose as well as to explain additional options now available, a new set of user input instructions is included in Appendix A. The SAAS3V program is documented in [1] and a listing of the SAAS3V MUTATE program in Appendix B.

SAAS3V can handle a maximum of 25 nodes in the I direction and 100 in the J direction, while the total number of nodal points may not exceed 1000. SAAS3VP, however, has been extended to facilitate 50 nodes in the I-direction and 100 in the J-direction while the total number of nodes may not exceed 2000. The (I,J) nodal coordinates are those of the transformed Laplacian (R,Z) grid, normalized such that all nodes along a constant I or J are equi-spaced and of unit distance apart [1].

4.1 Main Program Changes

In the main program of SAAS3V, the plotter is initialized before mesh generation, and the mesh plotted before actually solving the problem. Deformed grid and contour plotting is performed at the end of the program. Since additions to the program included various options for both mesh plotting and the plotting of output data, it became

less confusing to group all plotting options at the end of the main program (see Appendix B).

The original options of stopping the program after mesh generation and mesh plotting before solving the problem (for verification of the correctness of the input data), or of restarting the program for additional output information (without again solving the problem) are retained in SAAS3VP. Restarting is now also provided after mesh generation, in order to eliminate the need for regenerating the mesh once it has been stopped as explained above, or if the same problem has to be solved with different material properties. After non-linear problem solution, restarting is now also possible if one or more additional non-linear approximations are required. The program then restarts at the end of the previous non-linear approximation.

4.2 Modification of Subroutines MESH and POINTS

Modification of the mesh generator was motivated by three separate objectives:

1. To generate a mesh such that the element size decreases exponentially towards a point or points within the mesh.
2. To enforce the generation of internal points on straight lines.
3. To generate the mesh of a body with u-shaped boundaries.

In the SAAS3V mesh generator, input data is in the form of LINE SEGMENT CARDS, which specify the (I,J) and (R,Z) coordinates of two points A and B, say, located on a straight line in the R-Z (or X-Y) plane (see Appendix A). The mesh generator generates points between

points A and B, equally spaced, obtaining the number of points between A and B from the difference between their I or J values. In order to space the points exponentially between A and B, two additional values are specified on the LINE SEGMENT CARDS of SAAS3VP, viz., GRF and IGRF. Here GRF is the growth rate factor defined by the relation

$$L = s \sum_{n=0}^{N} (GRF)^n$$

where L is the distance between points A and B, s is the length of the smallest increment between A and B and N is the number of points generated between A and B (see Figure 4.1). The mesh generator calculates L and N from the (R,Z) and (I,J) coordinates of A and B, and s is calculated from L, N and GRF.

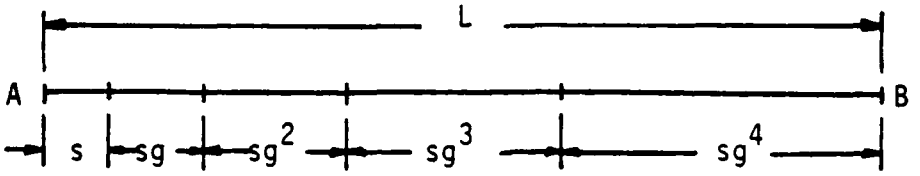

Figure 4.1 Nodal Point Spacing Increasing Exponentially from A to B. g = GRF = 1.5 and IGRF = +1 and N = 4.

The value of IGRF must be either -1 or +1. If GRF > 1 and IGRF = -1, nodal point spacing decreases exponentially from A to B. Conversely, if GRF > 1 and IGRF = +1, nodal point spacing increases exponentially from A to B. If IGRF equals zero or any other value than +1 or -1, points generated between A and B are equally spaced as normally done by the SAAS3V mesh generator. (Nodal points are necessarily also spaced evenly if GRF equals 1.0.) At present, exponential spacing of nodal points can only be performed if the boundaries consist of straight line segments, and not when the LINE SEGMENT CARDS contain data for the generation of circular arcs.

Internally generated points, i.e., nodal points not generated from data given by the LINE SEGMENT CARDS, are determined by a relaxation technique, so as to locate each internal point at a "happy medium", averaged between four of its eight surrounding nodal points. The number of iterations in the relaxation technique may be limited to obtain certain effects in the generated mesh by specifying a value for NLIM on the MESH GENERATION CONTROL CARD. Typical results are shown in Figure 4.2. In many applications, however, as was the case with the problems analyzed for this study, it may be desirable to generate internal points such that they necessarily lie in straight lines. Material deformations are best demonstrated by a deformed grid and then it is desirable to have the undeformed grid to also appear undeformed. The option of generating internal nodal points such that they lie in straight lines is achieved by giving NLIM the value of -1 on the MESH GENERATION CONTROL CARD. If this option is used in the example of Figure 4.2(b), the result obtained is that of Figure 4.3,

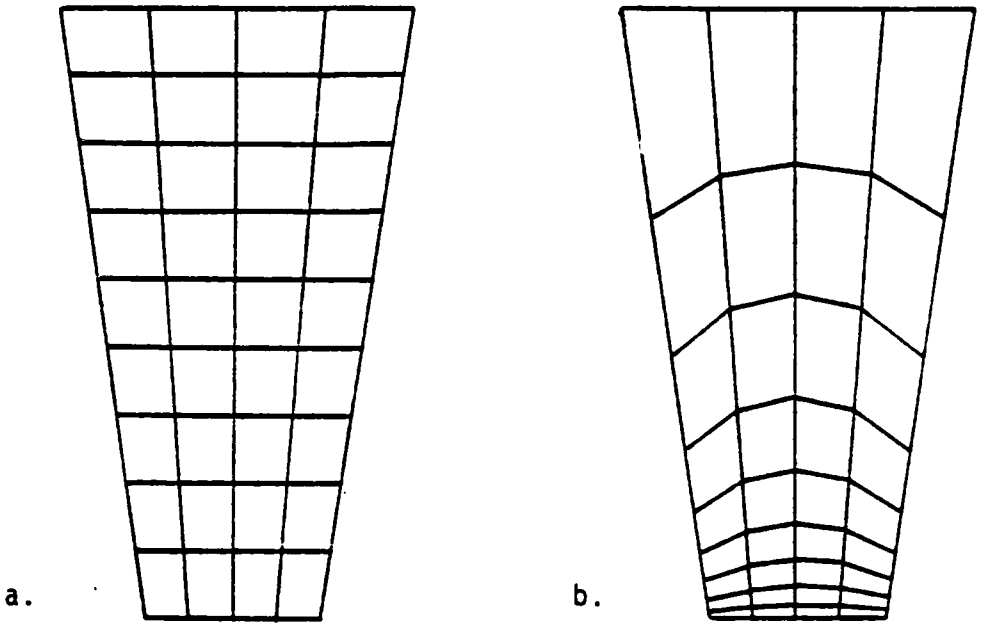

Figure 4.2 Internal Points Generated by the Relaxation Technique for (a) Equally Spaced Elements and (b) Elements Spaced Exponentially in the Vertical Direction.

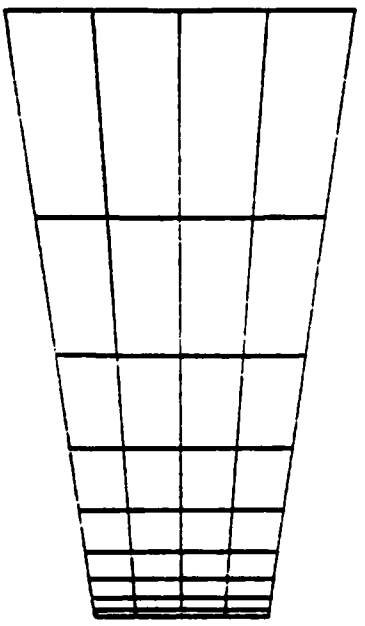

Figure 4.3 Internal Points Generated in Straight Lines.

and is achieved by interpolating internal points linearly between opposite line segment (boundary) nodal points.

Mesh generation could often be required on bodies with u-shaped boundaries such as the thick adherend adhesive joint analyzed in this study (see Figure 7.1). It is unavoidable for the SAAS3V mesh generator to assign nodal points and elements in the gaps between the upper or the lower adherends. The SAAS3VP mesh generator, however, will skip such areas not enclosed by four boundaries. It is important to note that with the SAAS3VP program, all boundaries must be covered by LINE SEGMENT CARDS, whereas in SAAS3V only one LINE SEGMENT CARD is required for each two opposite boundaries. No additional input data is required for this feature, and an unlimited number of u-shapes on any boundary is accommodated. Any area, however, enclosed by more than three sides will be fitted with elements. For example, Figure 4.4 shows a body which is unsuitable for mesh generation by the SAAS3V program. It is unavoidable for the SAAS3V mesh generator to fit the hashed areas with unwanted elements, and for the SAAS3VP mesh generator to fit the darkly hashed area only with unwanted elements.

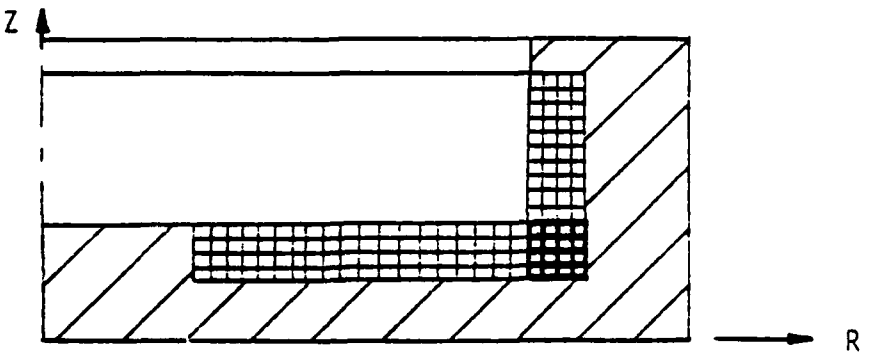

Figure 4.4 Example of a Body Unsuitable for Mesh Generation by the SAAS3V and SAAS3VP Programs.

4.3 Subroutine SCALEM

For problems with large aspect ratios such as lap joints, it is desirable to plot the generated mesh to a different scale in each direction. For the lap joints considered in this study, it was intended that more than one element be modeled through the thickness of the adhesive layer, h_o. Since $h_o << t$, where t is the adherend thickness, it also became desirable to plot the adhesive layer to larger scale than the adherends in the same direction. Subroutine SCALEM permits a user to scale the generated mesh such that arbitrary sections are enlarged or decreased individually. Up to a maximum of six different sections may be scaled in any one direction or in both directions simultaneously. The number of scale changes required in each of the I and J directions, NSCI and NSCJ, are included in the PLOT SCALE CARD and a number of SCALE CHANGE CARDS, equal to the maximum of NSCI and NSCJ, must then follow the PLOT SCALE CARD. Refer to Appendix A for more clarity.

In SAAS3V, nodal coordinates are adjusted for plotting the deformed element grid in subroutine CONTR. This function is now performed in subroutine SCALEM, after the mesh is scaled as described above, in order that the element deformations may be superimposed upon the enlargements brought about by the SCALE CHANGE CARDS.

4.4 Subroutines PLTSSD and INODE

Subroutine PLTSSD facilitates plotting of stresses, strains or displacements along any specified I or J coordinate, between arbitrary J_{min} and J_{max} or I_{min} and I_{max} coordinates respectively. The total

number of stress, strain or displacement plots is specified in the PLOT CONTROL CARD, and an equal number of SSD PLOT CARDS must follow the CONTOUR PLOT CARD specifying the necessary plotting information.

In SAAS3V, element stresses are identified by the element numbers, and nodal point displacements are identified by the node numbers. From a user's point of view, however, it is convenient to specify only nodal (I,J) coordinates for specifying plotting information. The variable NELMT was, therefore, included in SAAS3VP to identify each element by one specific node number, viz. the node corresponding to the smallest I and J coordinates of the four element nodes. Subroutine INODE was hence created to identify each node by its I and J coordinates. Refer to Appendix B.

4.5 Single Lap and Thick Adherend Preprocessors

During the course of the present study, many different cases were run in which only certain variables were changed, but for which the input data changed significantly. In order to facilitate the generation of input data, therefore, two simple preprocessors, SINGLE and THICK, were written in which only certain variables need to be changed, for example geometry and finite element parameters. These two preprocessors, included in Appendices C and D, generate complete sets of input data for the single lap and thick adherend joints respectively, and may easily be modified for other geometries too. The real benefit of using such preprocessors is in the generation of the line segment cards, especially if exponential spacing of the elements is required, and the size of the smallest elements is to be controlled.

Chapter 5

MATERIAL NON-LINEAR AND VISCOELASTIC CONSIDERATIONS

The SAAS3VP program accounts for material non-linearities by approximating non-linear stress-strain curves by bi-linear effective stress-effective strain curves. The program uses a method of successive approximations to obtain the effective stress function which is related to the von Mises yield criterion.

The SAAS3VP program is essentially restricted to elastic or elastic-plastic materials. However, as mentioned in Chapter 2, Sen and Jones [8] demonstrated the application of Schapery's direct method of Laplace transform inversion, using the SAAS3 program for calculating the associated elastic solution for the stresses, strains and displacements. The adhesive material property was considered to be linearly viscoelastic in the analysis of Sen and Jones.

In Schapery's direct method of transform inversion, it is assumed that a viscoelastic response, $\psi(t)$, is given by

$$\psi(t) = sL\{\psi(t)\} = s\bar{\psi}(s)\Big|_{s = 1/2t} \qquad [7]$$

where $\bar{\psi}(s)$ is the Laplace transform of $\psi(t)$ and may be obtained numerically for all non-negative values of the transform parameter, s. It is therefore only necessary to multiply the values of the transformed function by s and to obtain results at $s = 1/2t$.

The above assumption will hold and give good results if:

(i) The body is undisturbed for $t < 0$.

(ii) $\psi(t)$ is the solution to a problem in which all prescribed loads and displacements are step functions of time, applied at t = 0.

(iii) The derivative of $\psi(t)$ is a slowly varying function of log t.

(iv) Inertia is neglected.

As outlined by Sen and Jones [8], the SAAS3 finite element program was used to compute $\bar{\psi}(s)$, which, in this case represents stresses, strains or displacements. Here $\bar{\psi}(s)$ is the response to a unit step load $\bar{P}(s)$ such that

$$\bar{P}(s) = L\{P_o\ H(t)\} = P_o/s$$

where P_o is the actual load applied to the body, and

$$H(t) = \begin{cases} 0 & t < 0 \\ 1 & t \geq 0 \end{cases}$$

Material properties $\bar{E}(s)$ and $\bar{\nu}(s)$ are used such that

$$\bar{E}(s) = s\ \bar{E}_r(s)$$

and

$$\bar{\nu}(s) = s\ \bar{\nu}_r(s)$$

where $\bar{E}_r(s)$ and $\bar{\nu}_r(s)$ are the Laplace transforms of the time dependent relaxation modulus and Poisson's ratio respectively. Thus, for each time, there are corresponding values for the load $\bar{P}(s)$ and for elastic constants $\bar{E}(s)$ and $\bar{\nu}(s)$.

All time independent material properties remain unchanged, and the time dependent properties must be given by Laplace transformable

analytical expressions. A mathematical expression for the relaxation modulus, $E_r(t)$, for example, may be obtained from experimental data for a single relaxation test. Alternatively, if the test equipment is set up such that creep tests are easier to perform than relaxation tests, an analytical expression for the creep compliance $D_c(t)$ may be obtained and then $E_r(t)$ assumed to be equal to the inverse of $D_c(t)$. If the time dependence is not strong, then

$$E_r(t) \approx \frac{1}{D_c(t)}$$

The disadvantage of using Schapery's direct method is that it assumes the material to be linearly viscoelastic, i.e., $E_r(t)$ is independent of the threshold value for stress or strain at which the creep or relaxation tests are performed. The experimentally obtained creep data for FM 73 adhesive of Figure 7.4, for example, shows a decrease of 39% in creep compliance at t = 30 minutes, if the threshold stress is increased from 493 psi to 3041 psi (see Figures 7.5 and 7.6). The adhesive is therefore far from being linearly viscoelastic and in such cases, Schapery's quasi-elastic method may be applied which is based on the same assumptions as the direct method, but is equally applicable for linear and non-linear materials [9].

Schapery's quasi-elastic method consists of simply calculating the elastic response of the actual viscoelastic body to boundary conditions and material properties which are numerically equal to the instantaneous relaxation moduli or creep compliances associated with the viscoelastic problem. The difference between this quasi-elastic approximation and the exact viscoelastic solution can then either be

neglected, or else estimated by an established finite-difference integration technique, or possibly by a method of successive approximations [9]. In the example of a viscoelastic cantilever beam, Schapery [9] showed that the quasi-elastic method yields end displacements with negligible error over four decades of time as compared to the exact viscoelastic solution. In the example of the double lap joint, Sen and Jones [8] found the maximum difference between results obtained by the direct method and the quasi-elastic method to be less than 0.2% and the maximum error in results obtained by the quasi-elastic method was estimated to be 0.85% in shear stress, 0.77% in peel stress and 0.21% in the axial stress.

In the present analysis, stress-strain curves as a function of time are obtained from experimentally obtained creep data, and these curves are approximated by bi-linear stress-strain curves. The viscoelastic response to a load, $P_o = P_o H(t)$, is obtained for different times t by using Schapery's quasi-elastic method. The difference between this approximation and the exact viscoelastic solution was neglected due to the sound mathematical basis from which the quasi-elastic method was developed and due to the small estimated error in the double lap joint analysis of Sen and Jones [8].

Chapter 6

THE SINGLE LAP JOINT

6.1 Comparison with the Analysis of Humphreys [5]

The study performed by Humphreys was mainly on the bonding of composite adherends in single and double lap joints. However, two joints were analyzed using isotropic aluminum adherends, one in which the adhesive layer was entirely neglected. In the other, the adhesive represented a non-linear stress-strain curve which was approximated by a Ramberg-Osgood representation. In this part of the present study, the adhesive was treated as a linear elastic material and the loading coincided with the lowest value considered by Humphreys, for which the peak stresses were all within the linear range. The two different treatments for the adhesive response, therefore, do not contribute to differences in results obtained.

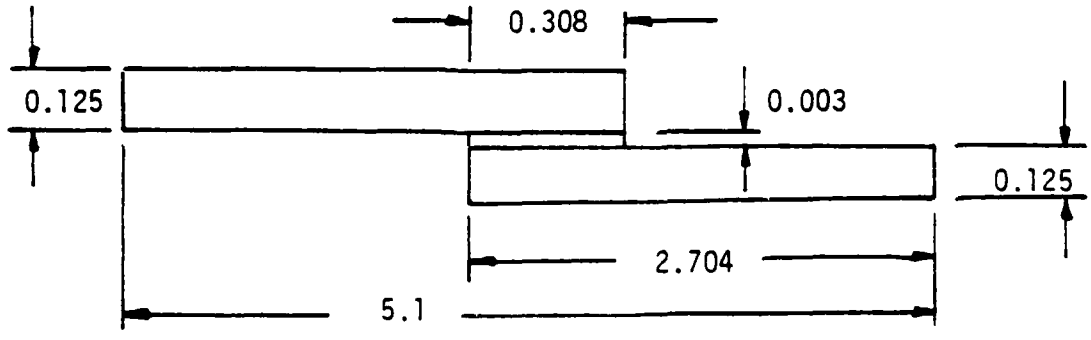

Figure 6.1 Geometry of Single Lap Joint for Comparison with Results of Humphreys [5]. Dimensions in Inches.

The geometry chosen for the single lap joint conforms with that used by Humphreys and is shown in figure 6.1. The boundary conditions and finite element discretizations as used by Humphreys are shown in figure 6.2. Two separate finite element discretizations were used in the present analysis for comparing results with Humphreys, and these, together with the boundary conditions are shown in figures 6.3 and 6.4. The only difference between the latter two figures is the use of either one or two elements through the adherend thicknesses. Since Humphreys utilized two elements through the adherend thickness over only short portions of the structure, it was expected that his results would lie somewhere between those of the present two analyses. A similar finite element mesh to that of Humphreys cannot be employed without the use of triangular elements for the transition from one to two elements through the adherend thicknesses. Such a use of triangular elements would make automatic mesh generation with the SAAS3VP program cumbersome and was not thought to be worth the effort.

The aspect ratio of the smallest elements in the adhesive layer, adjacent to the joint edges, is 2.5 for the present two analyses, as well as for Humphreys' analysis. From Figures 6.2 to 6.4, the boundary conditions are seen to be slightly different, but by St. Venant's principle, these differences could not have influenced the adhesive stresses significantly. Humphreys' finite element program, NONCOM1, employed constant stress triangular elements with three degrees of freedom per node, while the SAAS3VP program employed four-noded elements with two degrees of freedom per node. The order of the finite elements used in the two programs are the same, so that an equal degree

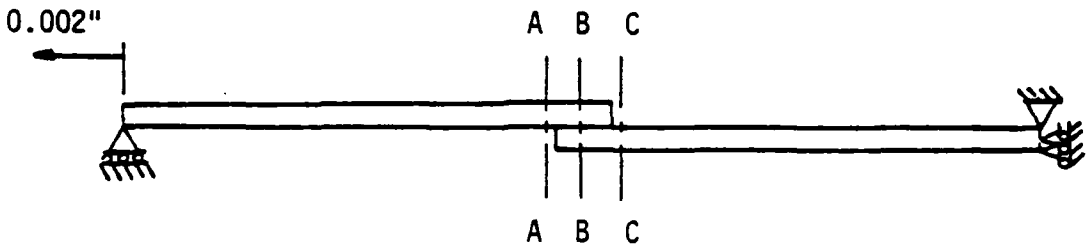

a)

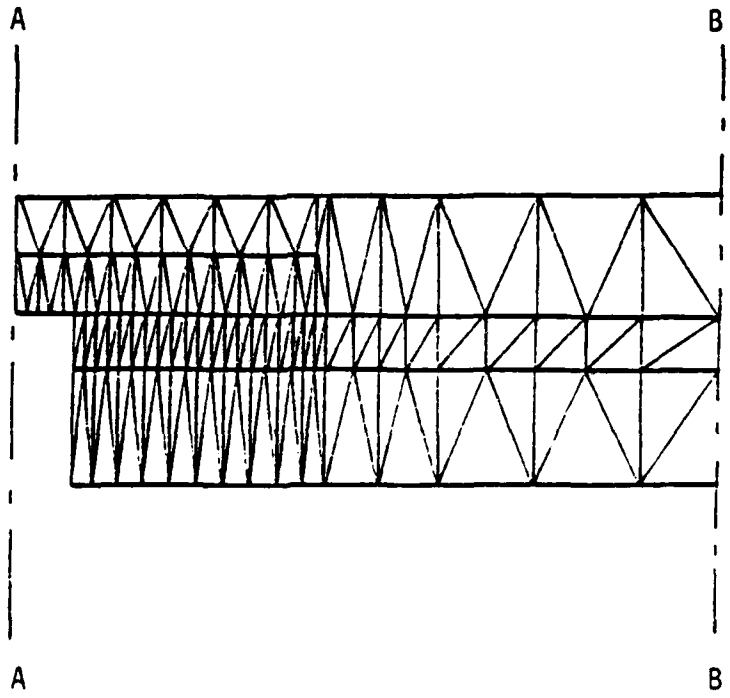

b)

Figure 6.2 (a) Boundary Conditions and (b) Finite Element Discretization of the Single Lap Joint as Used by Humphreys [5].

Note: The finite element discretization to the left of AA and to the right of CC is not known.

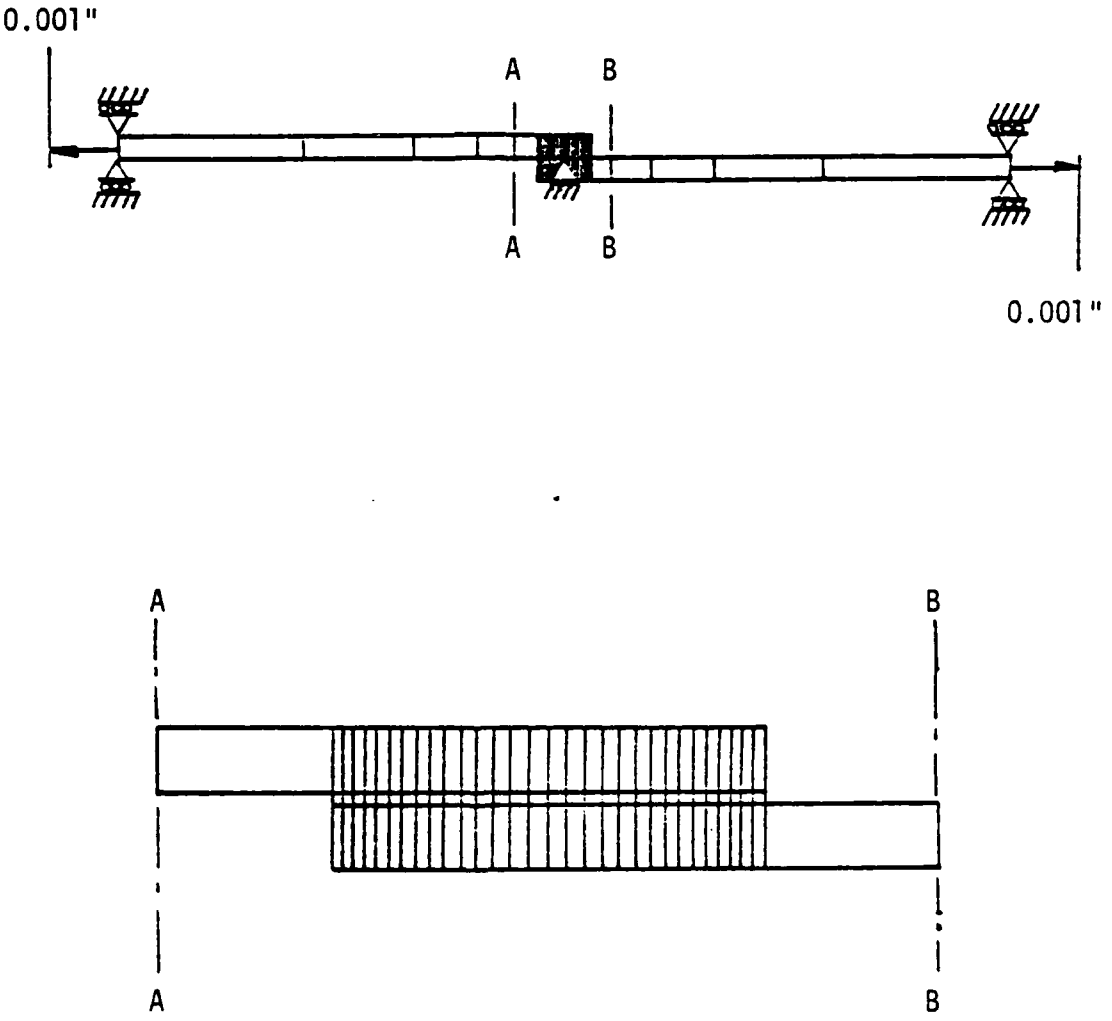

Figure 6.3 Finite Element Discretization I and Boundary Conditions, used to compare results with Humphreys.

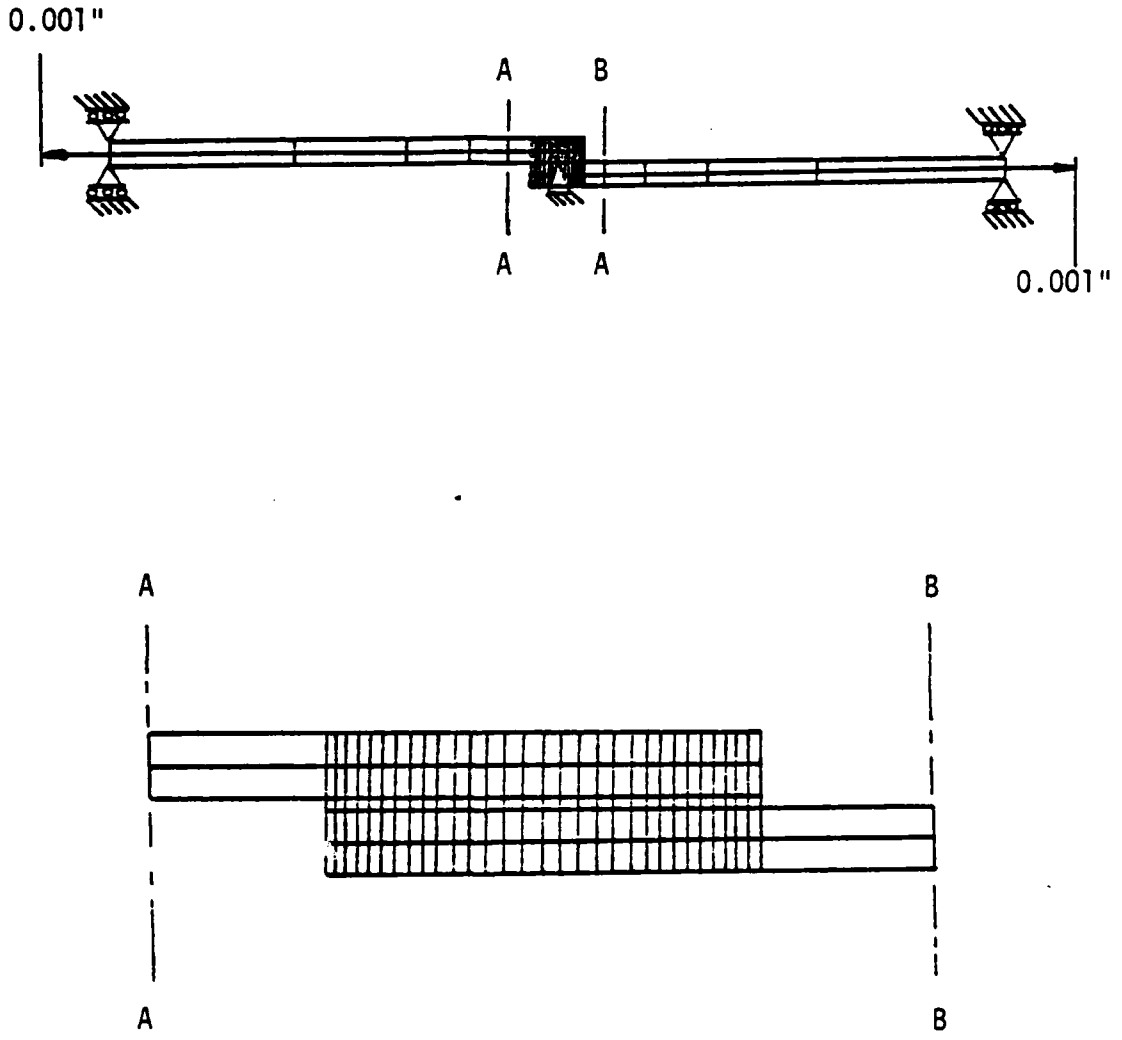

Figure 6.4 Finite Element Discretization II and Boundary Conditions, used to compare results with Humphreys.

of accuracy was expected.

As was considered by Humphreys, the adherends were chosen to consist of 2024-T4 aluminum, and Metlbond 1113 properties were used for the adhesive, which is an adhesive supported by a synthetic carrier cloth. The material properties are listed in Table 6.1. Some uncertainty with regards to the material properties used by Humphreys exists, however. The properties marked with an asterisk (*) in Table 6.1 are given in reference [5], from which it was initially assumed that the adhesive and adherends were both treated as isotropic materials. These properties in the present analyses yielded peel stresses of an order of magnitude higher than those obtained by Humphreys. Shear stresses were found to be in the order of 50% higher. Upon reference to the computer output of Humphreys, still available at V.P.I., it was found that the adhesive modulus in the direction normal to the shear plane, E_{33}, was taken to be one-tenth the moduli in the other two directions. All three Poisson's ratios were equal, which then make the adhesive orthotropic. Using the same properties in the SAAS3VP program yielded totally unrealistic results. The peel stresses were negative at the joint edges and a maximum at the joint center. It was not attempted to explain these results since such highly orthotropic properties do not represent any real adhesive.

The particular peak peel stress of Humphreys was also found to be in the order of 25% of that of his peak shear stress. From the analyses of Goland and Reissner and the conditions set for the ratios of the tensile and shear moduli to the thickness of the adhesive and the adherends, it was expected that the peak peel stress should at least

Table 6.1 Material Properties Used by Humphreys and in the Present Analysis for Comparing Results with Humphreys.

	Moduli (x 10^6 psi)						Poisson's Ratio's		
	E			G			ν		
2024-T4 Aluminum	10.600*			4.0*			.33*		
Metlbond 1113	.325*			.03625*			.366*		
	E_{11}	E_{22}	E_{33}	G_{12}	G_{13}	G_{23}	ν_{12}	ν_{13}	ν_{23}
Humphreys' Computer Printout	.3248	.3248	.03248	.03625	.03625	.03625	.366	.366	.366

*Reference [5].

be equivalent to the peak shear stress. In the present analyses, the peak peel stress exceeded the peak shear stress by about 30%. Neither of the two sets of results from this part of the present analysis are provided here since the finite element discretizations used are not considered to be good.

6.2 About Increasing the Number of Elements

This section deals with the influence of increasing the number of elements in the single lap joint on stresses in the adhesive layer. The number of elements in different sections of the structure was increased separately, while the number of elements in other sections were kept constant and to low values (to save on computer time). In order to make meaningful comparisons, it is necessary to always compare stresses at the same location in the structure. Changing the number of elements, however, changes the locations of elements as well. For the convenience of not having to interpolate stresses between element centroids, therefore, only the two elements marked "E_c" in Figure 6.5 were considered. The aspect ratio of these two elements were kept at 3.0 throughout this part of the study and, due to anti-symmetry, their stresses were always equal.

The joint geometry used was the same as that used for comparing results with Humphreys (Figure 6.1). Boundary conditions were changed, however, and are now defined in Figure 6.5. Material properties are given in Table 6.1, the adhesive being treated as an isotropic material.

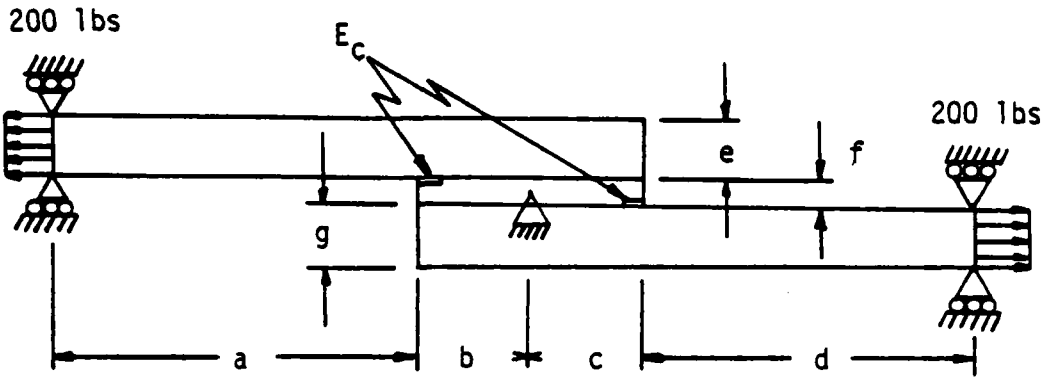

Figure 6.5 Boundary Conditions and Finite Element Configuration $\begin{matrix}(a,b,c,d)\\(e,f,g)\end{matrix}$ for the Single Lap Joint.

In the following four Subsections, 6.2.1 to 6.2.4, all stresses discussed refer to the stresses in the elements marked "E_c" in Figure 6.5. These stresses are listed in Tables 6.2 to 6.5, as well as percentage changes in these stresses from one case to the next, tabulated from top to bottom and not necessarily in case number order. Note that the elements "E_c" of Figure 6.8 do not necessarily represent the peak stresses in the adhesive layer, nor are the $\Delta\sigma$ values necessarily the largest change in stresses from one case to the next. They are, however, representative of the most important adhesive stresses and of whether further increase in the number of elements in any one section is desirable or not. The finite element configurations, for which stresses are listed in Tables 6.2 to 6.5, are listed in the form

$$\begin{matrix}(a,b,c,d)\\(e,f,g)\end{matrix}$$

where a to g refer to the number of elements in each section of the joint, defined in Figure 6.5. In Tables 6.2 to 6.5, NE_i is the number of elements in the particular joint section, i, and is varied independently of the number of elements in other sections.

6.2.1 Increasing the number of elements through the adherend thickness

Increasing NE_e, the number of elements through the adherend thickness, above 5, has a negligible effect on the adhesive peel stress σ_y and a small influence on the in-plane adhesive axial and shear stresses, σ_x and τ_{xy}, respectively. If NE_e is increased from 5 to 8, for example, σ_y is increased by 0.07%, σ_x by 1.15% and τ_{xy} by 0.39% (see Table 6.2). A larger number of elements through the adherend thickness, therefore, is not required for accurate adhesive stresses.

6.2.2 Increasing the number of elements through the adhesive layer thickness

Increasing NE_f, the number of elements through the adhesive layer thickness, above 5, has a negligible influence on the adhesive shear stress τ_{xy}, but a small influence on the peel and axial stresses, σ_y and σ_x, respectively. For example, if NE_f is increased from 6 to 8, σ_y is decreased by 0.56%, σ_x by 0.22% and τ_{xy} by 0.04% (see Table 6.3). The number of elements through the adhesive layer thickness, therefore, need not be more than through the adherend thickness, but must definitely not be less than 5 for stresses to be withinin about 5% accuracy.

Table 6.2 The Influence of NE_e, the Number of Elements Through the Adherend Thickness, on Adhesive Stresses.

Case No.	Element Config.	NE_e	Peel Stress		Axial Stress		Shear Stress		Maximum Principal Stress		
			σ_y (psi)	$\Delta\sigma_y$ (%)	σ_x (psi)	$\Delta\sigma_x$ (%)	τ_{xy} (psi)	$\Delta\tau_{xy}$ (%)	σ_{max} (psi)	$\Delta\sigma_{max}$ (%)	Angle (deg.)
B3*	(5,5,5,5) (5,4,5)	5	1278.8	-	607.9	-	386.5	-	1733.6	-	32.4
B4	(5,5,5,5) (5,4,5)	5	1311.5	2.56	591.7	-2.66	718.9	86.0	1755.6	1.27	31.7
B5	(5,5,5,5) (8,4,8)	8	1312.4	0.07	598.5	1.15	721.7	0.39	1760.7	0.29	31.8
B6	(5,5,5,5) (10,4,10)	10	1312.3	-0.01	601.2	0.45	722.7	0.14	1762.2	0.09	31.9

*Case No. B3 only was for elements spaced exponentially through the adherend thickness.

Table 6.3 The Influence of NE_f, the Number of Elements Through the Adhesive Layer Thickness, on Adhesive Stresses.

Case No.	Element Config.	NE_f	Peel Stress		Axial Stress		Shear Stress		Maximum Principal Stress		
			σ_y (psi)	$\Delta\sigma_y$ (%)	σ_x (psi)	$\Delta\sigma_x$ (%)	τ_{xy} (psi)	$\Delta\tau_{xy}$ (%)	σ_{max} (psi)	$\Delta\sigma_{max}$ (%)	Angle (deg.)
B6	(5,5,5,5) (10,4,10)	4	1312.3	-	601.2	-	722.7	-	1762.2	-	31.9
B7	(5,5,5,5) (10,6,10)	6	1276.8	-2.71	587.0	-2.36	721.4	-0.18	1731.5	-1.74	32.2
B8	(5,5,5,5) (10,8,10)	8	1269.7	-0.56	585.7	-0.22	721.1	-0.04	1725.8	-0.33	32.3
B9	(5,5,5,5) (10,10,10)	10	1267.6	-0.17	585.6	-0.02	720.9	-0.03	1724.1	-0.10	32.3

It must be pointed out, however, that NE_f being a large number relative to the adhesive thickness is due to extremely large stress gradients through the layer thickness close to the joint edge. Within a short distance from the edge, however, these gradients reduce sharply. As a consequence, NE_f may possibly be gradually reduced to one element as one moves away from the joint edge, by making use of triangular elements in the transition region.

6.2.3 Increasing the number of adherend elements in the axial direction

A surprisingly small number of elements in the adherends in the axial direction, outside the joint, NE_a, will cause negligible error in the adhesive stresses. For example, if NE_a is increased from only 3 to 5, σ_y decreases by 0.09%, σ_x by 0.36% and τ_{xy} by 0.23% (see Table 6.4). Further increase in NE_a has a negligible influence on all adhesive stresses.

6.2.4 Increasing the number of joint elements in the axial direction

Adhesive stresses are found to be heavily influenced by the choice of NE_b, the number of joint elements in the axial direction. Only if NE_b is increased from 15 to 20 does the increase in peel stress, $\Delta\sigma_y$, drop to 0.45%. The axial and shear stresses increase by 0.26% and 0.13%, respectively, for this change in NE_b (see Table 6.5).

In Table 6.5, the configuration for case no. D1 only had more elements in the left-hand half of the lap joint than in the right-hand half. The reason for investigating this configuration on adhesive stresses was to determine whether the use of fewer elements far away

Table 6.4 The Influence of NE_a, the Number of Elements in the Axial Direction of the Adherends, Outside the Joint, on Adhesive Stresses.

Case No.	Element Config.	NE_a	Peel Stress		Axial Stress		Shear Stress		Maximum Principal Stress		
			σ_y (psi)	$\Delta\sigma_y$ (%)	σ_x (psi)	$\Delta\sigma_x$ (%)	τ_{xy} (psi)	$\Delta\tau_{xy}$ (%)	σ_{max} (psi)	$\Delta\sigma_{max}$ (%)	Angle (deg.)
C7	(3,10,10,3) (5,4,5)	3	1497.2	-	639.2	-	753.6	-	1935.3	-	30.2
C6	(5,10,10,5) (5,4,5)	5	1495.8	-0.09	636.9	-0.36	751.9	-0.23	1932.3	-0.16	30.1
C5	(8,10,10,8) (5,4,5)	8	1495.2	-0.04	636.3	-0.09	751.4	-0.07	1931.2	-0.06	30.1
C1	(10,10,10,10) (5,4,5)	10	1495.0	-0.01	636.1	-0.03	751.3	-0.01	1930.9	-0.02	30.1
C4	(12,10,10,12) (5,4,5)	12	1495.0	0.00	636.0	-0.02	751.2	-0.01	1930.8	-0.01	30.0

Table 6.5 The Influence of NE_b, the Number of Elements in the Axial Direction in Half the Joint Length, on Adhesive Stresses.

Case No.	Element Config.	NE_b	Peel Stress		Axial Stress		Shear Stress		Maximum Principal Stress		
			σ_y (psi)	$\Delta\sigma_y$ (%)	σ_x (psi)	$\Delta\sigma_x$ (%)	τ_{xy} (psi)	$\Delta\tau_{xy}$ (%)	σ_{max} (psi)	$\Delta\sigma_{max}$ (%)	Angle (deg.)
B4	(5,5,5,5) (5,4,5)	5	1311.5	-	591.7	-	718.9	-	1755.6	-	31.7
C7	(5,10,10,5) (5,4,5)	10	1497.2	14.16	639.2	8.03	753.6	4.83	1935.3	10.24	30.2
C8	(5,15,15,5) (5,4,5)	15	1524.9	1.85	644.4	0.81	757.2	0.48	1960.6	1.31	29.9
C9	(5,20,20,5) (5,4,5)	20	1531.8	0.45	646.1	0.26	758.2	0.13	1967.0	0.33	29.9
C10	(5,25,25,5) (5,4,5)	25	1533.4	0.10	646.3	0.03	758.2	0.00	1968.2	0.06	29.8
D1*	(5,25,10,3) (5,4,5)	-	1302.7	-15.0	561.0	-13.2	676.4	-12.0	1703.2	-13.5	30.6

*Case No. D1 only, had less elements in the right hand adherend and half joint length than in the left.

from one joint edge (the left edge, for example) would, due to St. Venant's Principle, maybe have negligible effect on the stresses at that joint edge. If this were so, a great saving on number of elements (and computer time) could be made. However, as can be seen from Cases C10 to D1 in Table 6.5, this does not appear to be the case. It is therefore advisable to model the antisymmetric structure with an antisymmetric finite element discretization.

6.3 Linear Elastic Analysis with an Improved Mesh

Considering the results obtained from the foregoing analysis, a finite element discretization was chosen such that an increase in the number of elements in any section by 25% is estimated to cause a change in any stress in the adhesive layer of less than 0.2%. The element configuration as defined in Figure 6.5 is given by

$$\begin{matrix}(a,b,c,d)\\(e,f,g)\end{matrix} = \begin{matrix}(5,20,20,5)\\(10,10,10)\end{matrix}$$

The mesh plot for this configuration is shown in Figure 6.6. The geometry and loading conditions were chosen to remain the same as defined in Figures 6.1 and 6.5 for the foregoing analysis, respectively. Linear elastic material properties were assumed for this investigation, which also remained as given in Table 6.1, with the adhesive treated as an isotropic material.

Distributions for peel, axial, shear and principal stresses in the interface layer are given in Figures 6.7 to 6.10, respectively. All variables are non-dimensionalized as indicated, and the end stress, p = 1600 psi, was chosen to be low enough so that the peak stresses do

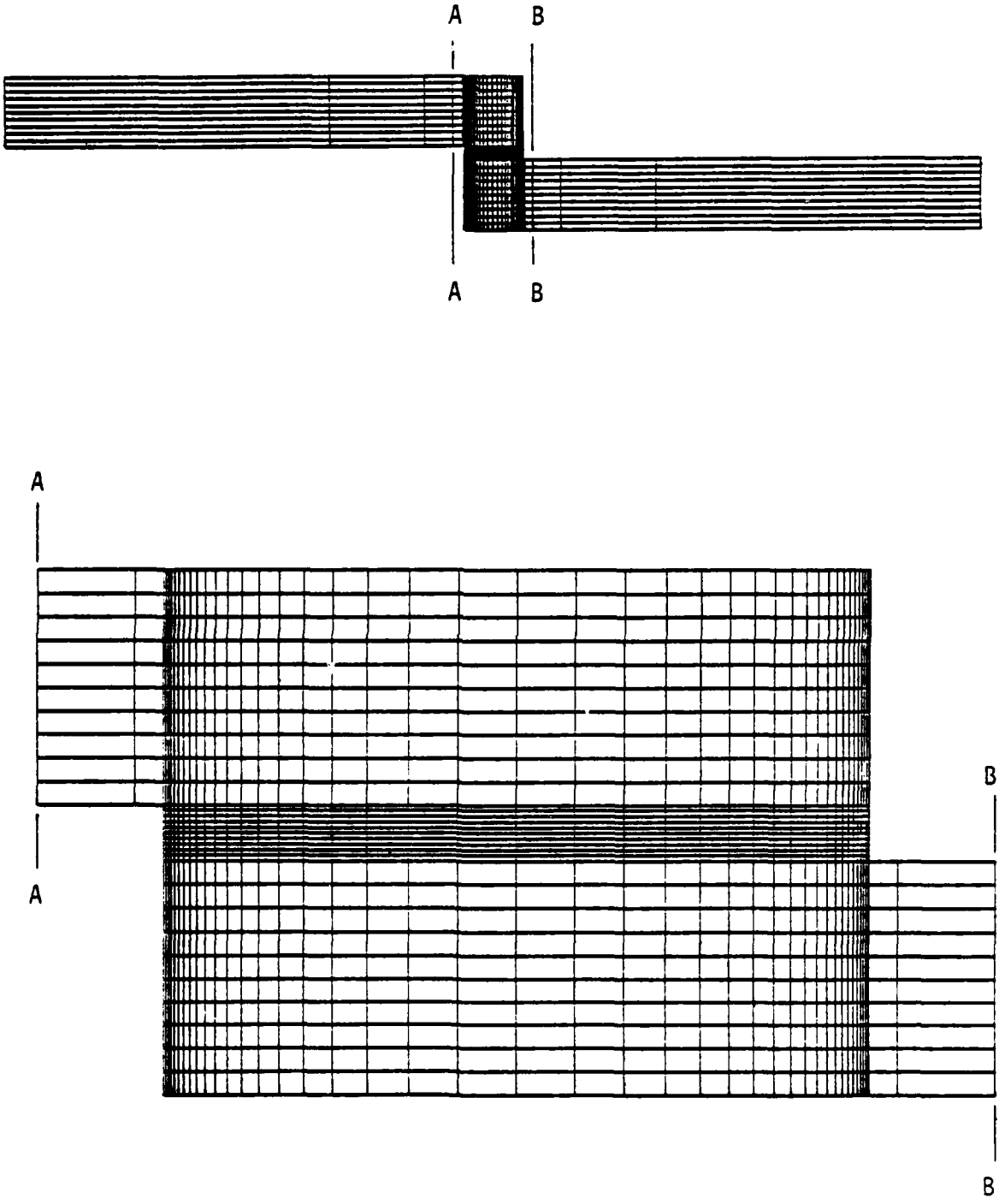

Figure 6.6 Improved Finite Element Mesh Configuration Used for the Single Lap Joint Analysis.

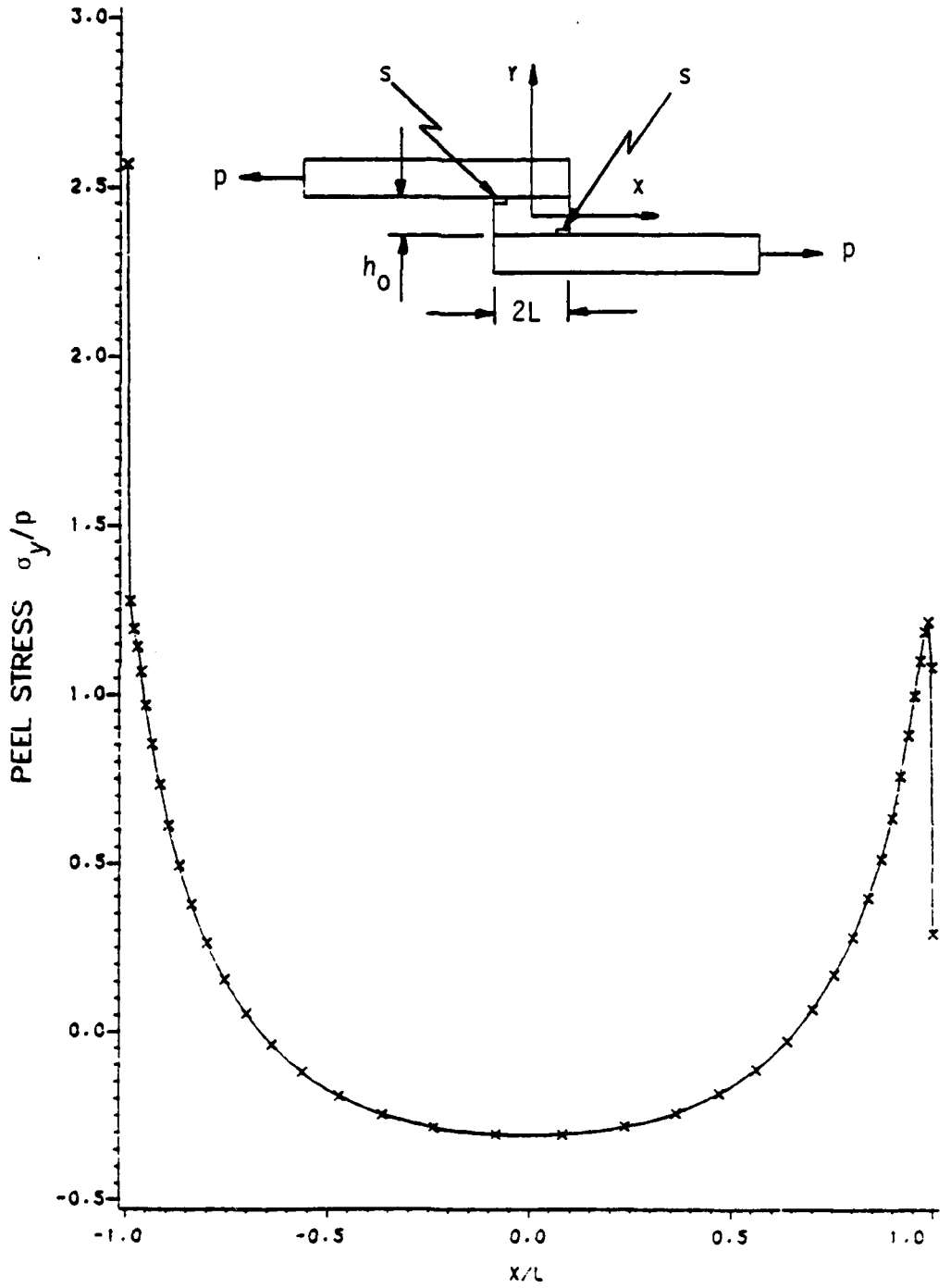

FIGURE 6.7 ADHESIVE PEEL STRESS AT THE INTERFACE ($Y=H_o/2$) OF THE SINGLE LAP JOINT

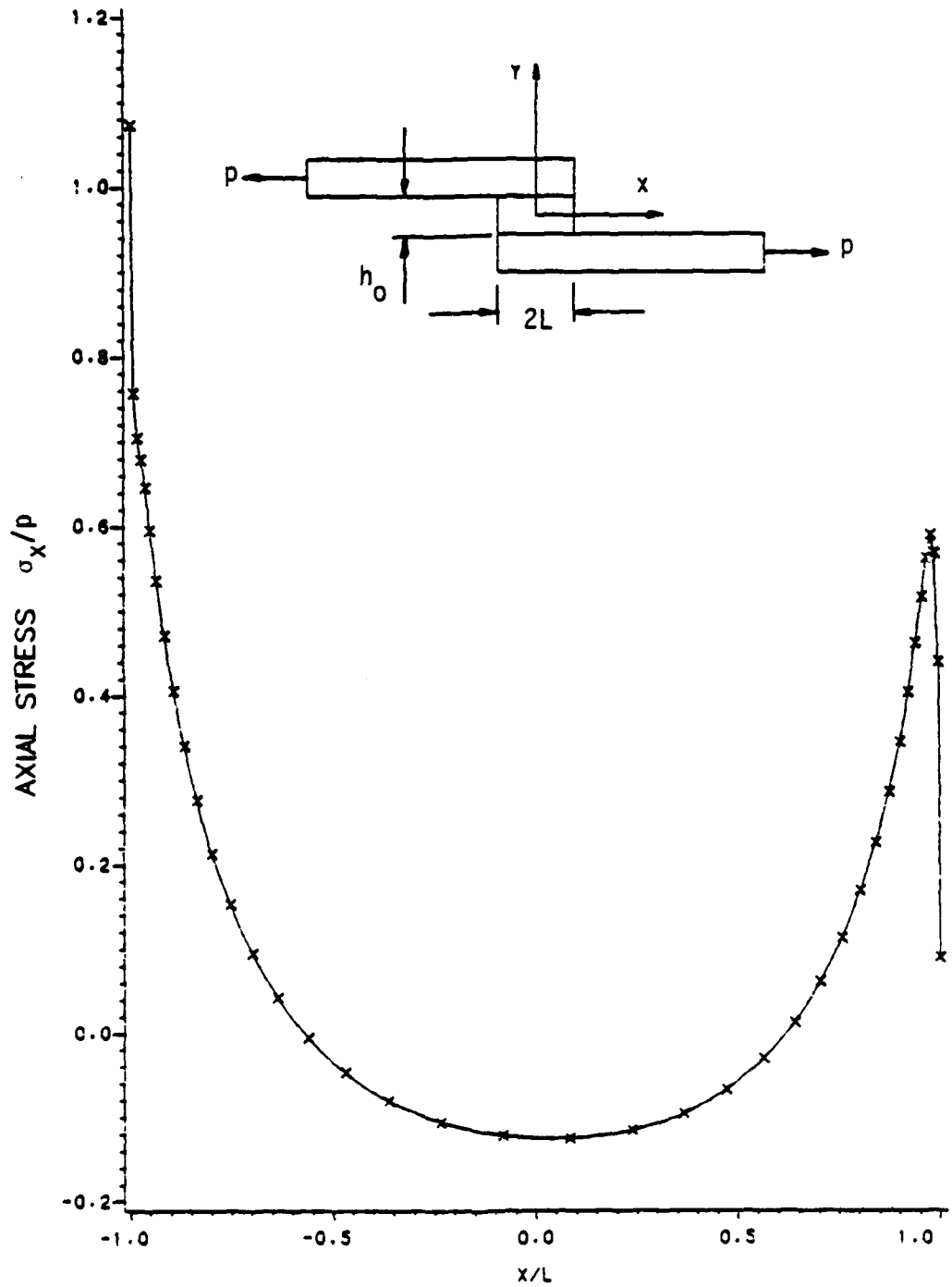

FIGURE 6.8 ADHESIVE AXIAL STRESS AT THE INTERFACE ($Y=H_o/2$) OF THE SINGLE LAP JOINT

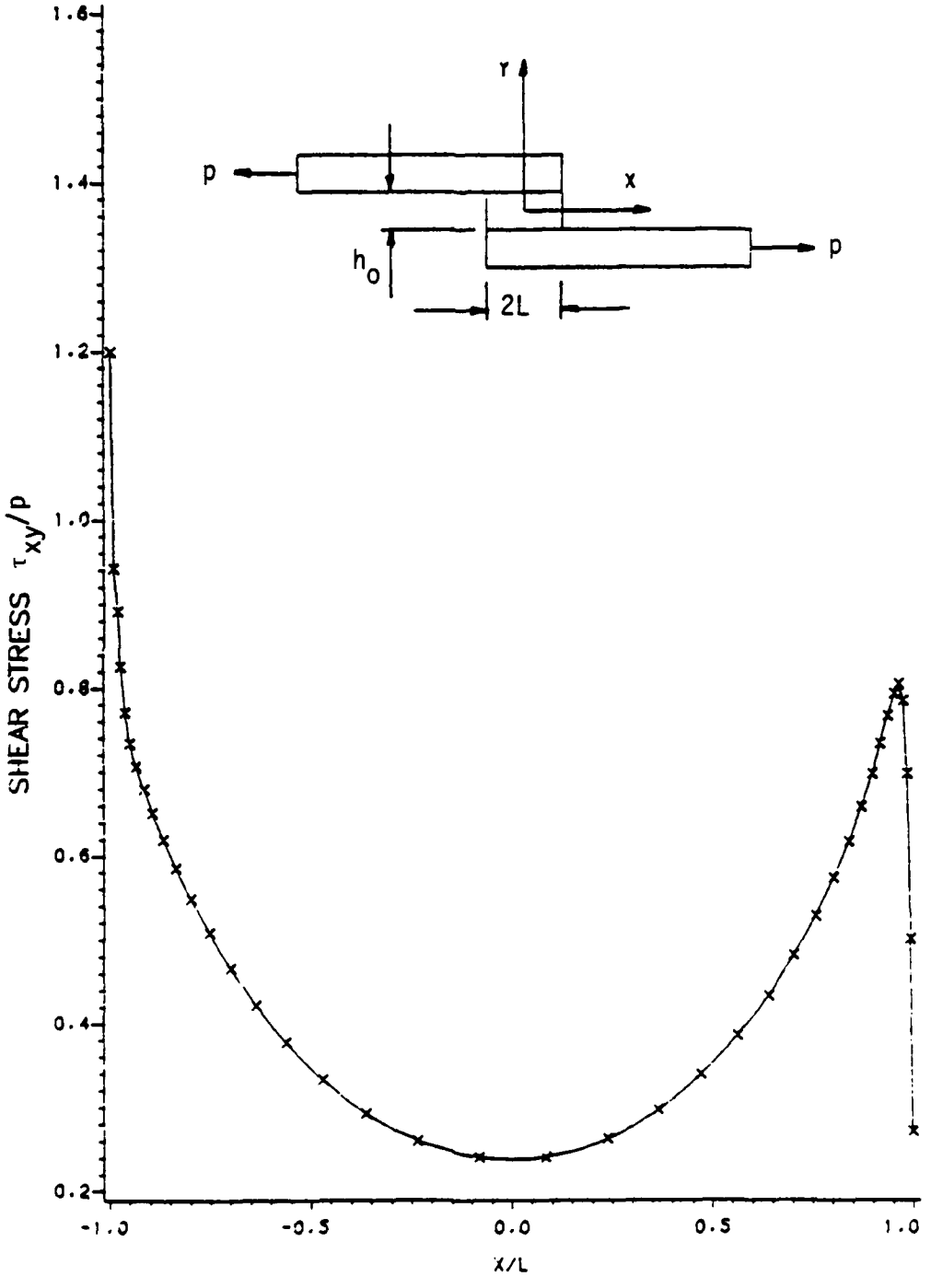

FIGURE 6.9 ADHESIVE SHEAR STRESS AT THE INTERFACE ($Y=H_o/2$) OF THE SINGLE LAP JOINT

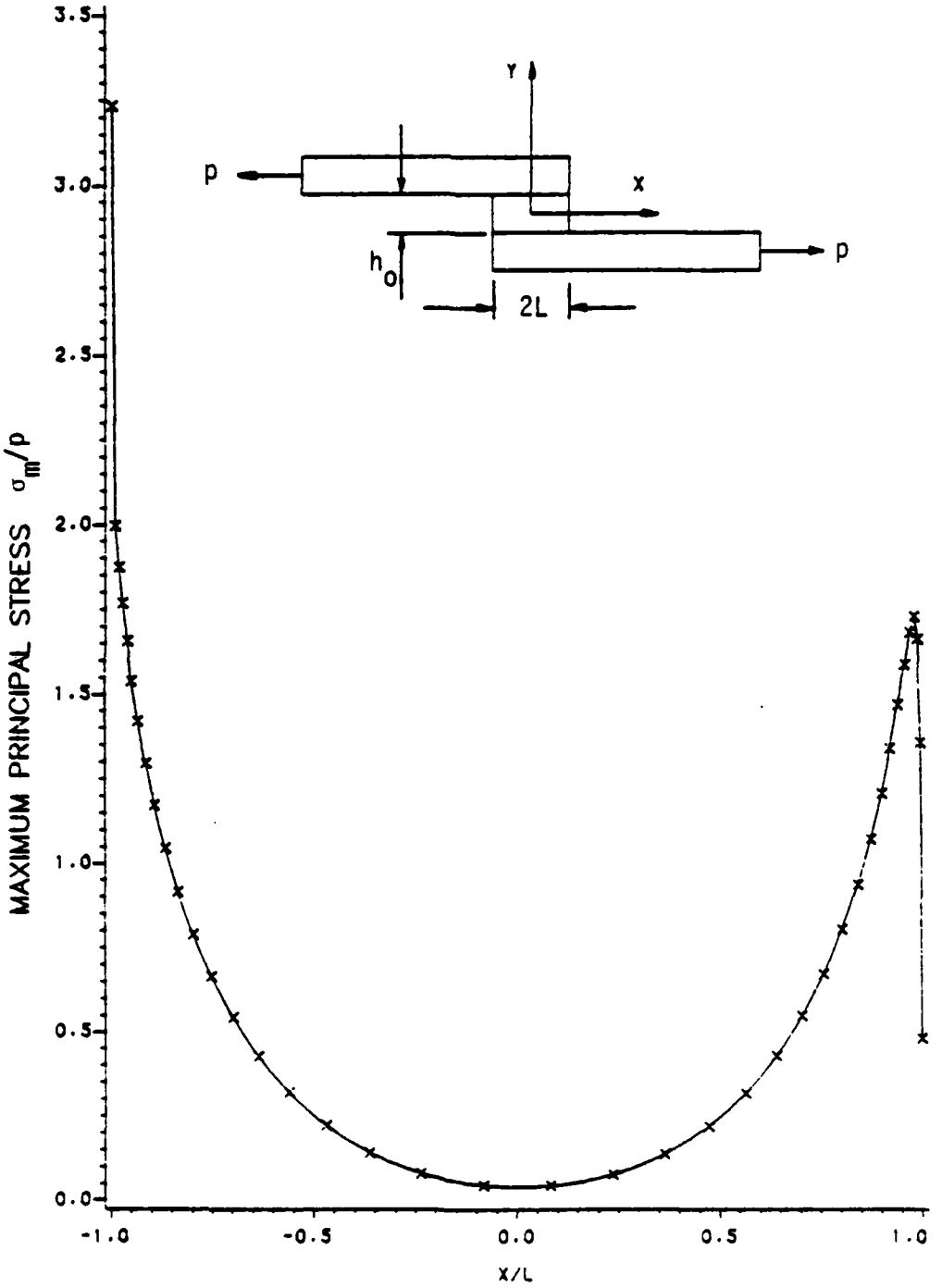

FIGURE 6.10 ADHESIVE MAXIMUM PRINCIPAL STRESS AT THE INTERFACE ($Y=H_o/2$) OF THE SINGLE LAP JOINT

not enter far into the material non-linear range. These peak stresses at the extreme left-hand side of Figures 6.7 to 6.10 are representative of the stress singularities at the positions marked "s" on Figure 6.7, which are due to the geometric discontinuities at that region.

There is another source of error in the stresses, not only in proximity to the stress singularities, but also close to any free edge with high stress gradients. Consider Figure 6.11 which shows a free body diagram of an element adjacent to the free edge in the adhesive. Since we are dealing with constant stress finite elements, the boundary loads of the element shown are constant, and it can be seen that these loads cannot place the element in equilibrium, due to the free edge, free of normal and shear stresses. If the stress gradients are high, which in this case they are, the imbalance is severe, and the resulting calculated stresses are inaccurate. In the real material, element boundary loads are not uniformly distributed along the element boundaries as they are assumed to be in Figure 6.11 and in the finite element analysis, and in this manner such an element would be held in equilibrium and stresses would no longer be inaccurate. With the use of higher order finite elements, however, boundary conditions can be satisfied exactly and this source of error will be greatly reduced.

From the distribution of stress in Figure 6.9 in the vicinity of $x/L = -1$, it is noticed that the shear stress tends to reach a peak value close to the joint edge. From the fifth element away from the left-hand edge and closer, however, the stress gradient suddenly increases at a steeper rate, indicating that these values are inaccurate due to the reasons discussed above. The same phenomenon occurs in

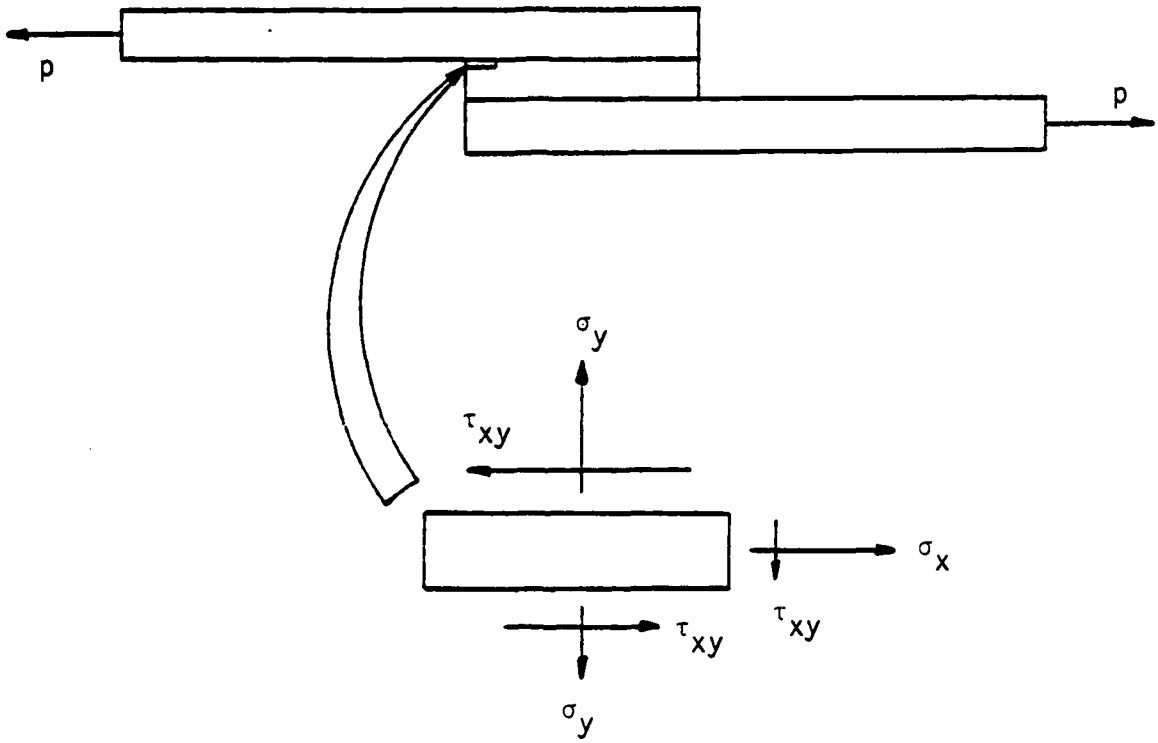

Figure 6.11 Stresses Caused by Edge Loads on an Element Adjacent to the Joint Edge.

Figures 6.7, 6.8 and 6.10, but there only in the two elements closest to the edge, x/L = -1. In the rest of this study, therefore, unless otherwise stated, when stresses or strains at the joint edge are produced or discussed, those stresses in the two columns of elements closest to both joint edges are ignored or omitted, and results in the elements third from the edges will be implied. Also, when stresses or strains at the interface between the adhesive and the adherends are discussed, the results in the interface layer elements are implied. The non-symmetry of stress distributions about the line x/L = 0 is due to the difference in stresses between the upper and lower interfaces.

From Figures 6.8 and 6.9, the finite element method also indicates that the axial and shear stresses tend to drop to zero at the free edge, x/L = 1, due to the zero normal and shear stress boundary conditions at free edges. Note, however, that the peel stress need not be zero at the joint edges, even though Figure 6.7 indicates it to be nearly so in the element adjacent to the edge, x/L = 1. The normal (peel) stress on the upper surface of the top adherend is zero everywhere due to the zero normal stress boundary condition, and this stress remains approximately zero all the way through the adherend close to the right-hand free edge. This is the reason for the adhesive peel stress (and hence also the maximum principal stress since other stresses are zero) to be very low in the element adjacent to the free edge, at $(x,y) = (L,h_o/2)$.

The variation of stresses through the adhesive thickness is shown in Figures 6.12 to 6.15 for peel, axial, shear and maximum principal stress respectively. The variation of stresses are shown at

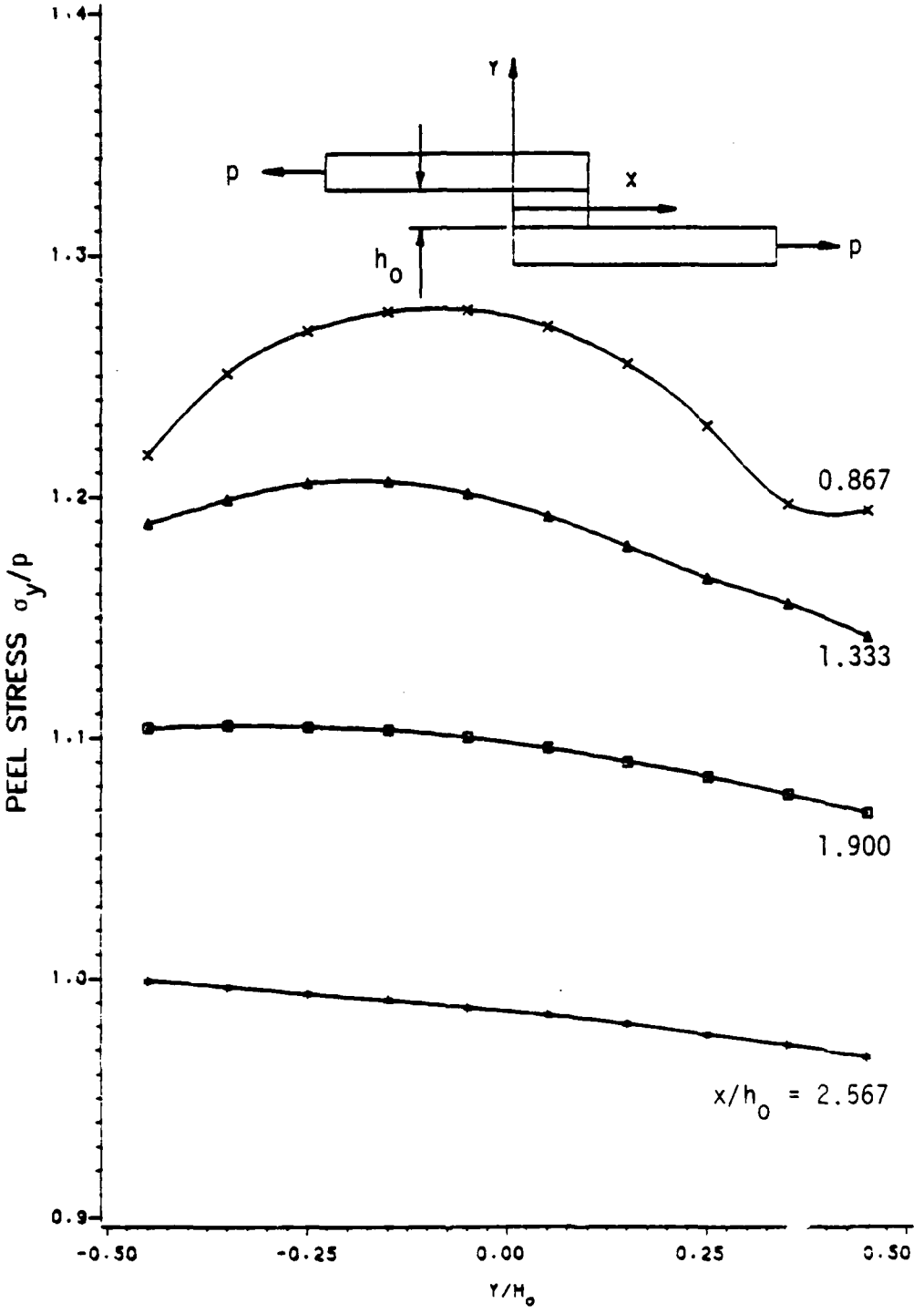

FIGURE 6.12 VARIATION OF PEEL STRESS THROUGH THE ADHESIVE THICKNESS AS A FUNCTION OF THE AXIAL POSITION IN THE SINGLE LAP JOINT

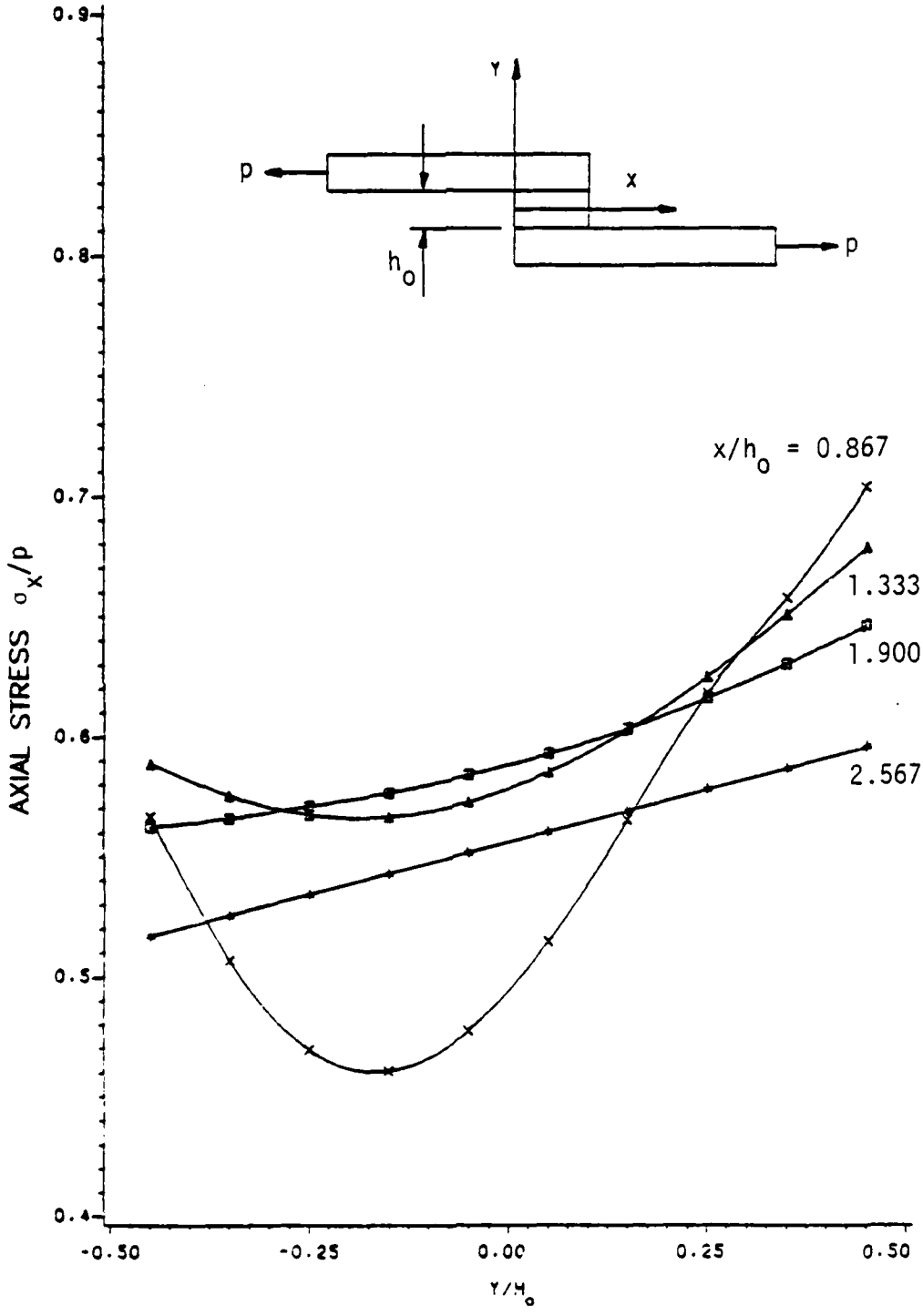

FIGURE 5.13 VARIATION OF AXIAL STRESS THROUGH THE ADHESIVE THICKNESS AS A FUNCTION OF THE AXIAL POSITION IN THE SINGLE LAP JOINT

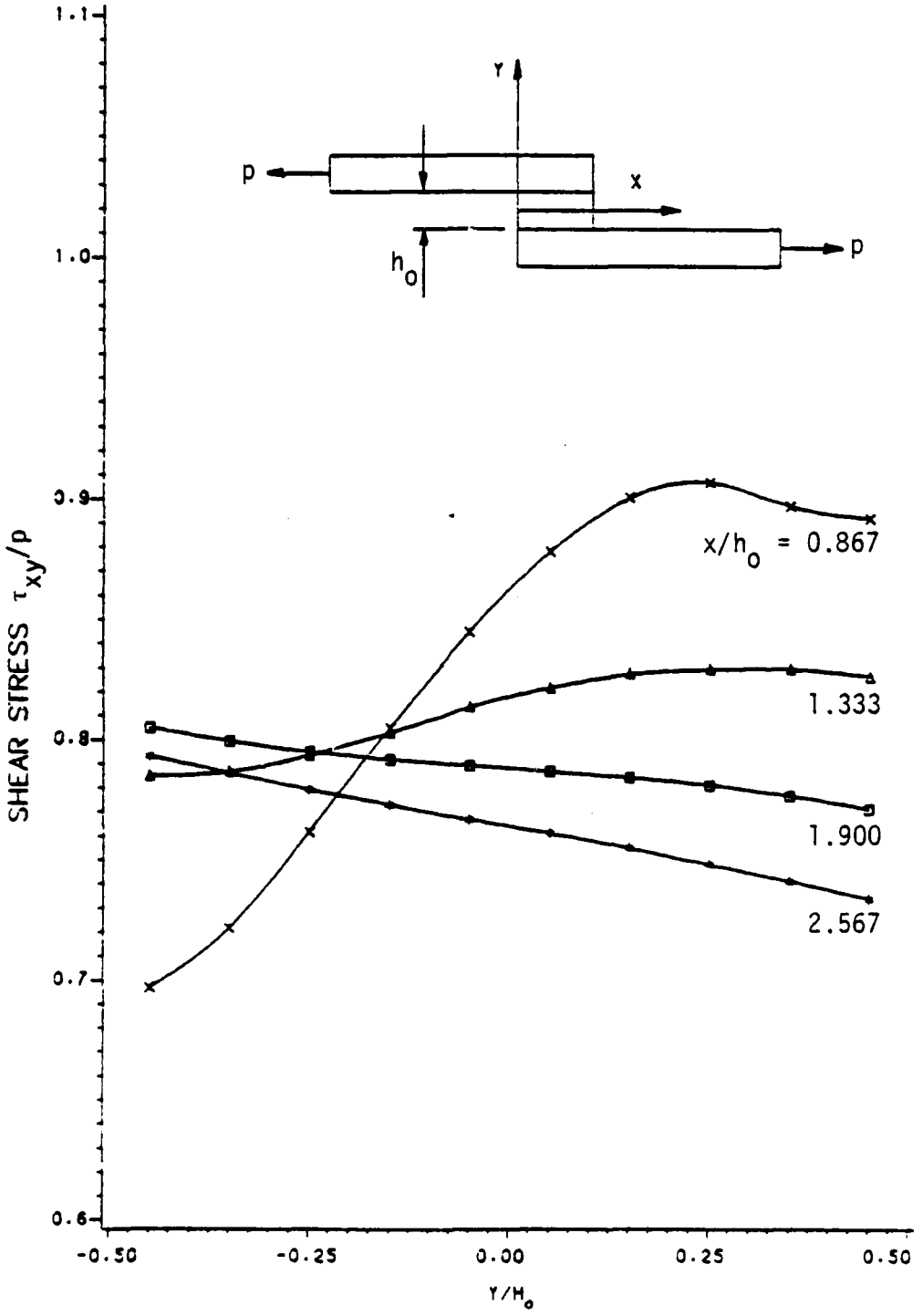

FIGURE 6.14 VARIATION OF SHEAR STRESS THROUGH THE ADHESIVE THICKNESS AS A FUNCTION OF THE AXIAL POSITION IN THE SINGLE LAP JOINT

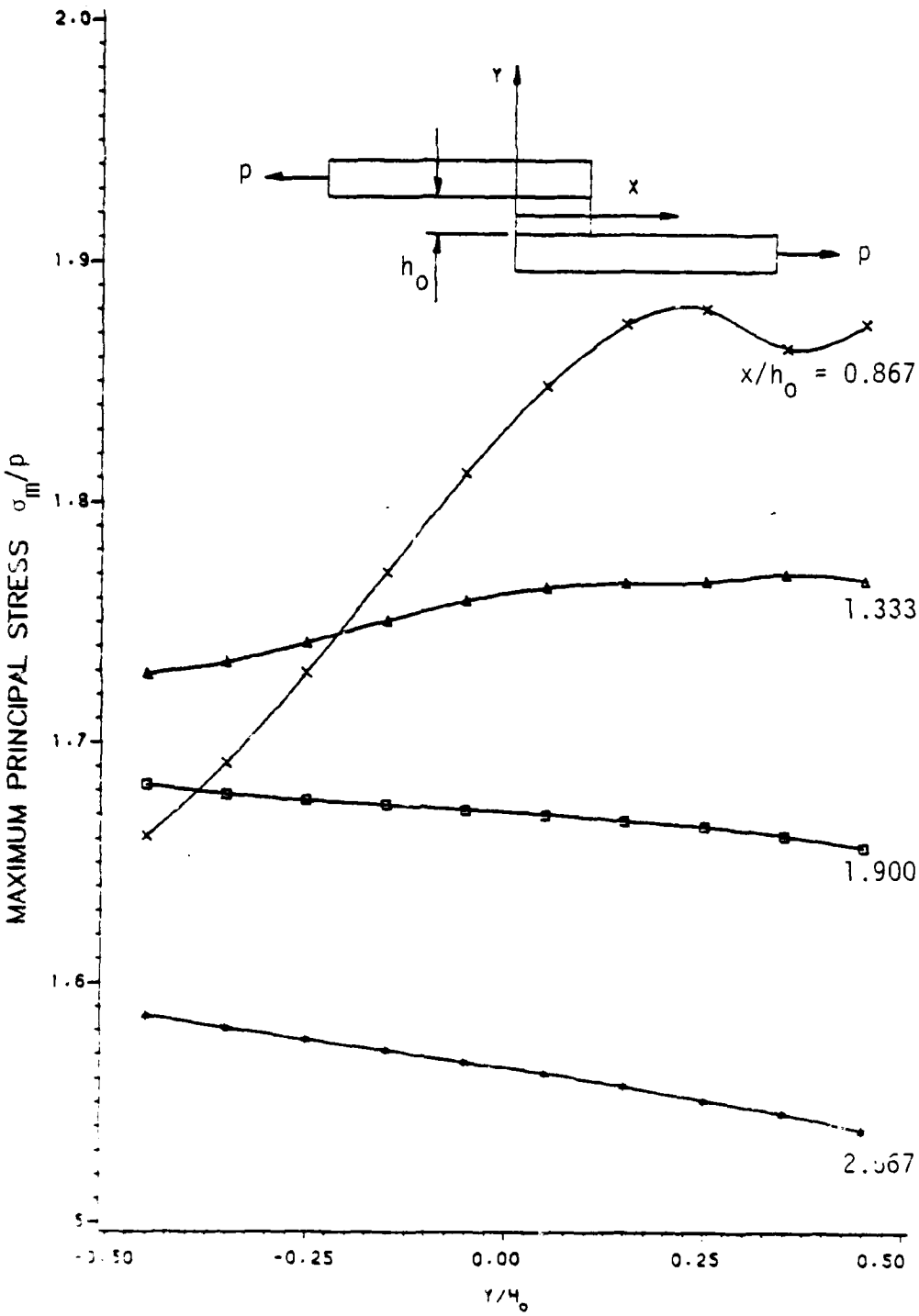

FIG. 5 VARIATION OF MAXIMUM PRINCIPAL STRESS THROUGH THE ADHESIVE THICKNESS AS A FUNCTION OF THE AXIAL POSITION IN THE SINGLE LAP JOINT

four locations along the axial direction of the joint, which coincide with the third to sixth element centroids from the left-hand joint edge, $x = 0$.

At first glance, the variation of stresses through the adhesive thickness does not appear to be significant. However, due to the small thickness of the adhesive layer (0.003 inches), the peak stress gradients (change in stress per unit distance) are 2.0, 8.7, 2.7 and 1.9 times higher in the thickness direction than in axial direction for peel, axial, shear and maximum principal stresses, respectively. It is also noticed from Figures 6.12 to 6.15 that the transverse stress gradients are highest at the joint edges and that in these regions they are least uniform. Just a short distance away from the edges ($x \approx 2\ h_o$), however, the transverse stress gradients reduce significantly and also become uniform through the adhesive thickness.

The positions of maximum stress are also found from Figures 6.12 to 6.15 and are of interest for establishing failure criteria. The peak peel stress, being about 40% higher than the peak shear stress, occurs at $y/h_o = -0.075$, not far from the center of bond (Figure 6.12). It is important to note, however, that the maximum principal stress has a peak value of 47% higher than that of the peel stress and occurs at about $y/h_o = 0.2$ (Figure 6.15). A relative maximum value of the latter stress also occurs at the upper interface, being not much lower than the peak value. The angles of maximum principal stress are 36° and 37° respectively for the above-mentioned two peak values, measured counter-clockwise from the positive x-direction.

6.4 Viscoelastic Analysis and Comparison with Nagaraja and Alwar [19]

The geometry of the single lap joint analyzed by Nagaraja and Alwar is given in Figure 6.16. Actual dimensions were not provided in reference [19], but were chosen for the present analysis to conform with Nagaraja and Alwar's geometry ratios, inserted in the top of Figure 6.16. Nagaraja and Alwar obtained stresses at two levels which, from reference [19], appear to be at distances $h_o/12$ from the interface between the adhesive and each adherend. The geometry for the present analysis was thus chosen such that these levels would coincide with the centroid of the first element to the inside of the interface layer elements, if an interface layer thickness of 0.0003 inches and 10 elements through the thickness of the adhesive (including the interface elements) are used.

Finite element discretizations and boundary conditions for the present analysis are given in Figure 6.17. The applied load at the end of the right-hand adherend was chosen to give an average shear stress equivalent to that of Nagaraja and Alwar, if this load is divided by the shear area, or joint length. Nagaraja and Alwar employed 18-degree-of-freedom triangular elements which should give much more accurate results than the 8-degree-of-freedom quadrilateral elements of the SAAS3VP program. The number of degrees of freedom per node may be used as a guide for comparing accuracies between analyses using different kinds of elements. Since Nagaraja and Alwar's elements had 6 degrees of freedom per node and the SAAS3VP program elements 2, to obtain a comparable accuracy as that of the former, it was estimated that three times as many elements, equally spaced in

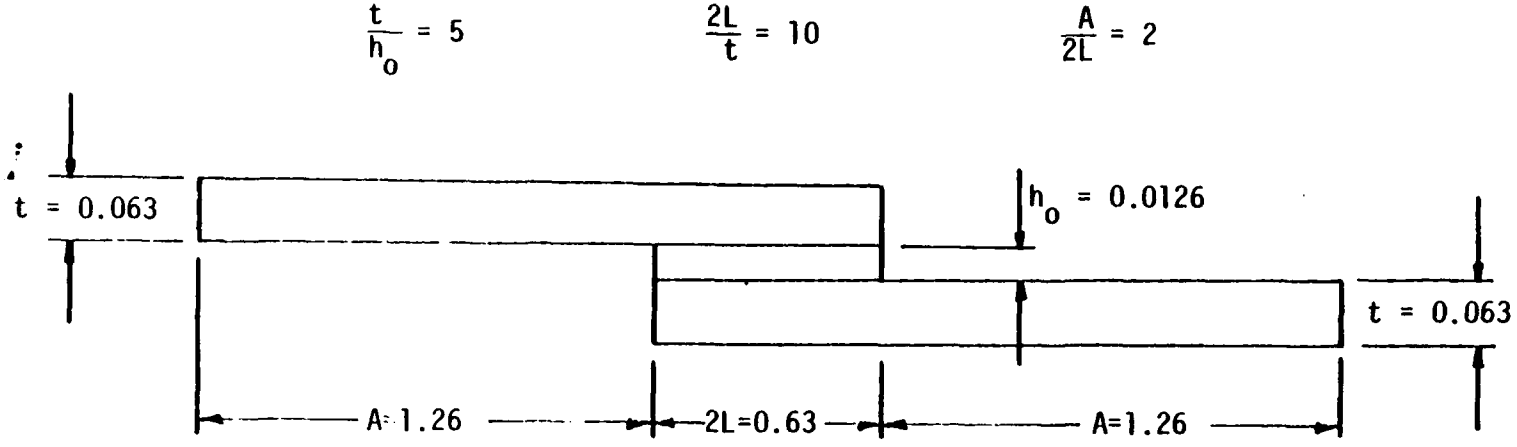

Figure 6.16 Geometry of the Single Lap Joint as Used by Nagaraja and Alwar [19]. Dimensions (in Inches) not Given in Reference 19, but Were Deduced for the Present Analysis.

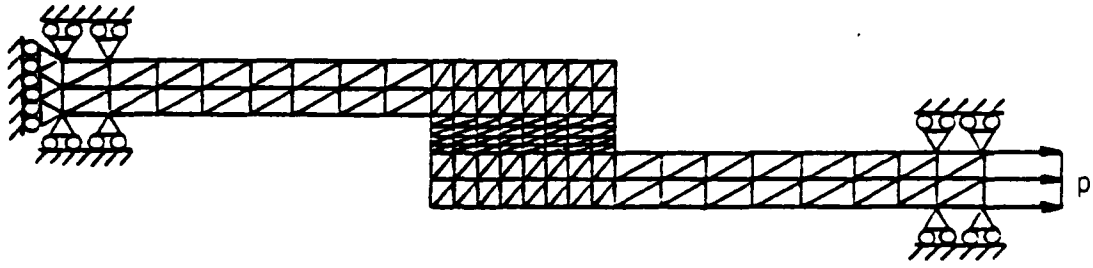

a)

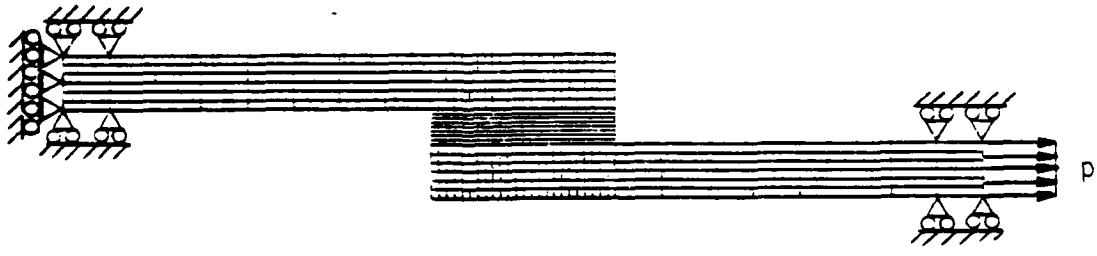

b) p = 1423 psi

Figure 6.17 Finite Element Discretizations and Boundary Conditions as Used by (a) Nagaraja and Alwar [19], and (b) in the Present Analysis for the Single Lap Joint.

each direction should be used in the present analysis. The number of elements in the axial direction in the joint section and in the thickness direction of the adherends were, therefore, taken to be three times that of Nagaraja and Alwar. Only ten elements, however, were used through the adhesive thickness and eight along the axial direction of the adherends since, as it was determined in Section 6.2, a greater number would not influence the calculated adhesive stresses significantly.

Material properties used by Nagaraja and Alwar and in the present analysis are given in Table 6.6. Nagaraja and Alwar, however, did not provide Young's modulus for the Aluminum for which the value in Table 6.6 was assumed. The relaxation moduli were determined experimentally by Nagaraja and Alwar, to which they fitted a Prony's Series for use with Schapery's direct method of transform inversion. Schapery's quasi-elastic method was used in the present analysis in which the viscoelastic material properties were assumed to be equivalent to the elastic properties for each value of time. These methods and their validity were discussed in Chapter 5.

Adhesive peel and shear stresses at a distance $h_o/12$ from the interface between the adhesive and the upper adherend for time t = 10 days are given in Figures 6.18 and 6.19 respectively, denoted by a + sign. These stresses are superimposed upon those of Nagaraja and Alwar for times t = 10, 100 and 1000 days and do not compare well with the stresses at time t = 10 days of the latter. It was therefore decided to use a refined finite element mesh, shown in Figures 6.20, which is based on the same principles that determined the mesh used

Table 6.6 Time Dependent Material Properties Used for the Single Lap Joint by Nagaraja and Alwar [19], and, for Comparison with Their Results in the Present Analysis.

		Young's Modulus E (psi)	Poisson's Ratio ν
Aluminum Adherends		10.3×10^6*	0.30
	Time (days)	Relaxation Modulus $E_r(t)$ (psi)	Poisson's Ratio ν
Araldite Adhesive	10	8.194×10^6	0.33
	100	3.073×10^6	0.33
	1000	1.138×10^6	0.33

*This value assumed

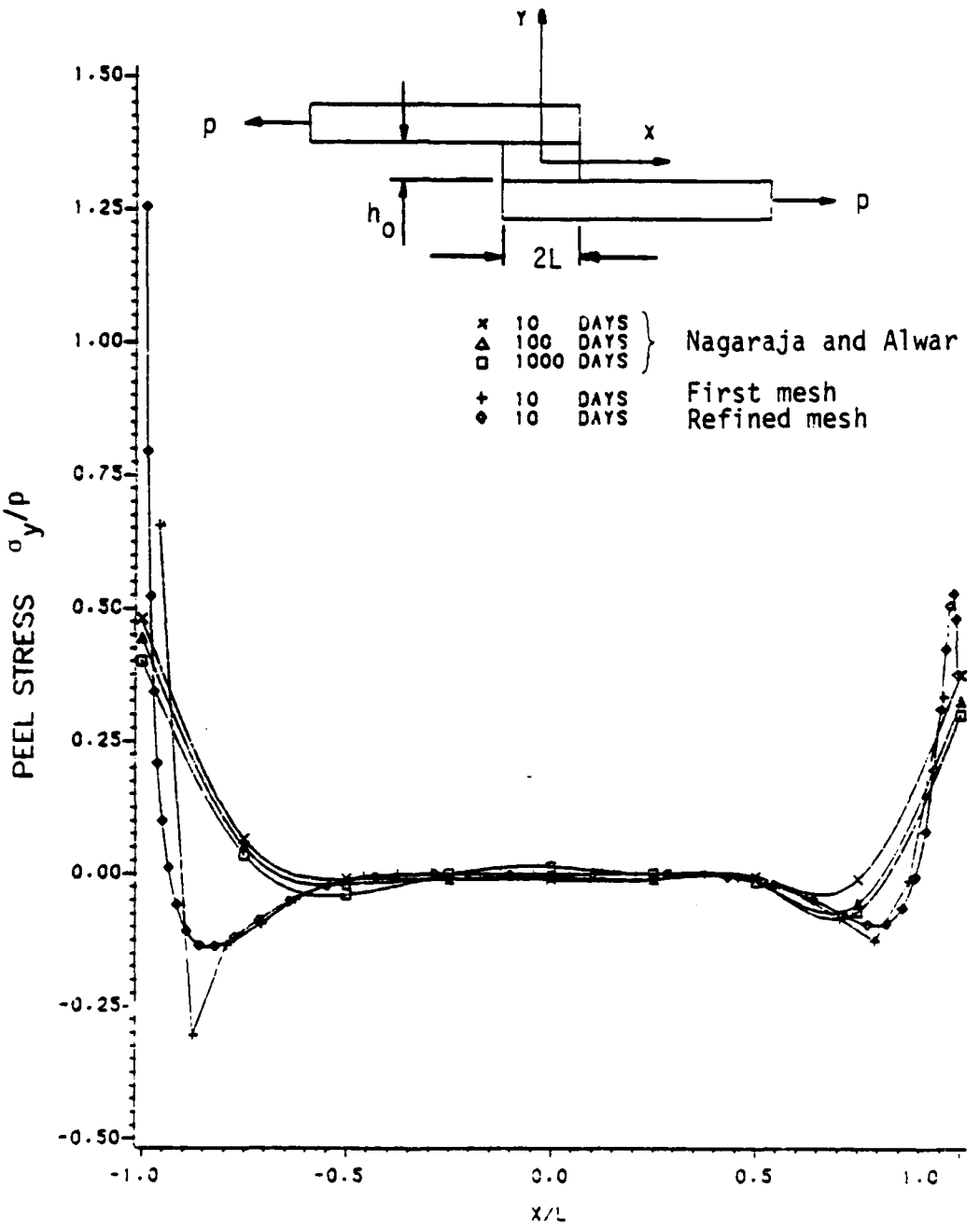

FIGURE 6.18 ADHESIVE PEEL STRESS IN THE SINGLE LAP JOINT AT $Y=H_o/12$ AND COMPARISON WITH THAT OF NAGARAJA AND ALWAR (19)

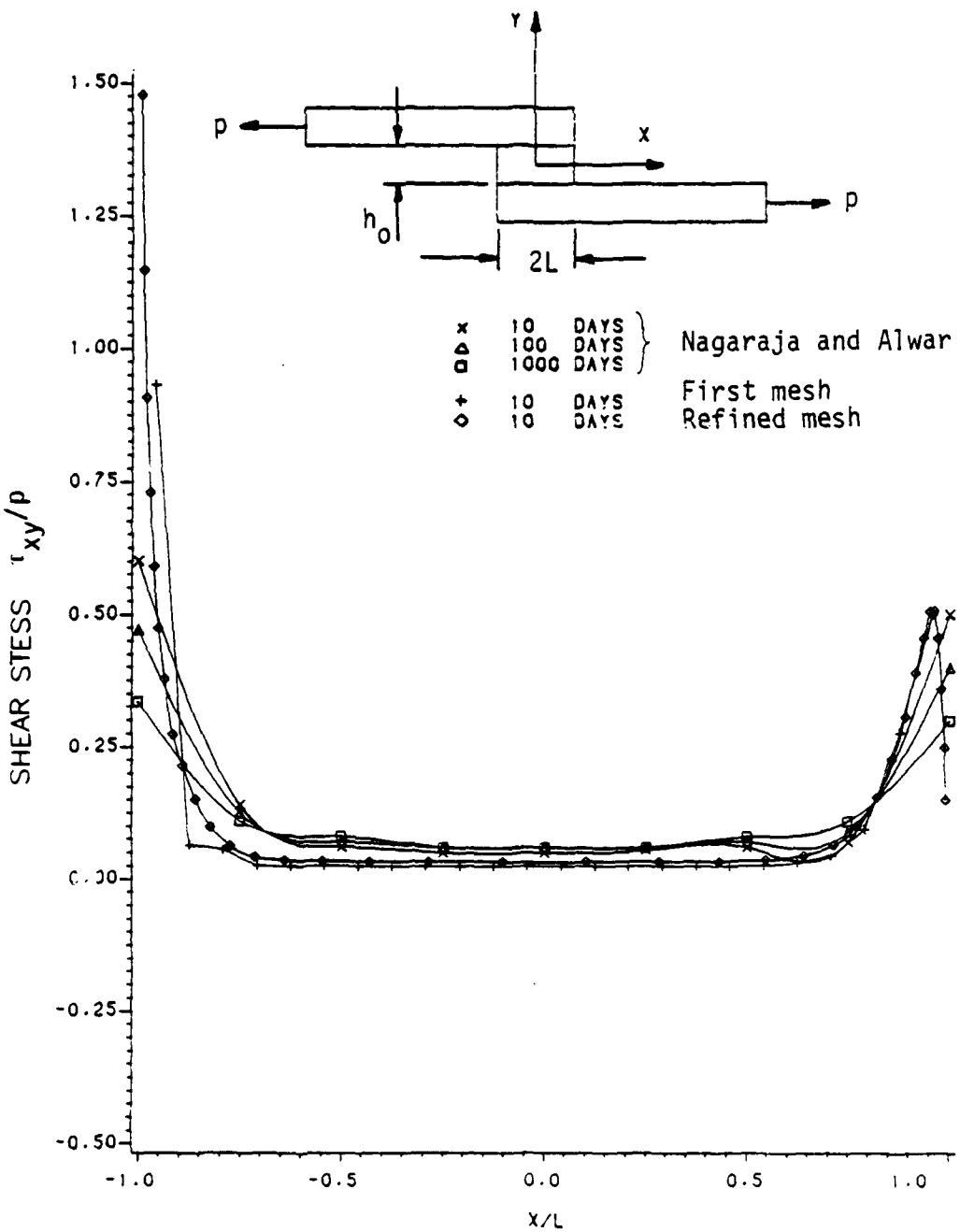

FIGURE 6.19 ADHESIVE SHEAR STRESS IN THE SINGLE LAP JOINT AT $Y=H_o/12$ AND COMPARISON WITH THAT OF NAGARAJA AND ALWAR (19)

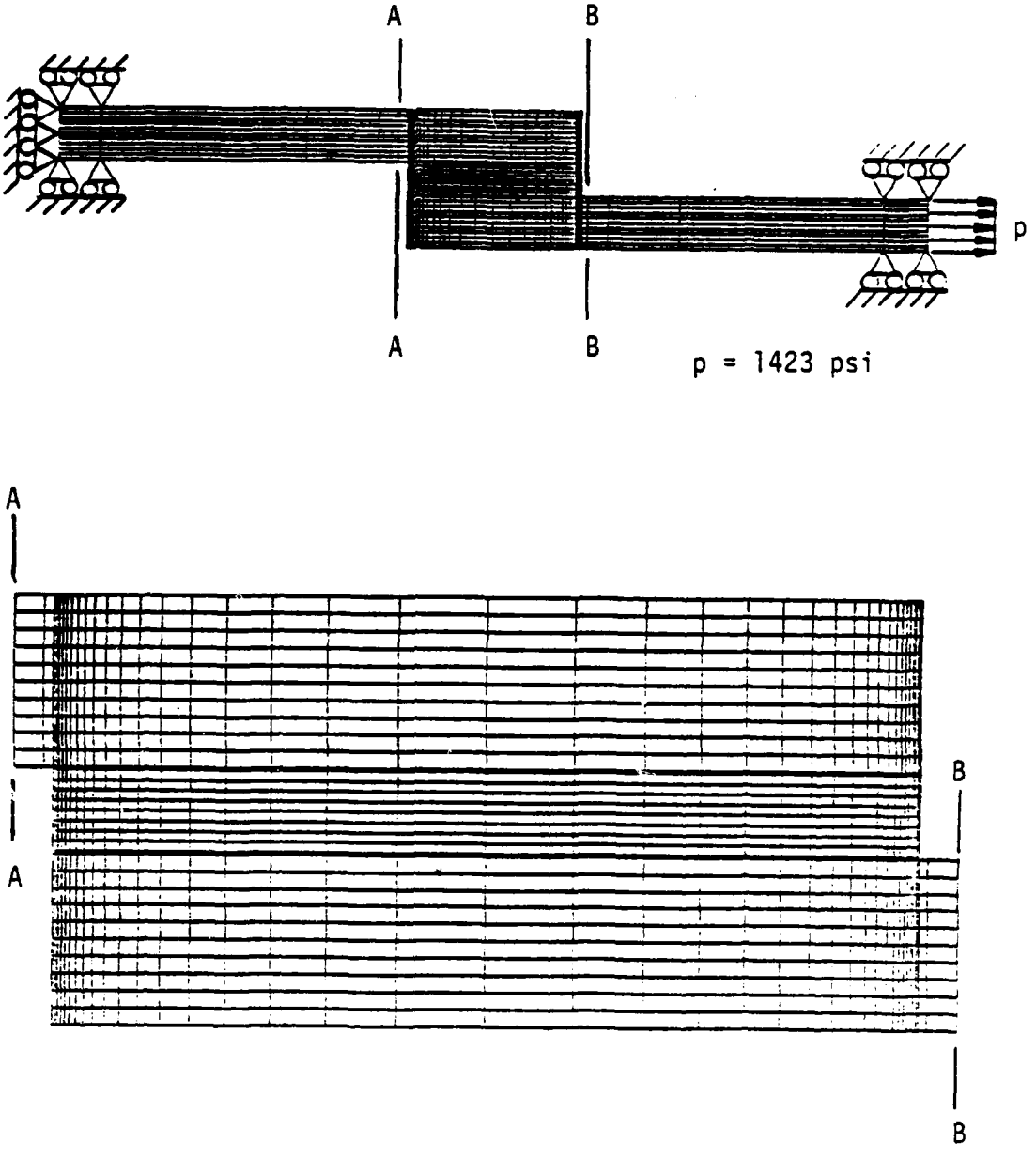

Figure 6.20 Improved Finite Element Discretization and Boundary Conditions for the Single Lap Joint and for Comparing Results with Nagaraja and Alwar [19].

for the analysis of Section 6.3. Boundary conditions are also shown in Figures 6.20, and are the same as those used by Nagaraja and Alwar. Peel and shear stresses from this analysis are also superimposed on the previously mentioned stresses in Figures 6.18 and 6.19, denoted with a ◇ sign. It is seen that the peel and shear stresses are both much higher than those of Nagaraja and Alwar in the proximity of the stress singularity on the left-hand side. Just a short distance away from the left-hand edge, much better agreement is obtained for the shear stress, but the peel stress decreases faster and to lower values than that of Nagaraja and Alwar. Close to the right-hand edge (away from a stress singularity) reasonably good agreement is obtained in the case of the shear stress but, again, not in the case of the peel stress. The shear stress for the present analysis in Figure 6.19 is seen to tend to satisfy the zero stress boundary condition on the right-hand side but that of Nagaraja and Alwar does not. The opposite is rather expected due to the higher order elements of the latter.

Nagaraja and Alwar did compare their results with those of Goland and Reissner and found good comparison for their peel stress and poor agreement for their shear stress. However, the stiffness to thickness ratios of the adherends and the adhesive of Nagaraja and Alwar do not satisfy the requirements as layed down by Goland and Reissner for the analyses to be valid, so that this comparison of Nagaraja and Alwar is not valid either.

Peel, axial, shear and maximum principal stresses for times $t = 10$, 100 and 1000 days are shown for the latter analysis mentioned above (i.e., using the improved finite element discretization), in

Figures 6.21 to 6.24, respectively. These stresses, however, are at the interface, $y = h_o/2$, and not at $y = h_o/12$ as before. Peak peel and shear stresses for time t = 10 days are therefore higher than those of Figures 6.18 and 6.19. Similar redistributions of stresses are obtained as by Nagaraja and Alwar, i.e., peak stresses reduce significantly with increasing time. The reduction in peak stresses are 46%, 73%, 57% and 62% for peel, axial, shear and maximum principal stresses, respectively. Peel and shear stresses are seen to be zero, or close to zero, over the central 50% of the joint, which indicates that the overlap region is unnecessarily long for structural purposes and the level of loading considered. The peel stress distribution of Figure 6.21 is seen to be somewhat different from that of Figure 6.7 of the previous section. This is also due to the length of the overlap region and the low level of loading in the present case.

The distributions of adhesive peel, axial, shear and maximum principal strains at the interface, for times t = 10, 100 and 1000 days, are given in Figures 6.25 to 6.28. As may be expected from a constant load test over the time span of 10 to 1000 days, peak peel, shear and maximum principal strains are found to increase tremendously (see Figures 6.25, 6.27 and 6.28). The peak axial strain increases very little although in the proximity of $x/L = \pm 0.85$, percentage increase in the axial strain is relatively high (see Figure 6.26). The peak shear strain is found to be higher than all the other strains, while the peak shear stress was found to be higher than only that of the peel stress.

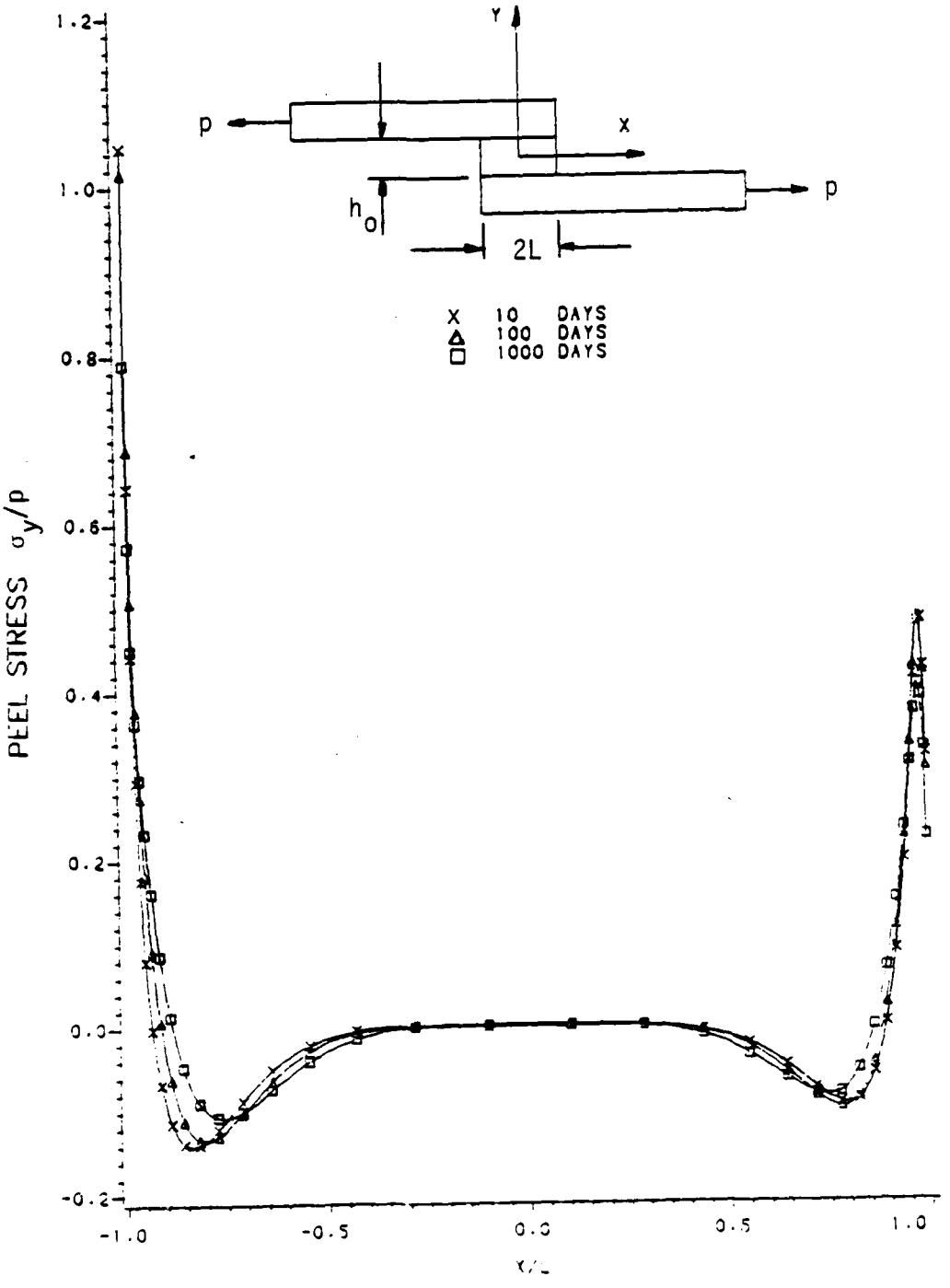

FIGURE 6.21 TIME DEPENDENCE OF ADHESIVE PEEL STRESS AT THE INTERFACE ($Y=H_o$) OF THE SINGLE LAP JOINT

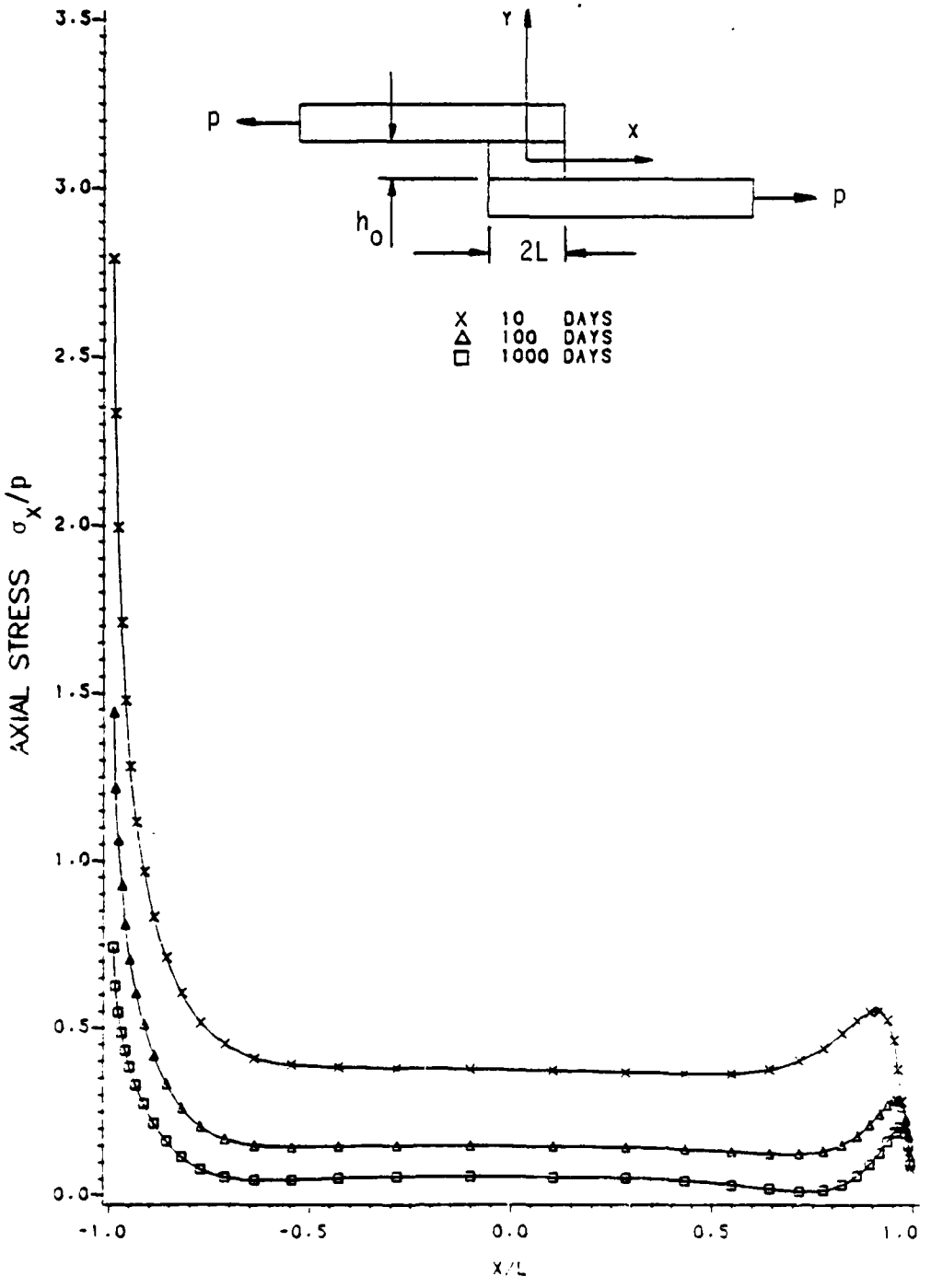

FIGURE 6.22 TIME DEPENDENCE OF ADHESIVE AXIAL STRESS AT THE INTERFACE ($Y=H_o$) OF THE SINGLE LAP JOINT

AD-A135 963 VISCOELASTIC ANALYSIS OF ADHESIVE STRESSES IN BONDED JOINTS(U) VIRGINIA POLYTECHNIC INST AND STATE UNIV BLACKSBURG DEPT OF E... L R BOTHA ET AL. MAY 83 2/2

UNCLASSIFIED VPI-E-83-17 N00014-82-K-0185 F/G 11/1 NL

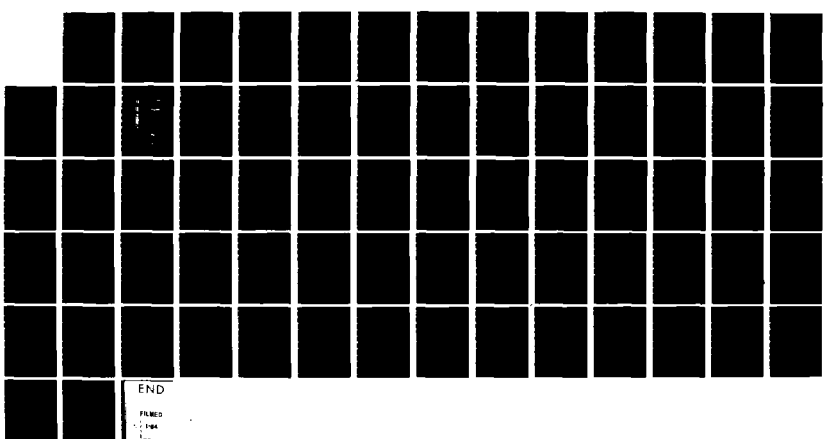

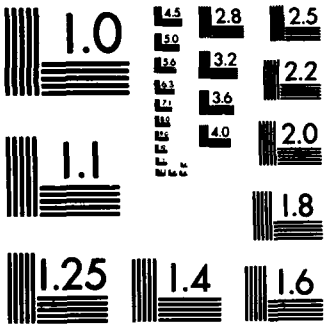

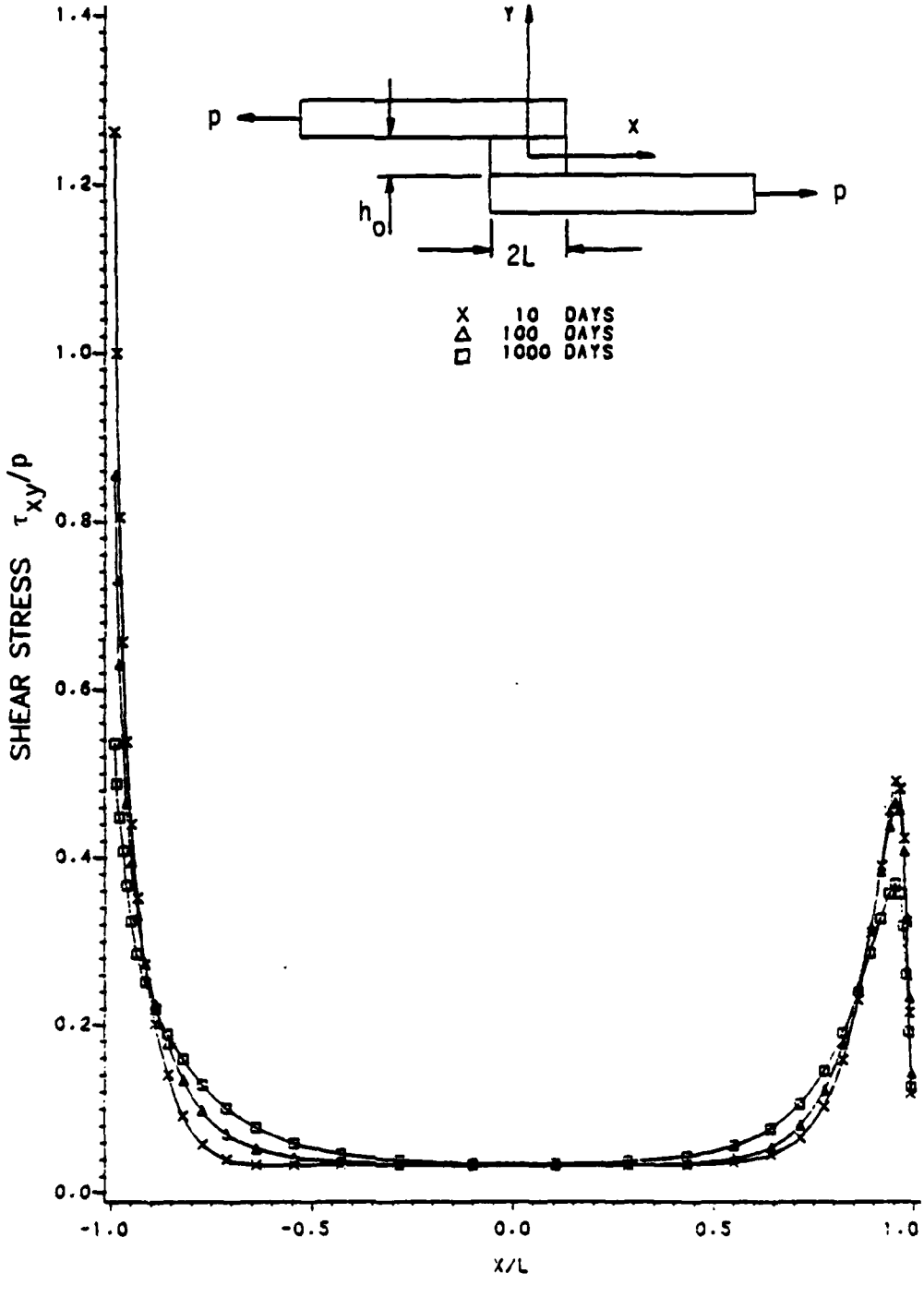

FIGURE 6.23 TIME DEPENDENCE OF ADHESIVE SHEAR STRESS AT THE INTERFACE ($Y=H_o/2$) OF THE SINGLE LAP JOINT

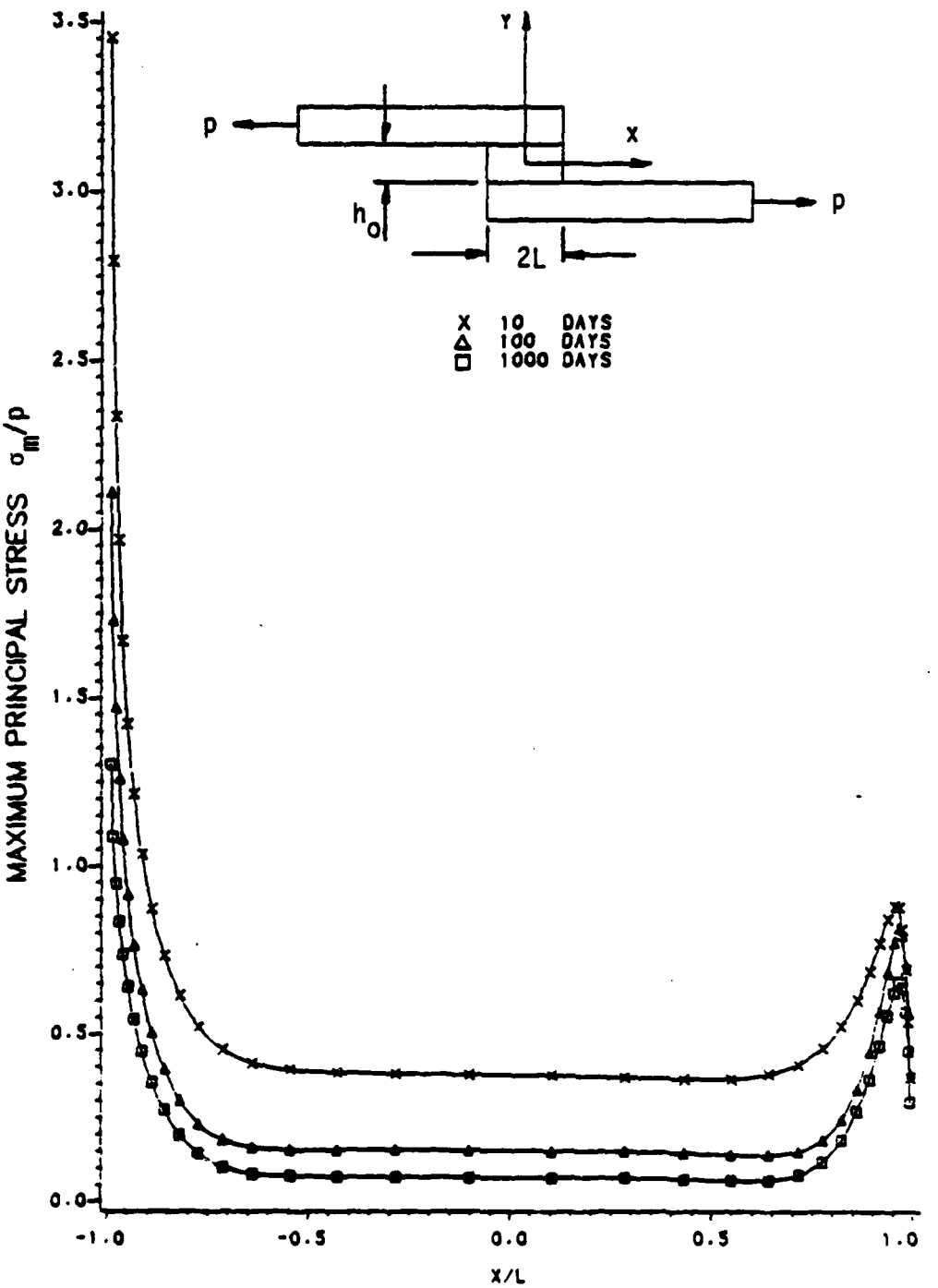

FIGURE 6.24 TIME DEPENDENCE OF ADHESIVE MAXIMUM PRINCIPAL STRESS AT THE INTERFACE ($Y=H_o/2$) OF THE SINGLE LAP JOINT

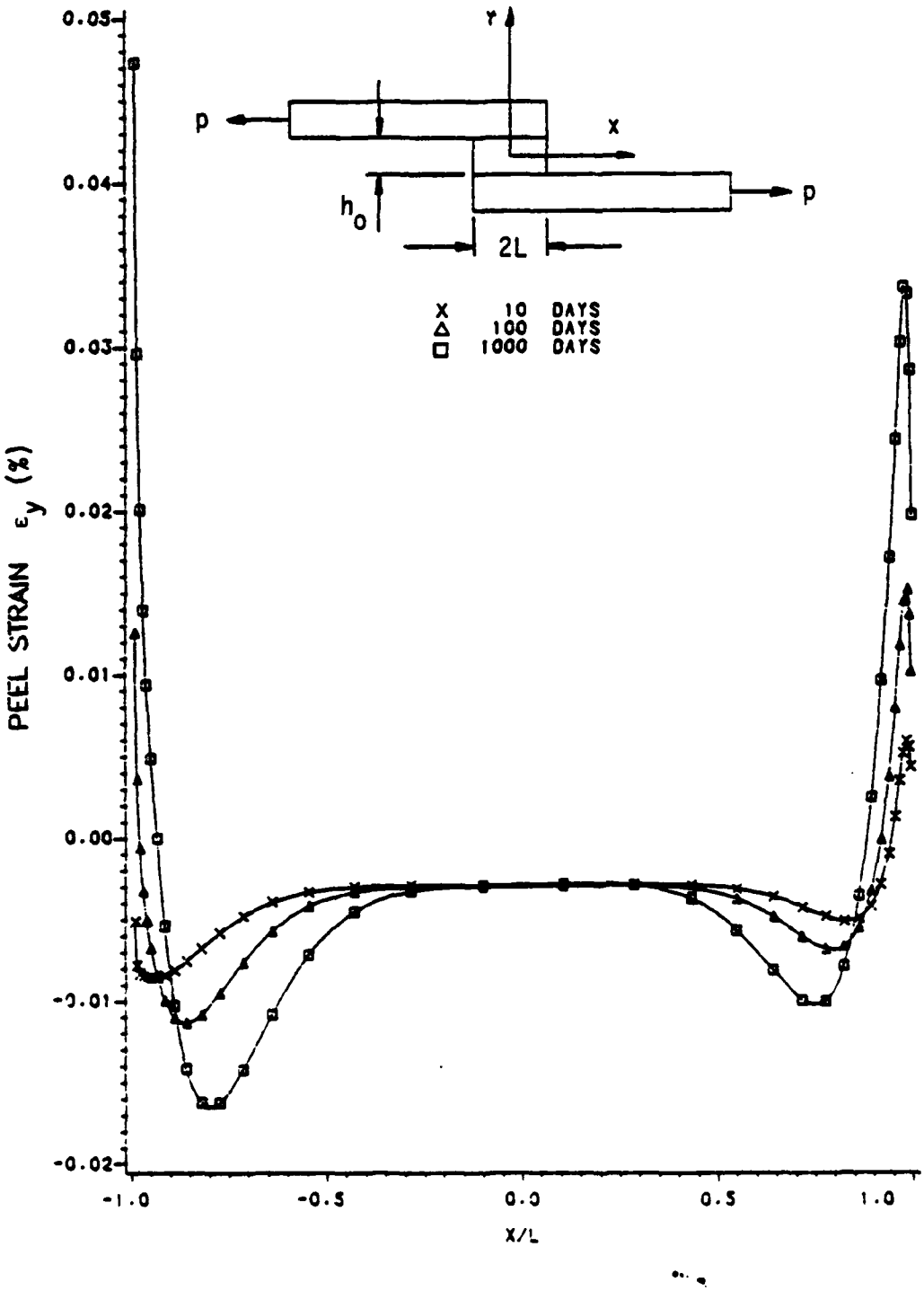

FIGURE 6.25 TIME DEPENDENCE OF ADHESIVE PEEL STRAIN AT THE INTERFACE ($Y=h_o/2$) OF THE SINGLE LAP JOINT

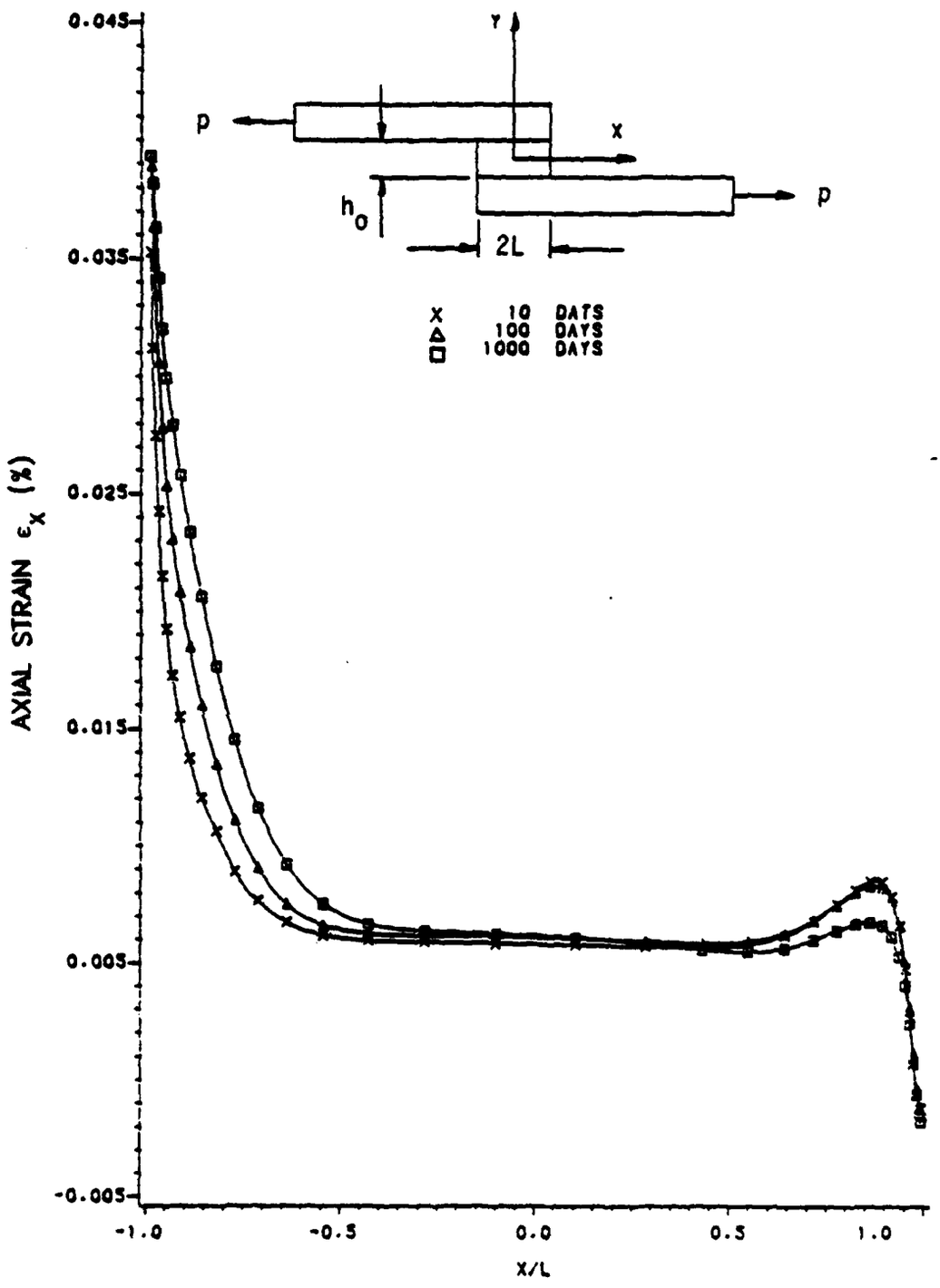

FIGURE 6.26 TIME DEPENDENCE OF ADHESIVE AXIAL STRAIN AT THE INTERFACE ($Y=H_o/2$) OF THE SINGLE LAP JOINT

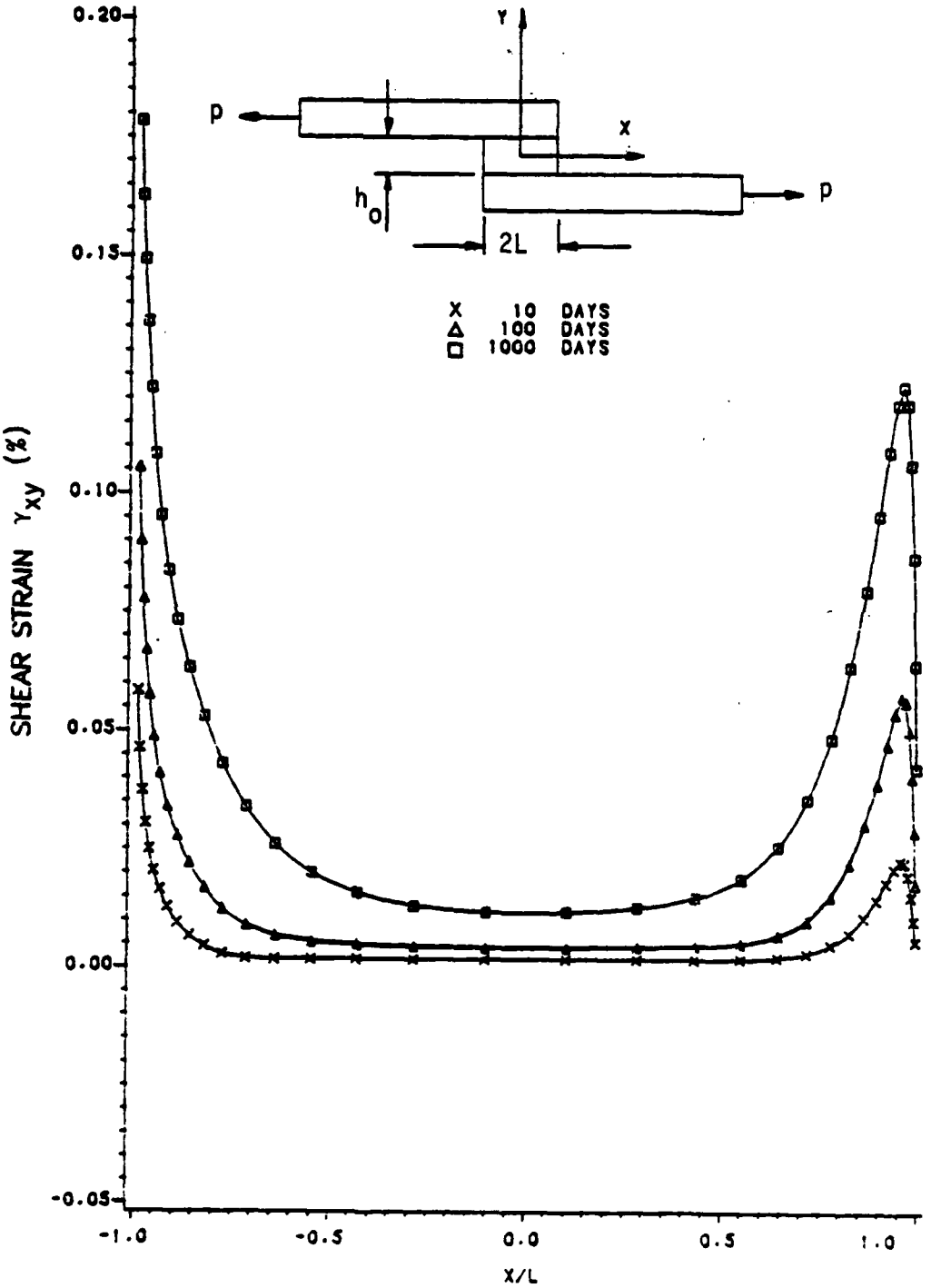

FIGURE 6.27 TIME DEPENDENCE OF ADHESIVE SHEAR STRAIN AT THE INTERFACE ($Y=H_o/2$) OF THE SINGLE LAP JOINT

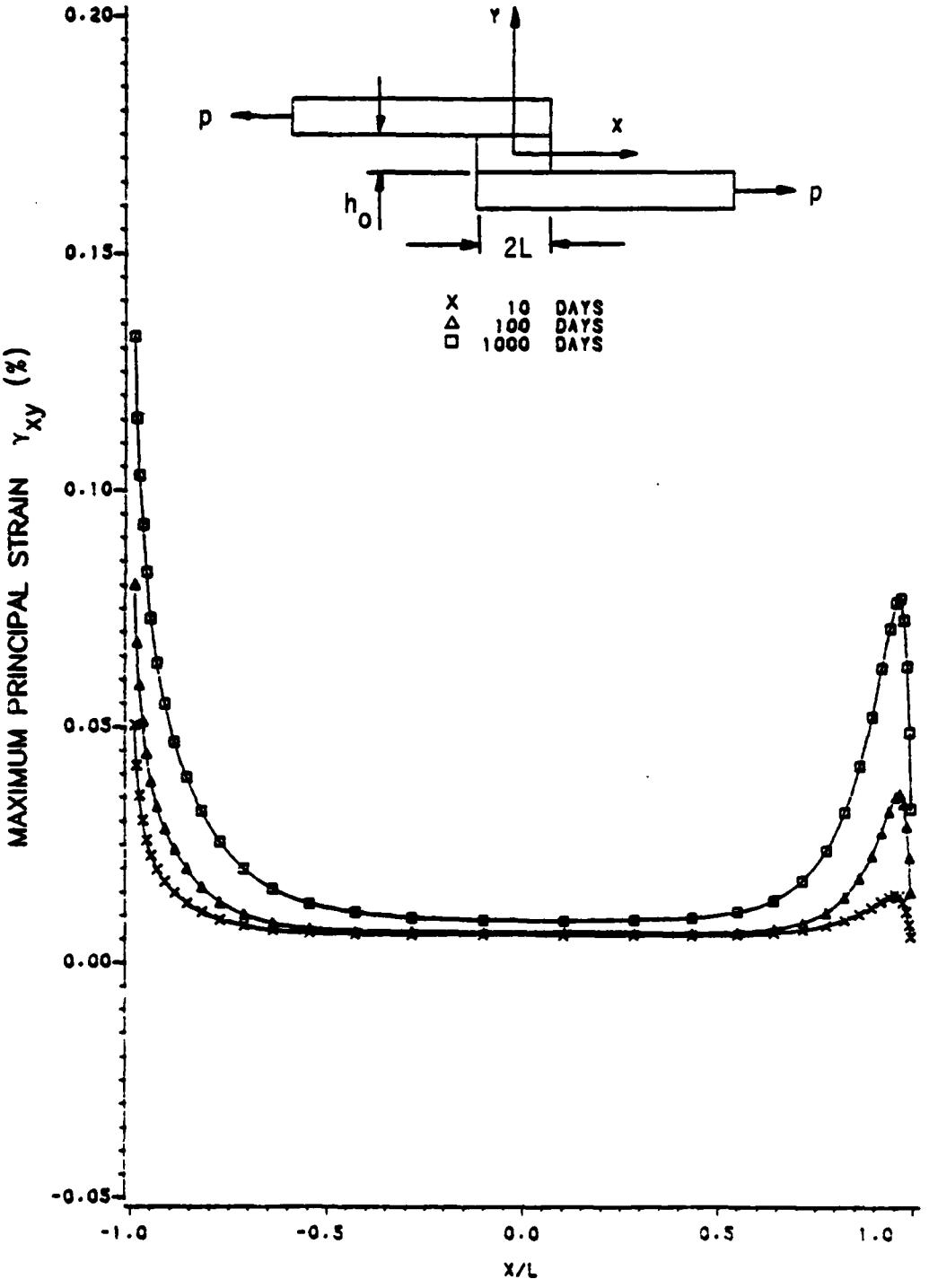

FIGURE 6.28 TIME DEPENDENCE OF ADHESIVE MAXIMUM PRINCIPAL STRAIN AT THE INTERFACE ($Y=h_o/2$) OF THE SINGLE LAP JOINT

6.5 Influence of the Interface Layer Stiffness on Adhesive Stresses

The purpose for investigating the influence of the interface layer stiffness on adhesive stresses was discussed in Chapter 1. One case presented here is the same analysis as that of Section 6.3, since the same finite element discretization, geometry, boundary conditions and linear elastic material properties are used. The stiffness ratio E_i/E_a, where E_i and E_a are the Young's moduli of the interface layer and of the adhesive respectively, was 1.0 for this analysis. Two other cases were run in which only E_i was changed such that E_i/E_a was 0.1 and 10.0, respectively. Adhesive stress distributions at the interface, $y = h_o/2$, are given in Figures 6.29 to 6.32 for peel, axial, shear and maximum principal stresses, respectively. Results for the three cases E_i/E_a = 0.1, 1.0 and 10.0 are superimposed for each stress, and show the influence of the interface layer stiffness clearly. Stresses are non-dimensionalized as before, being divided by the loads applied to the ends of the adherends.

Raising the interface layer stiffness to an order to magnitude above that of the adhesive has little influence on the overall peel and shear stresses (see Figures 6.29 and 6.31). The peak peel stress, for example, is raised by 11% and the peak shear stress by just 5%. The shear stress at the center of the overlap region is noticed to be lowered slightly. The peak axial stress, however, is increased by 160%, raising it to a value higher than either the peak peel or shear stresses. This behavior can easily be understood by comparing the situation with that of stiff fibers in a matrix of "soft" polymeric material under axial load. Most of the load is carried by the fibers.

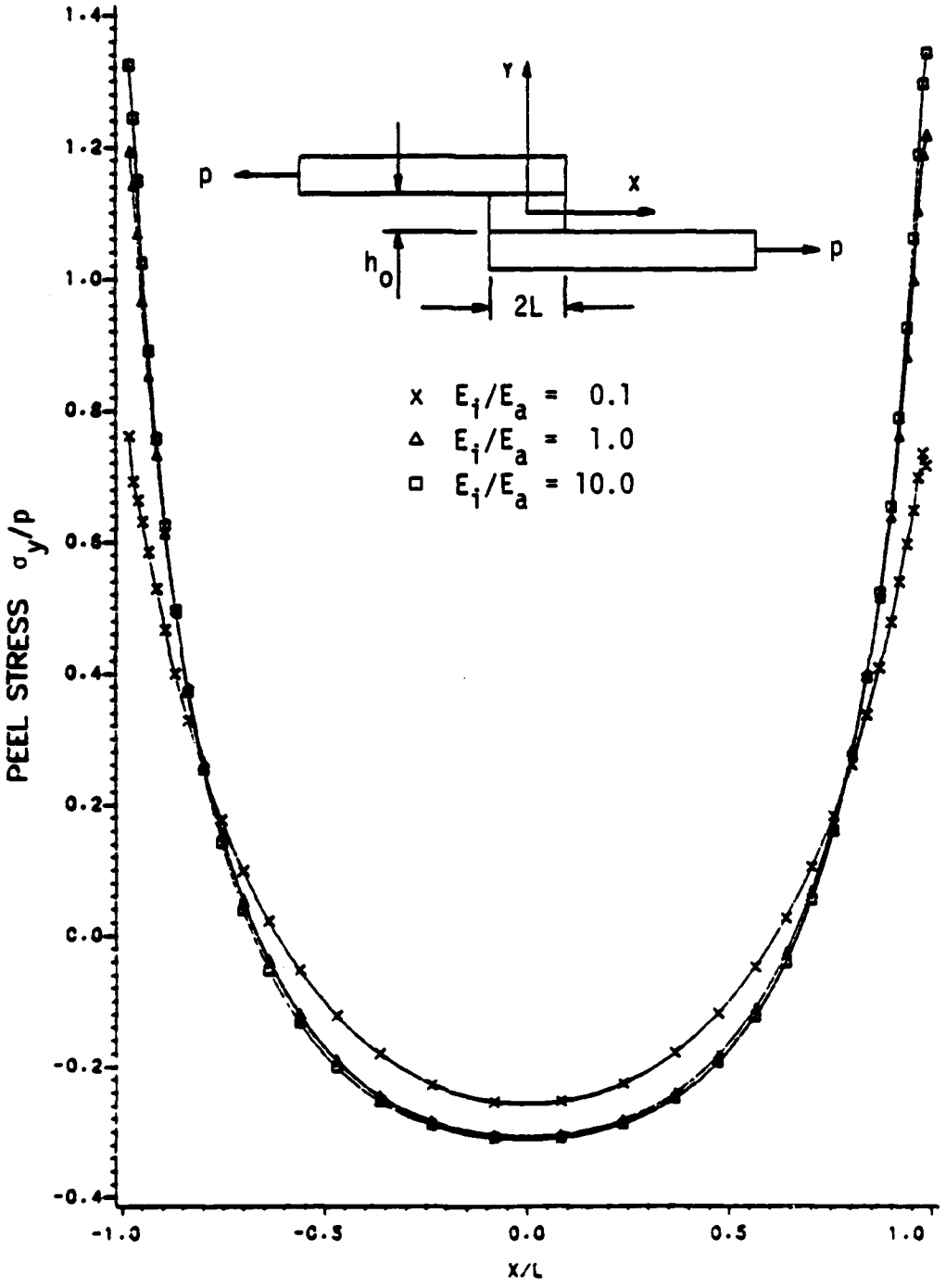

FIGURE 6.29 ADHESIVE PEEL STRESS AT THE INTERFACE ($Y=H_o/2$) OF THE SINGLE LAP JOINT AS A FUNCTION OF ^{E_i} INTERFACE LAYER STIFFNESS

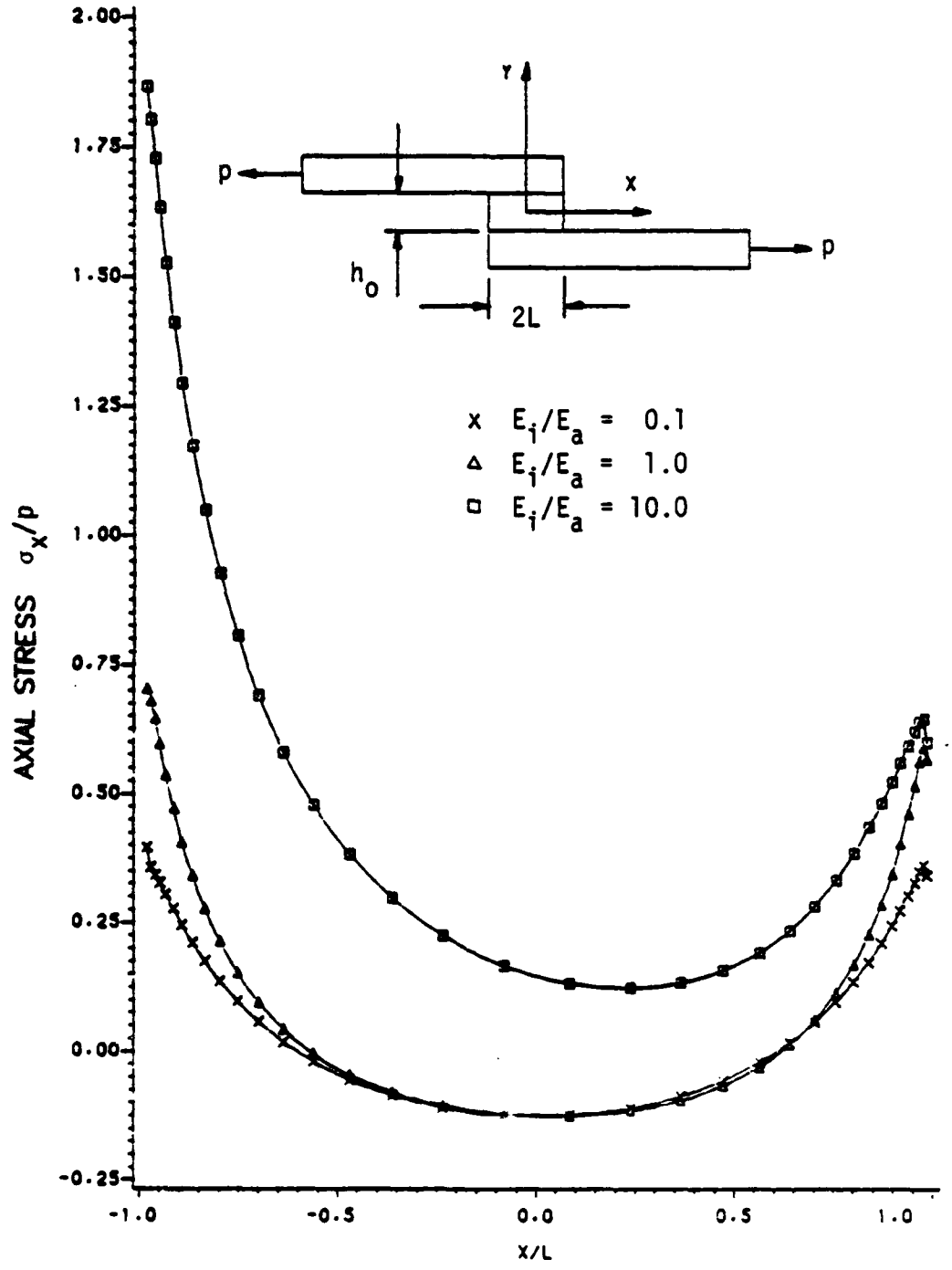

FIGURE 6.30 ADHESIVE AXIAL STRESS AT THE INTERFACE ($Y=H_o/2$) OF THE SINGLE LAP JOINT AS A FUNCTION OF INTERFACE LAYER STIFFNESS

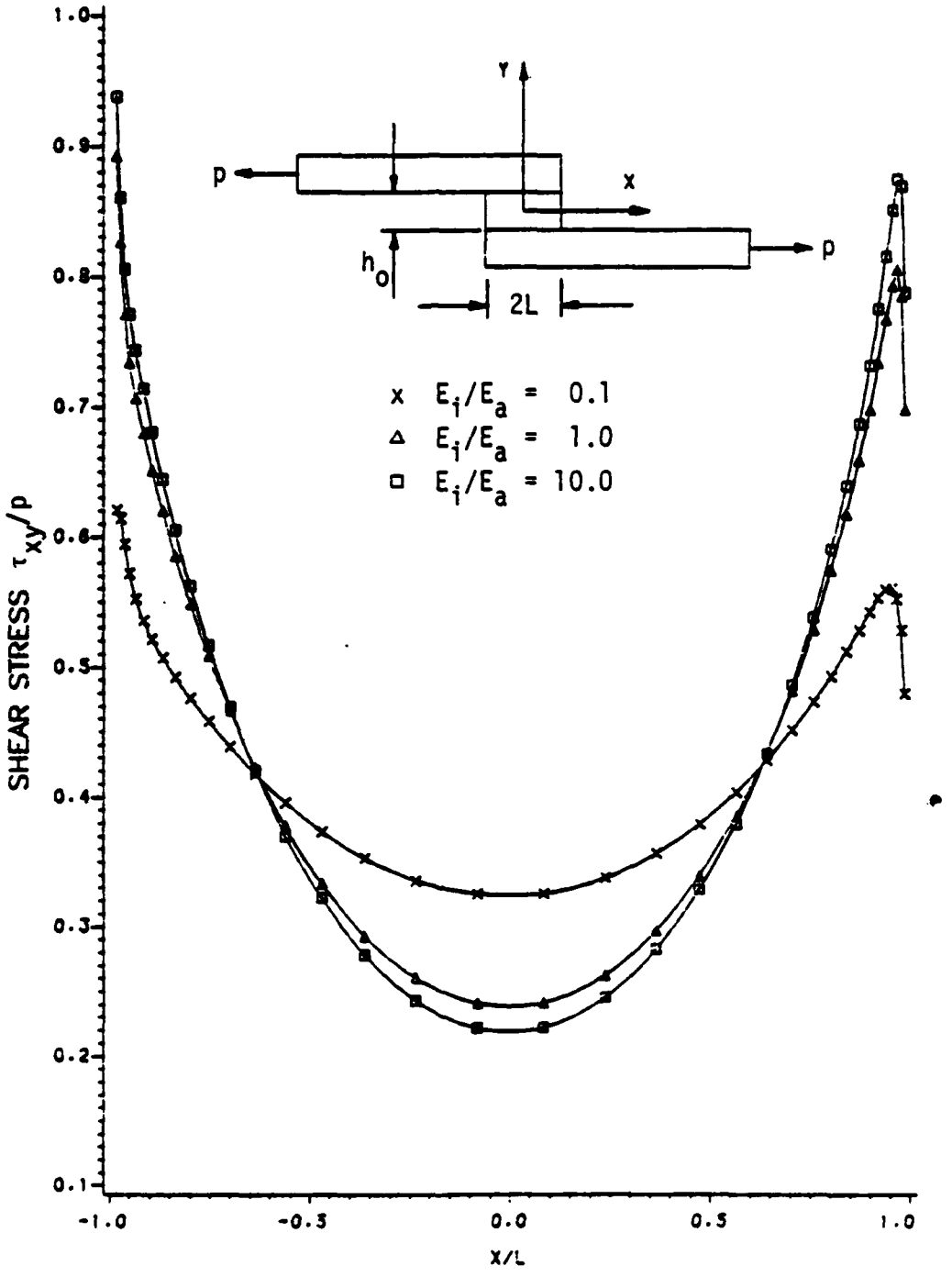

FIGURE 6.31 ADHESIVE SHEAR STRESS AT THE INTERFACE ($Y=H_o/2$) OF THE SINGLE LAP JOINT AS A FUNCTION OF INTERFACE LAYER STIFFNESS

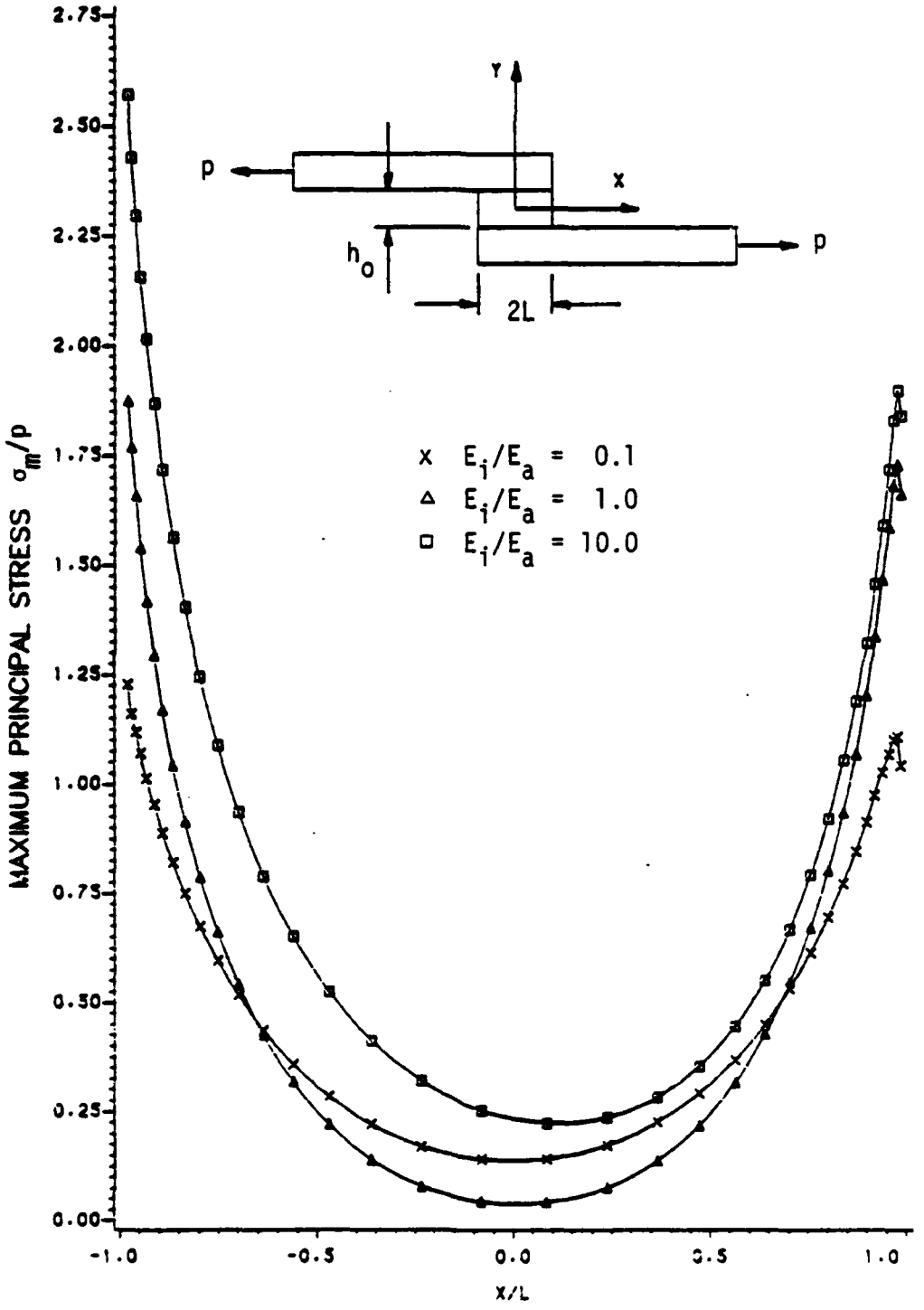

FIGURE 5.32 ADHESIVE MAXIMUM PRINCIPAL STRESS AT THE INTERFACE ($Y=H_a/2$) OF THE SINGLE LAP JOINT AS A FUNCTION OF INTERFACE LAYER STIFFNESS

due to equal straining of the fibers and the matrix. In our case we have two thin stiff interface layers on each side of a thicker and softer material, the adhesive. In most analytical studies the axial stress is completely neglected and in closed form analytical studies (for example, Goland and Reissner [2], Hart-Smith [3] and Delale and Erdogan [4]) it is assumed to be zero. The effect of the high axial-stress is that it causes the peak maximum principal stress to be raised to nearly 200% higher than the peak peel stress and 260% higher than the peak shear stress. The angle of maximum principal stress at $x/L = -1$ is also increased from 37° to 54°, measured counterclockwise from the positive x-axis.

Lowering the interface layer stiffness by an order of magnitude below that of the adhesive decreases the peak stresses by 36%, 43%, 30% and 35% for peel, axial, shear and maximum principal stress, respectively. Note from Figure 6.31 that the shear stress distribution is much more uniform throughout the length of the adhesive layer in the case of the lower interface layer stiffness. This is true for stresses in other directions also, but is not as pronounced as in the case of the shear stress. The shear stress must also necessarily become more uniform if the peak values are lowered, since it is through shear that most of the load must be transferred from the one adherend to the other.

Chapter 7

THE THICK ADHEREND SPECIMEN

7.1 Geometry and Finite Element Discretization

The geometry of the thick adherend specimen is chosen to be the same as that given by Krieger [24], and is defined in Figure 7.1. Krieger considered two values for the adhesive thickness, viz. 0.005 and 0.002 inches. Only the former thickness was considered in the present analysis, however.

The finite element mesh was chosen through experience gained and stress distributions obtained from the foregoing analyses of the single lap joint. This mesh is shown in Figure 7.2, with more detail of the central region shown in figure 7.2(b). The interface layers, modelled as part of the adhesive, are 0.0003 inches thick and contain only one element through their thickness. Ten equally spaced elements are modeled through each adherend thickness and 10 elements through the adhesive thickness. These numbers are the same as what was used for the single lap joint in the foregoing analysis. The adherends outside the gaps of the thick adherend joint are similar in nature to the central joint sections of both joints, and comparable element densities are, therefore, required in the axial direction of these sections. Thirteen elements were modelled in the axial direction of each adherend outside the gaps and 28 in the axial direction in the joint section. These element densities are, however, less than in the joint section of the single lap joint, since it was decided to limit

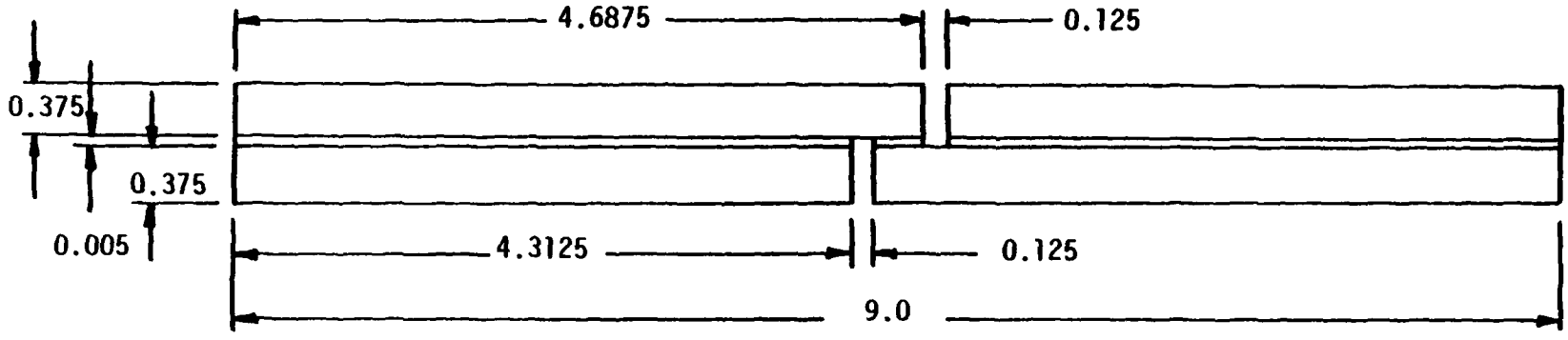

Figure 7.1 Geometry of the Thick Adherend Specimen for Comparison with Results of Krieger [24]. Dimensions in Inches.

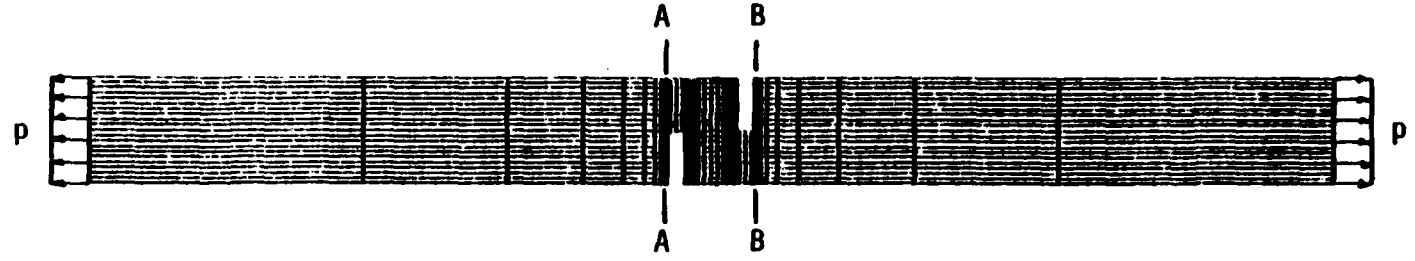

a) p = 1600 psi, Applied to Adherends Only.

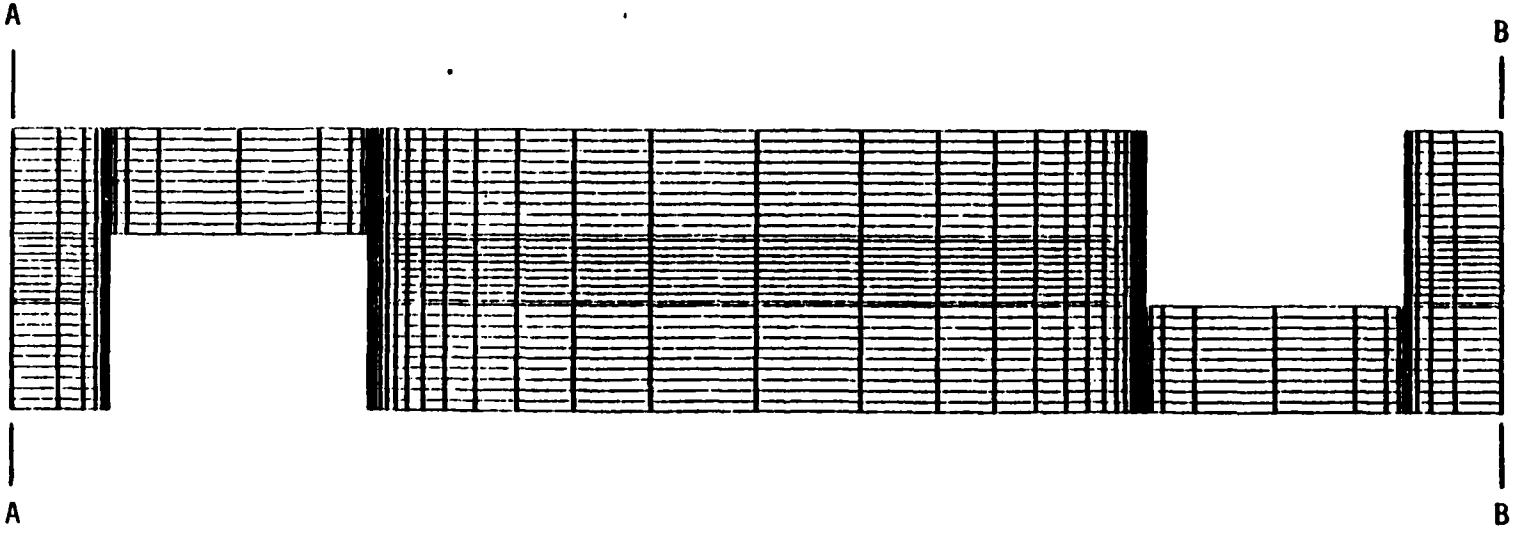

b)

Figure 7.2 (a) Boundary Conditions and Finite Element Discretization of the Thick Adherend Specimen and (b) Finite Element Discretization of Central Region of (a).

the total number of nodes to less than 2000, for economical reasons. For each increment in time, the total computer cost of generating the mesh and performing five non-linear iterations was $64.57 for the present thick adherend analysis, using the idle execution priority. Ten elements were modeled in the axial direction of each gap, which yields a comparable element density of that of the single lap adherends outside the joint section. The total number of nodes is 1965. The aspect ratio of the smallest elements adjacent to the edges either side of the gaps was chosen to be 3.0, lying lengthwise in the interface layers, since it was expected that stress gradients in this geometry would also be greater in the transverse direction than in the axial direction, close to the joint edges.

The boundary conditions for the finite element analysis are also shown in Figure 7.2. The end stress, p = 1600 psi, is the same as that used in the experimental analysis of Krieger [24], and this load was not applied to the adhesive, but over the two adherend ends only.

7.2 Material Properties

Material properties for the thick adherend joint were chosen to conform with test specimens currently available at V.P.I., intended for testing by B. Barthelemy in the near future. The test specimens were supplied by R. B. Krieger, Jr., of the American Cyanamid Company, Havre de Grace, Maryland, and have the same geometry as that of Figure 7.1. The type of aluminum used is not known, but its properties were supplied together with the test specimens by Krieger, and are listed in Table 7.1. The test specimens contain FM-73 adhesive, which

Table 7.1 Material Properties for the Thick Adherend Specimen

	Time t (min)	Elastic Modulus E (psi)	Plastic Modulus E_1 (psi)	$\frac{E_1}{E}$	Yield Stress σ_y (psi)	Poisson's Ratio ν
Aluminum[1]	-	10.3×10^6	-	-	-	0.33
FM-73[2] Adhesive	1	481,700	284,600	0.5908	1660	
	10	463,800	250,400	0.5399	1690	
	30	439,400	234,100	0.5328	1740	
FM-73 M[3] Adhesive	-	-	-	-	-	0.32

(1) Supplied by R. B. Krieger, American Cyanamid Co., to B. Bartholemy, V.P.I. (unpublished).

(2) Derived from creep data supplied by Brinson et al. [48] (see Figure 7.6).

(3) Romanko and Knauss [27].

is assumed to be isotropic in the present analysis.

Experimental creep data for FM-73 adhesive from Peretz and Weitsman [29] and Brinson et al. [48] is shown in Figures 7.3 and 7.4, respectively. From these sets of creep data, isochronous stress-strain data points were derived for times t = 1 and 15 minutes for the former and for times t = 1, 10 and 30 minutes for the latter. The isochronous curves for time t = 1 minute are shown in Figure 7.5 for comparison purposes. Figure 7.5 also has one stress-strain data point which was derived from the time dependent creep compliance for FM-73 adhesive at time t = 1 minute, given by Romanko and Knauss [27]. Note that this latter data point of Romanko and Knauss is for 25°C and the isochronous curves of both Brinson et al. and Peretz and Weitsman are for 30°C. It is expected that at 30°C, the data point of Romanko and Knauss would shift closer to the isochronous curve of Peretz and Wietsman and further away from that of Brinson et al. Since it is not known how much this shift will be, however, the data of Brinson et al. was chosen to obtain material properties for input to the finite element program in the present analysis.

Bi-linear isochronous stress-strain curves were fitted to the stress-strain data points obtained from the creep data for Brinson et al. and are shown in Figure 7.6 for times t = 1, 10 and 30 minutes. The corresponding elastic and plastic moduli, E and E_1, and values of yield stress, σ_y, used in the SAAS3VP program for the non-linear visco-elastic analysis, are listed in Table 7.1. Poisson's ratio for FM-73 adhesive, also listed in Table 7.1, was determined by Romanko and Knauss [27], using holographic interferometry. The evaluation was

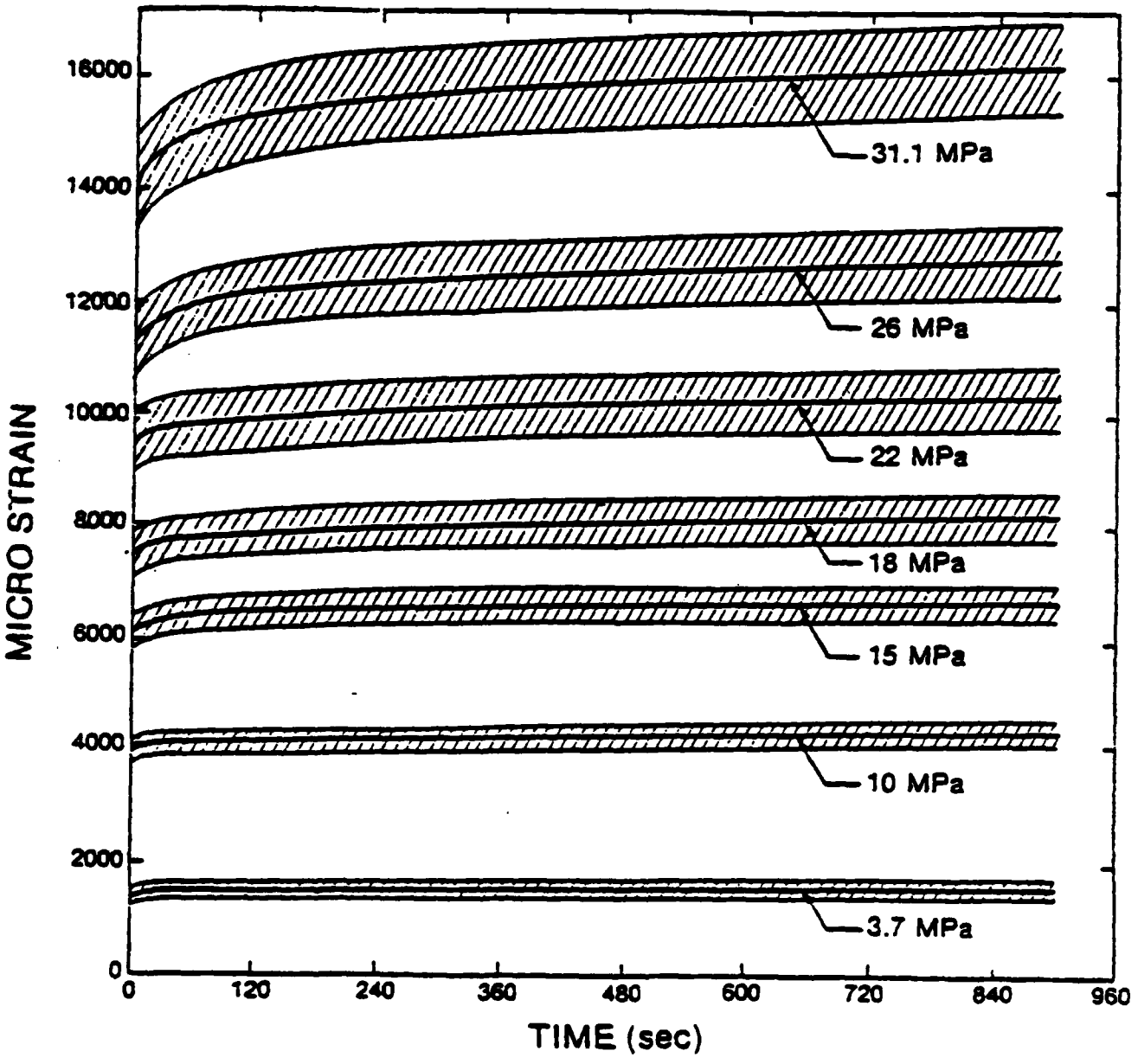

Figure 7.3 Experimental Creep Data for FM-73 U Adhesive at 30°C and 55% R.H. Reproduced from Peretz and Weitsman [29].

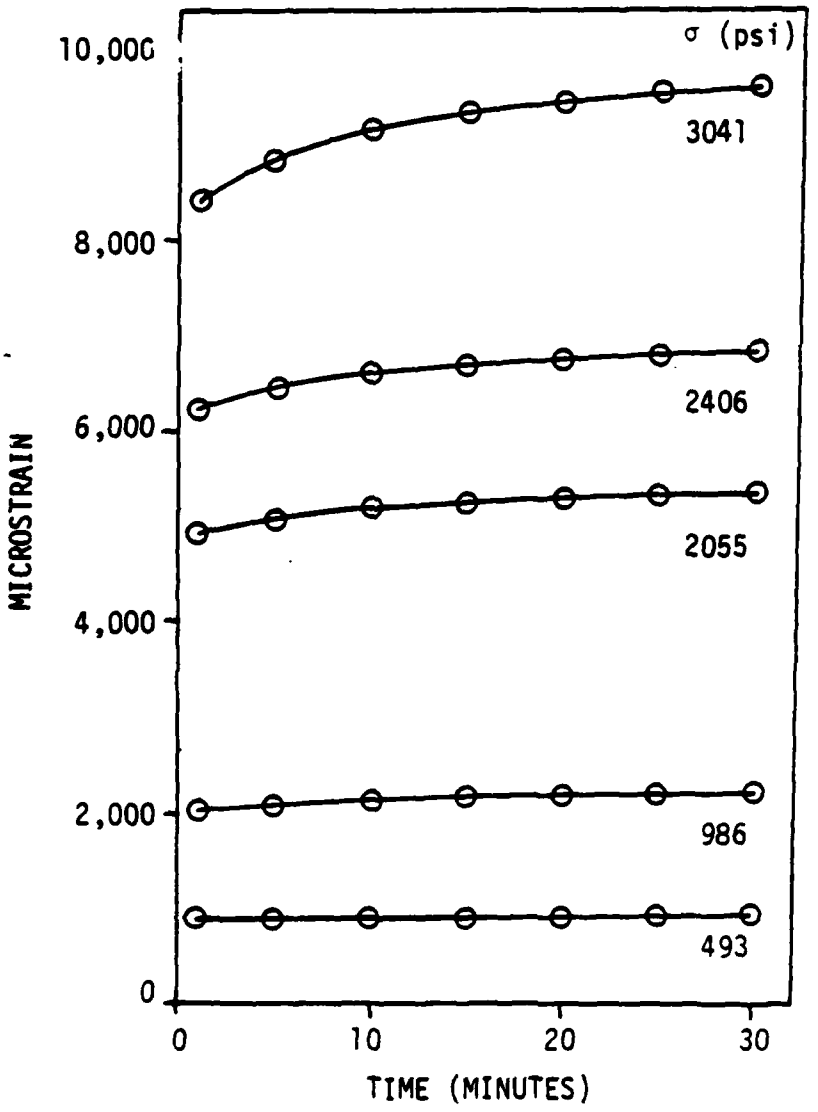

Figure 7.4 Experimental Creep Data for FM-73 Adhesive at 30°C as Supplied by Brinson et al.

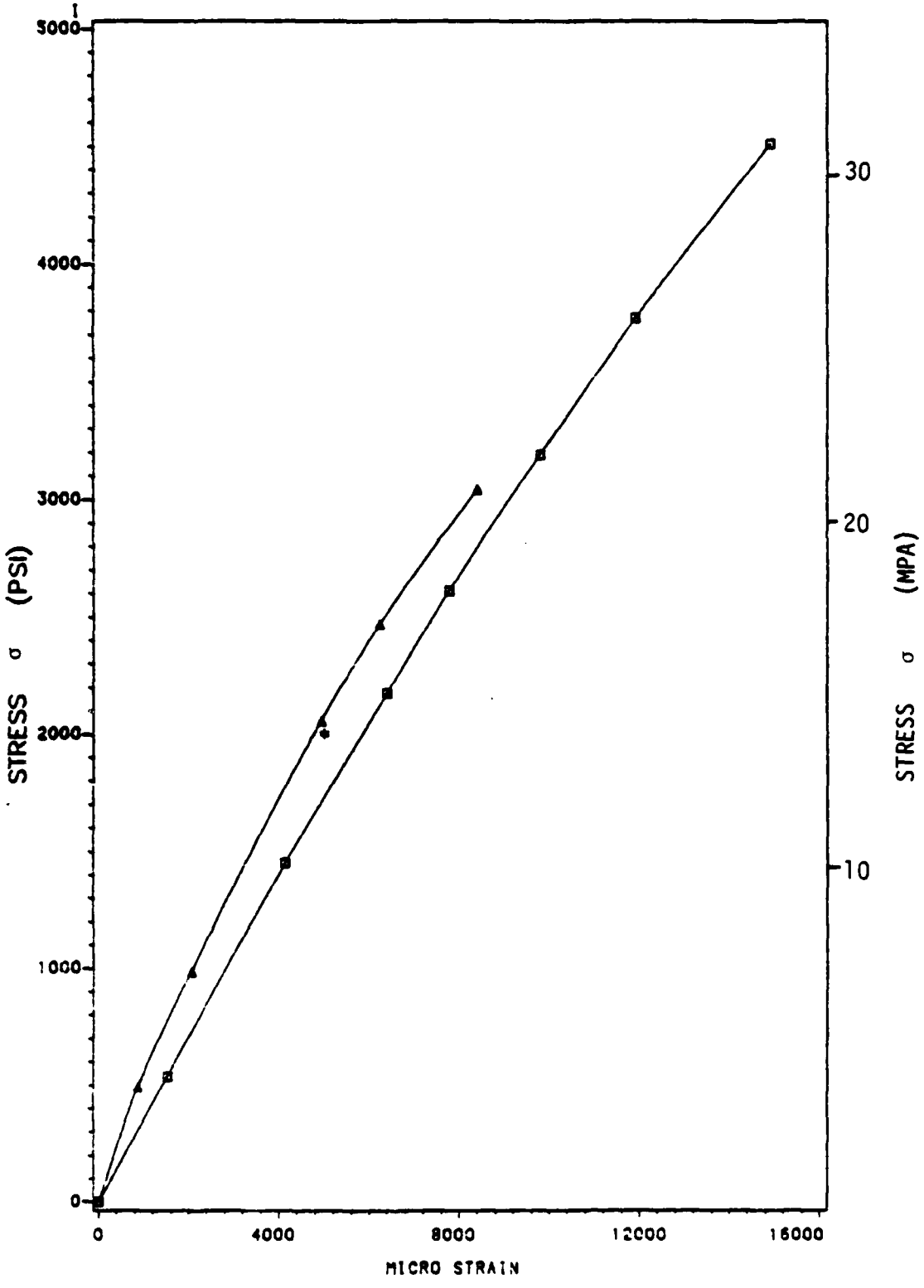

FIGURE 7.5 ISOCHRONOUS STRESS-STRAIN CURVES FOR FM-73 ADHESIVE AT TIME T = 1 MINUTE

- • DERIVED FROM 1/D(T) FOR 2000 LBS. AT 25°C OF ROMANKO AND KNAUSS (27)
- △ DERIVED FROM CREEP DATA AT 30°C OF BRINSON ET. AL. (48)
- □ DERIVED FROM CREEP DATA AT 30°C OF PERETZ AND WEITSMAN (29)

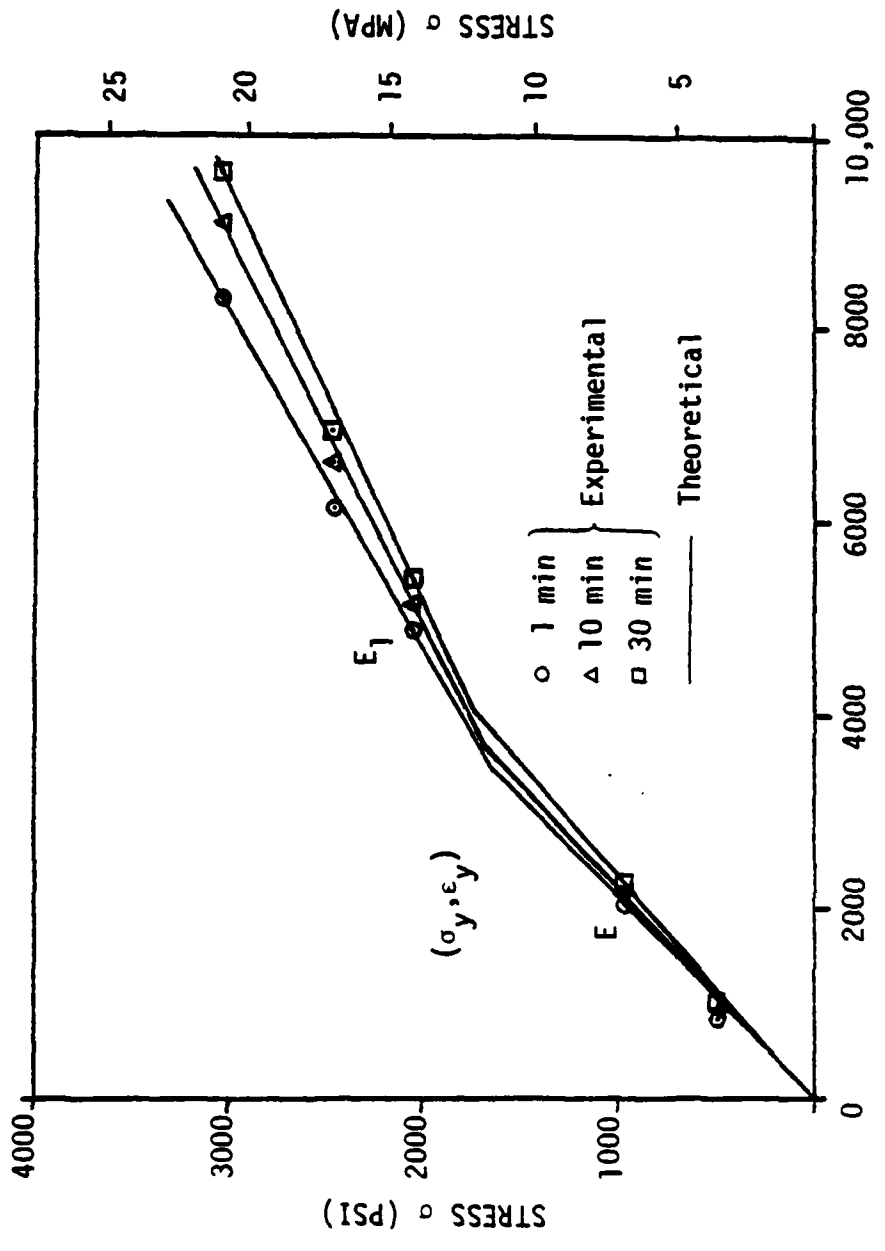

Figure 7.6 Bi-linear Isochronous Curves for FM-73 Adhesive Fitted to Stress-Strain Data Points Derived from the Creep Data of Brinson et al. [48].

performed at 25°C, and, over a time scale of more than 30 days, Poisson's ratio was found to be independent of time, in spite of a measurable creep over this period. The adhesive tested by Romanko and Knauss was supported with a Dacron mat carrier cloth and was also supplied by the American Cyanamid Company [27].

7.3 Non-Linear Viscoelastic Analysis

The time dependence of adhesive peel, axial, shear and maximum principal stresses are shown in Figures 7.7 to 7.10, respectively. As in the previous section on the single lap joint, stresses are non-dimensionalized with respect to the end load, p, and plotted as functions of non-dimensionalized distance along the length of the overlap region. The peel, axial and maximum principal stresses are seen to be all but uniform over the length of the joint section. The shear stress is also far from being evenly distributed over the joint section; the peak value for time t = 1 minute at the edge, x/L = -1, is 64% higher than at the center, x/L = 0. The non-uniformity of the shear stress, however, is not nearly as bad as was found for the single lap joint in the preceding chapter (Figure 6.9).

The peel and axial stresses of Figures 7.7 and 7.8, respectively, are seen to approach certain limits at the joint edges, but at the left-hand edge, x/L = -1, these stresses suddenly jump to higher values than what their tendencies predict. Even though stresses in the two elements closest to the joint edges are not shown, as explained in Section 6.3, the presence of the stress singularity at $(x,y) = (-L,h_o/2)$ clearly also influences the stresses in the third element from

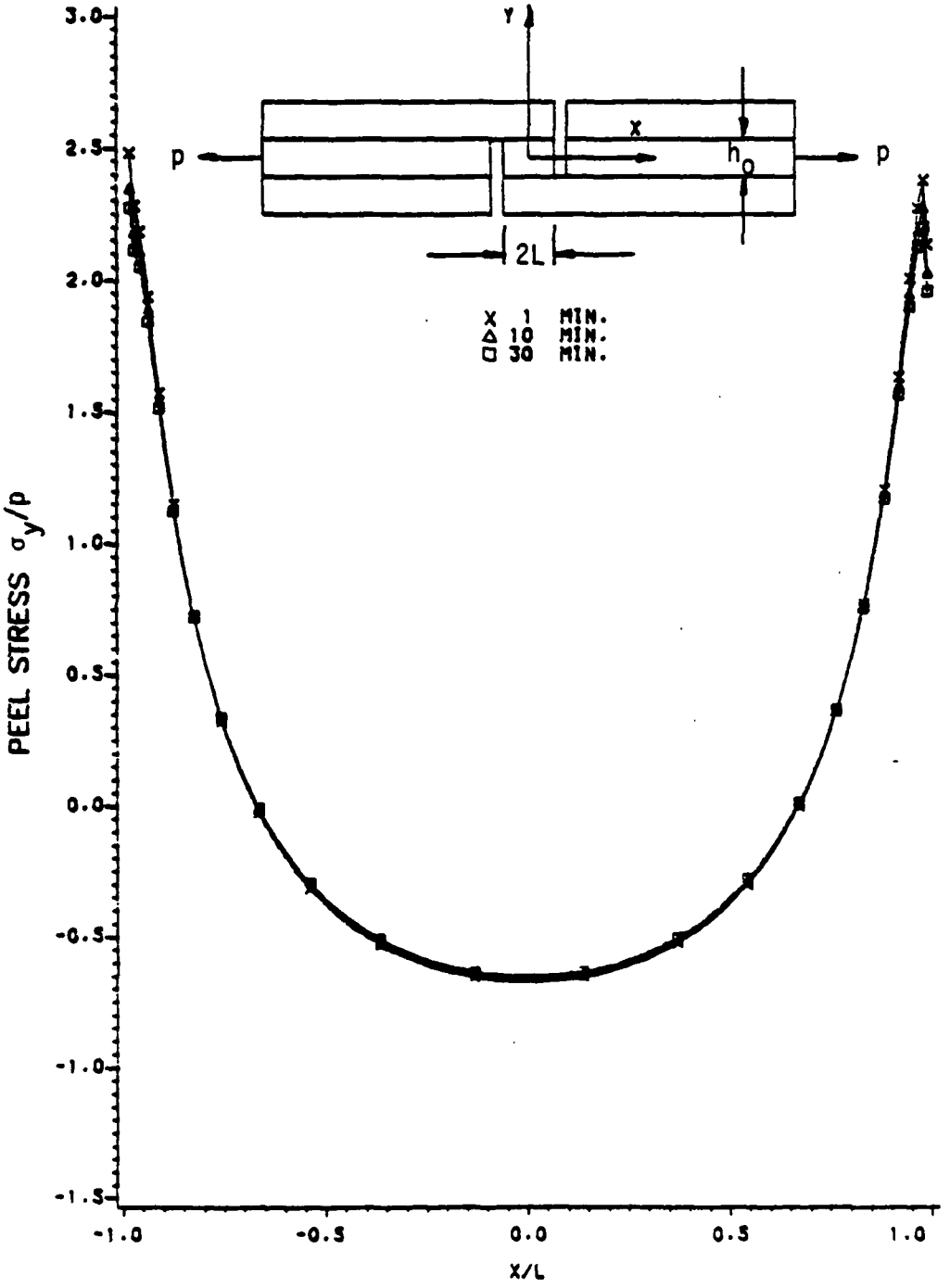

FIGURE 7.7 TIME DEPENDENCE OF ADHESIVE PEEL STRESS AT THE INTERFACE ($Y=H_o/2$) OF THE THICK ADHEREND SPECIMEN

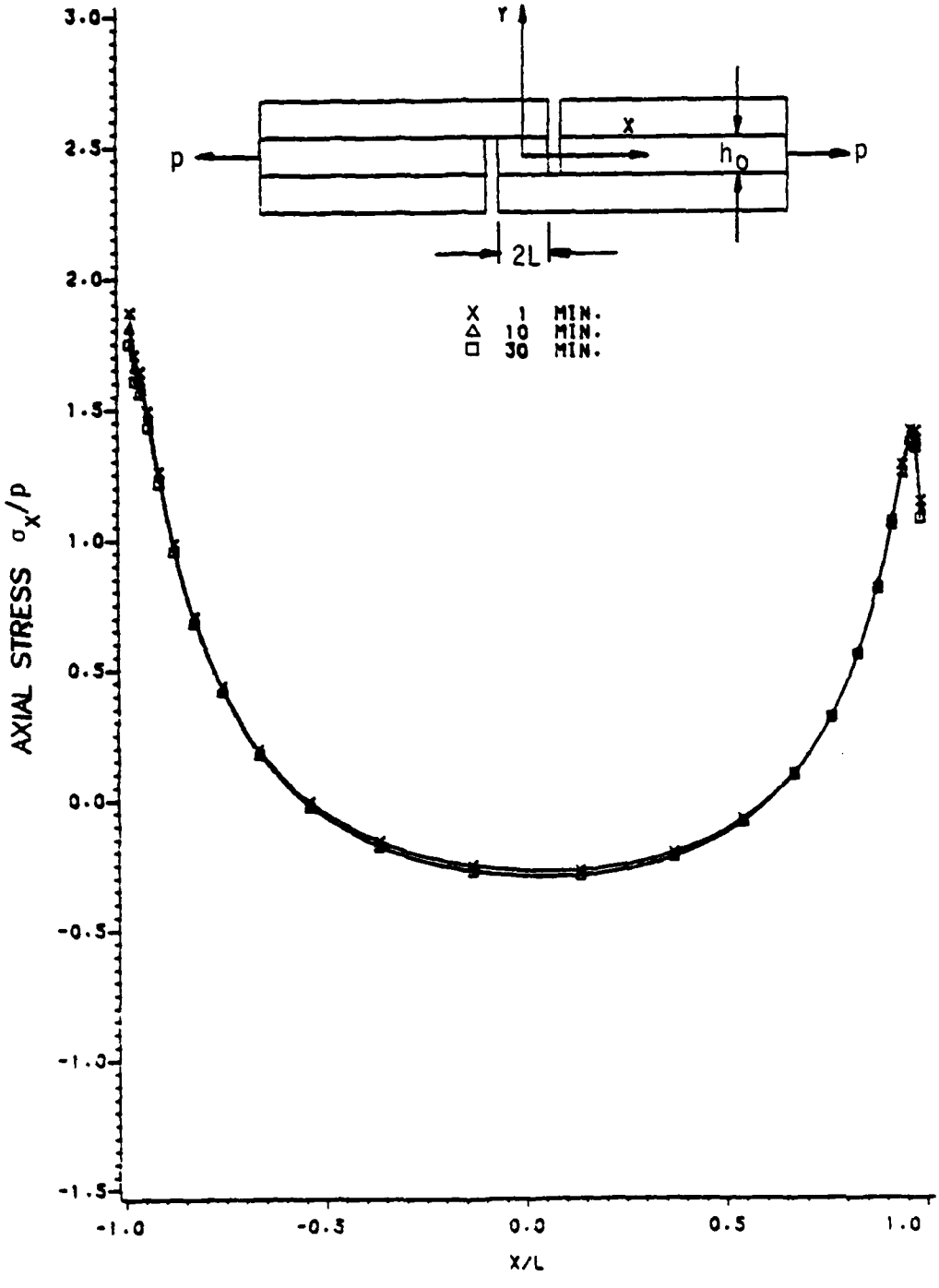

FIGURE 7.8 TIME DEPENDENCE OF ADHESIVE AXIAL STRESS AT THE INTERFACE ($Y=H_o/2$) OF THE THICK ADHEREND SPECIMEN

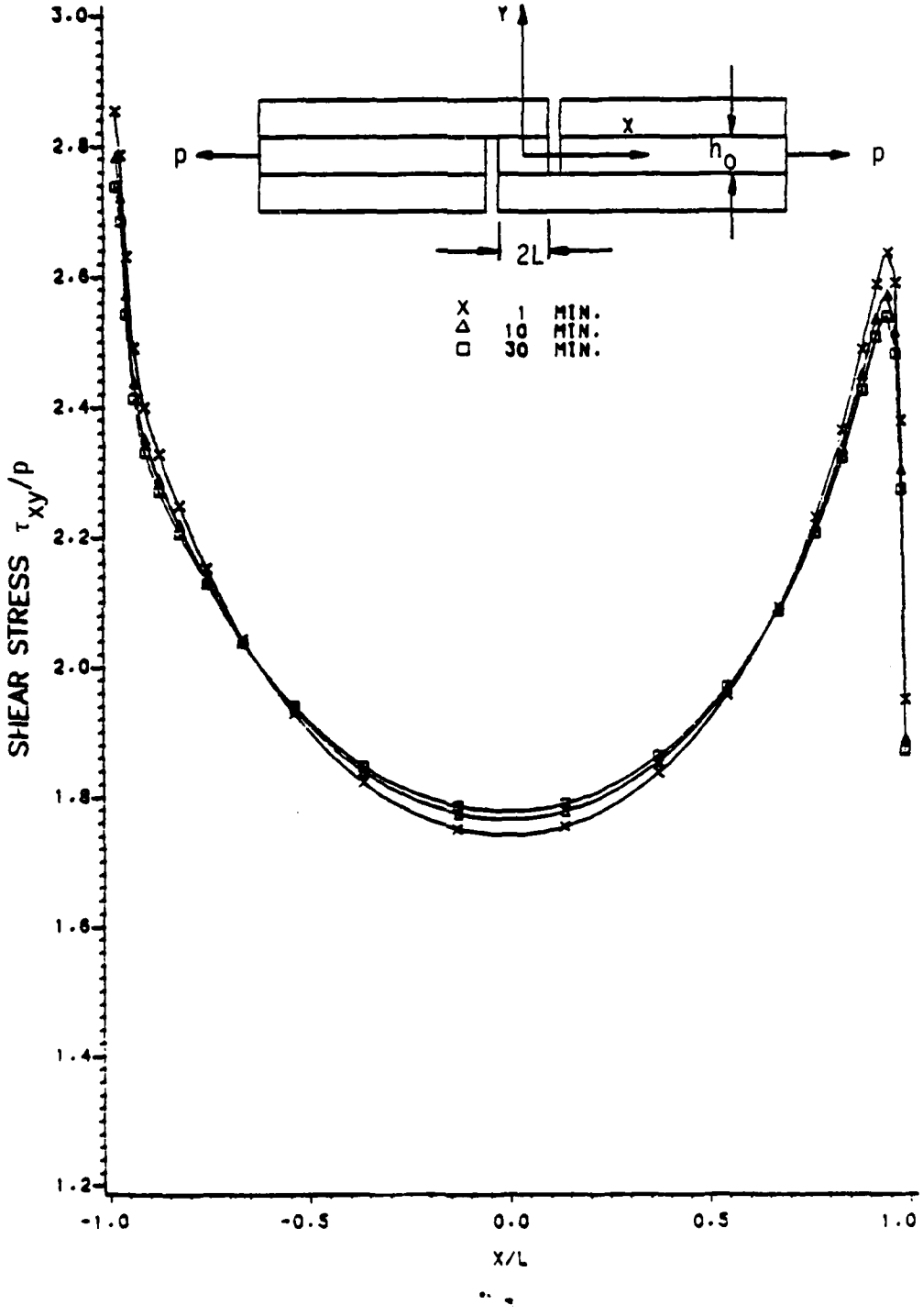

FIGURE 7.9 TIME DEPENDENCE OF ADHESIVE SHEAR STRESS AT THE INTERFACE ($Y=H_o/2$) OF THE THICK ADHEREND SPECIMEN

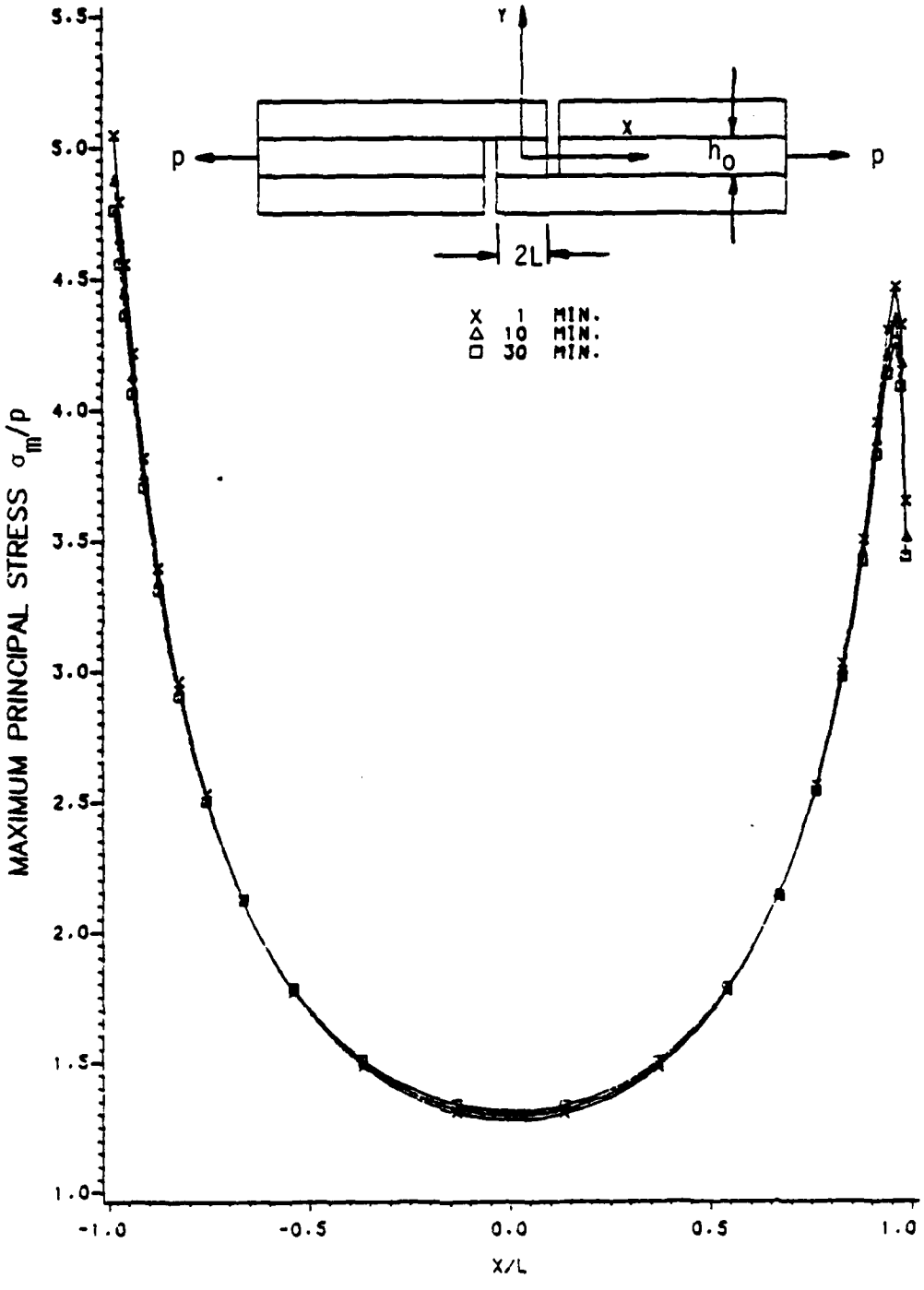

FIGURE 7.10 TIME DEPENDENCE OF ADHESIVE MAXIMUM PRINCIPAL STRESS AT THE INTERFACE ($Y=H_o/2$) OF THE THICK ADHEREND SPECIMEN

the left-hand joint edge. The stress singularity is the same as that discussed in Section 6.3. If the stress values for the third element from the joint edge are also ignored, the maximum stress relaxations from time t = 1 minute to t = 30 minutes are 7%, 5%, 4% and 5% for the peel, axial, shear and maximum principal stresses, respectively. The redistribution of stresses over the time scale of 1 to 30 minutes for a constant load is therefore very small.

The time dependence of adhesive strains at the interface, $y = h_o/2$, of the thick adherend specimen are shown in Figures 7.11 to 7.14 for peel, axial, shear and maximum principal strains, respectively. It is seen from Figures 7.11 and 7.12 that the peel and axial strains also change very little with time. The shear and maximum principal strains, however, are heavily dependent on time, as can be seen from Figures 7.13 and 7.14, respectively. From time t = 1 to 30 minutes, these strains increase by 15% and 13% at x/L = -1, respectively. At the center of the overlap region, increases in shear and maximum principal strains are greater than at the edges, being 22% and 21%, respectively, over the same time span. The tendency, therefore, is to move to a slightly more evenly distributed strain with increasing time.

Adhesive stresses in the upper interface layer, $y = h_o/2$, which include the regions to the outside of the gaps of the thick adherend specimen are shown in Figures 7.15 to 7.18, for the time t = 1 minute only. It is important to note that the peel, axial and maximum principal stresses of Figures 7.15, 7.16 and 7.18, respectively, are higher at the edges on the outside of the gaps than at the edges of the overlap or joint region. The peel stress outside the joint section,

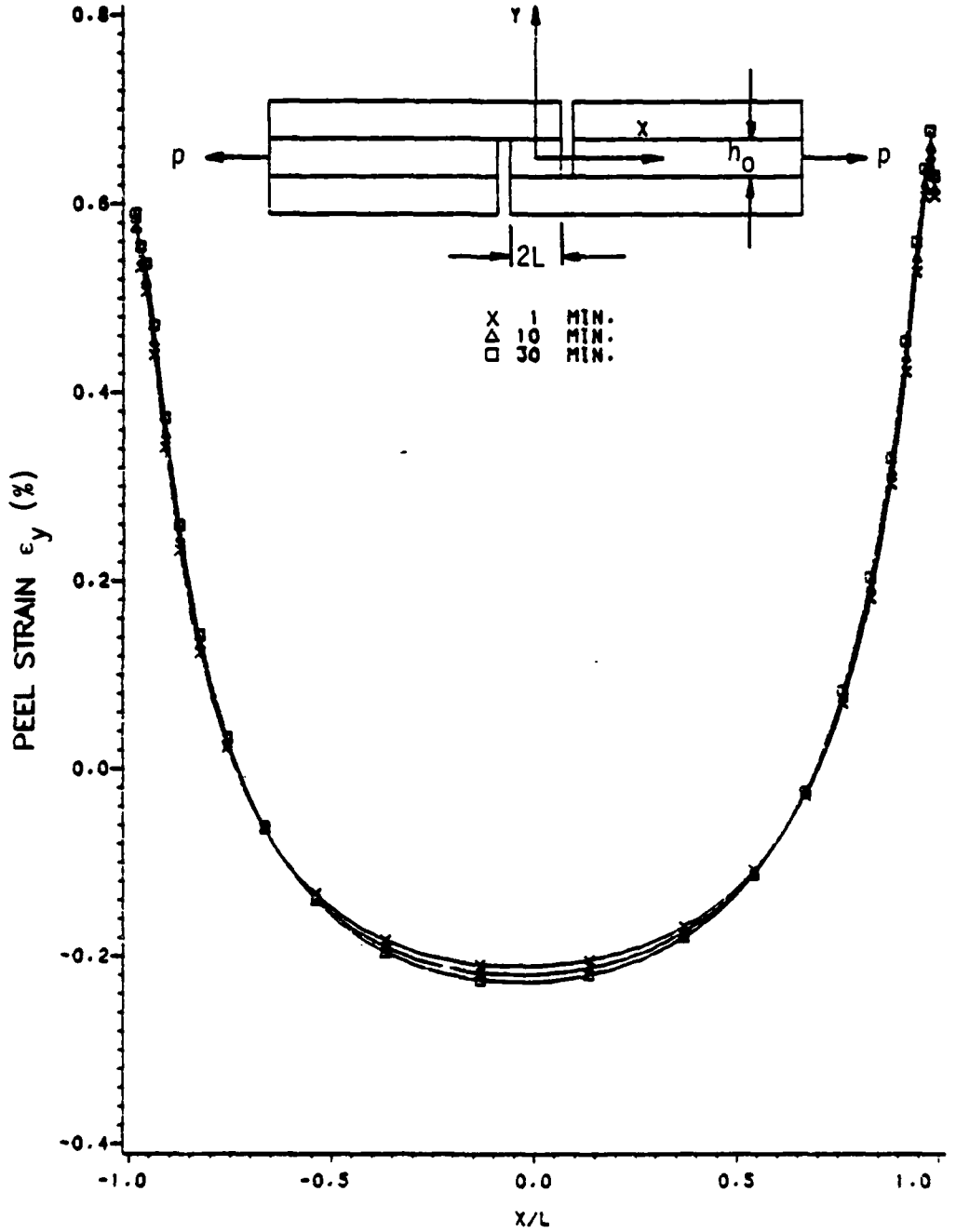

FIGURE 7.11 TIME DEPENDENCE OF ADHESIVE PEEL STRAIN AT THE INTERFACE ($Y=H_o/2$) OF THE THICK ADHEREND SPECIMEN

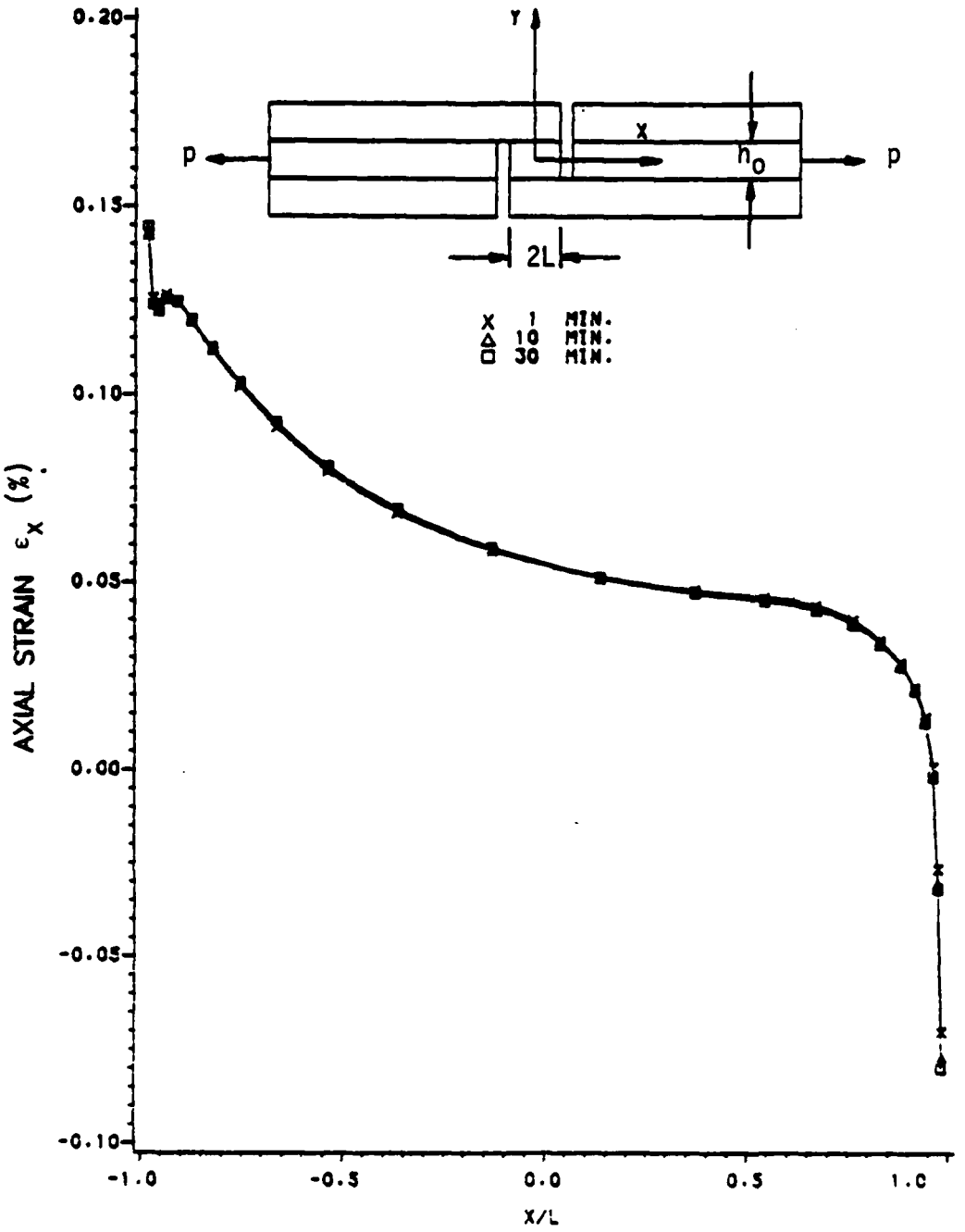

FIGURE 7.12 TIME DEPENDENCE OF ADHESIVE AXIAL STRAIN AT THE INTERFACE ($Y=H_o/2$) OF THE THICK ADHEREND SPECIMEN

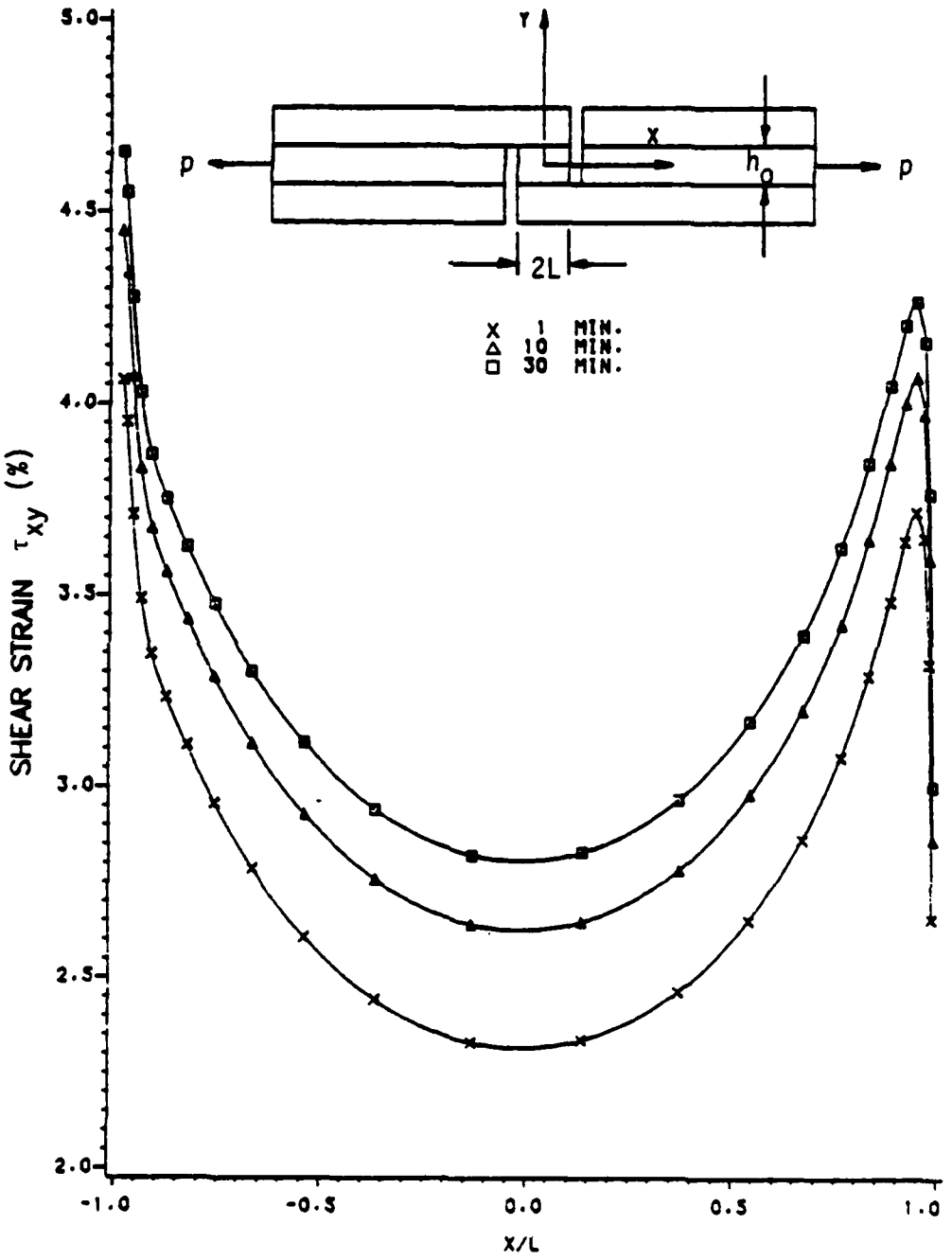

FIGURE 7.13 TIME DEPENDENCE OF ADHESIVE SHEAR STRAIN AT THE INTERFACE ($Y=H_o/2$) OF THE THICK ADHEREND SPECIMEN

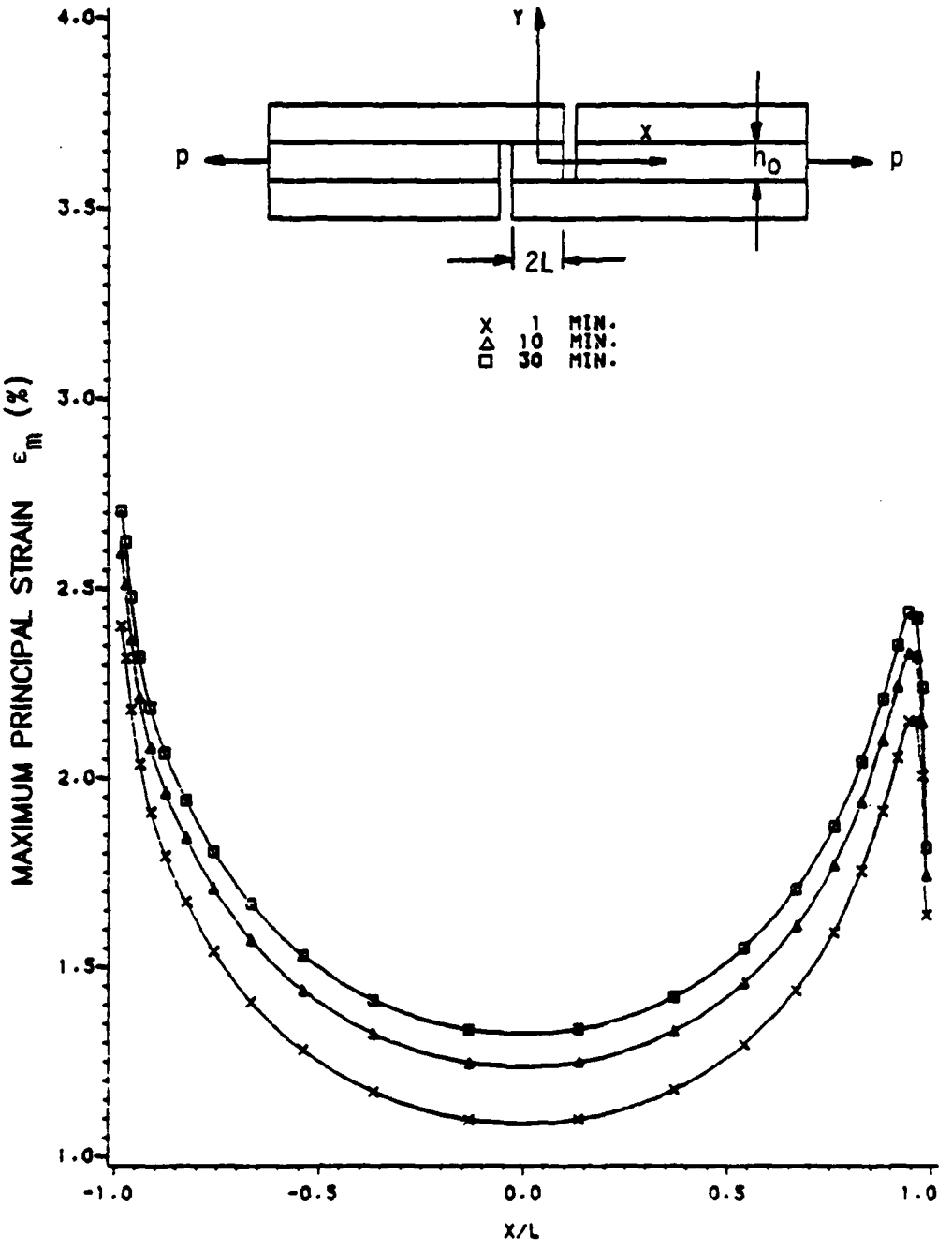

FIGURE 7.14 TIME DEPENDENCE OF ADHESIVE MAXIMUM PRINCIPAL STRAIN AT THE INTERFACE ($Y=H_o/2$) OF THE THICK ADHEREND SPECIMEN

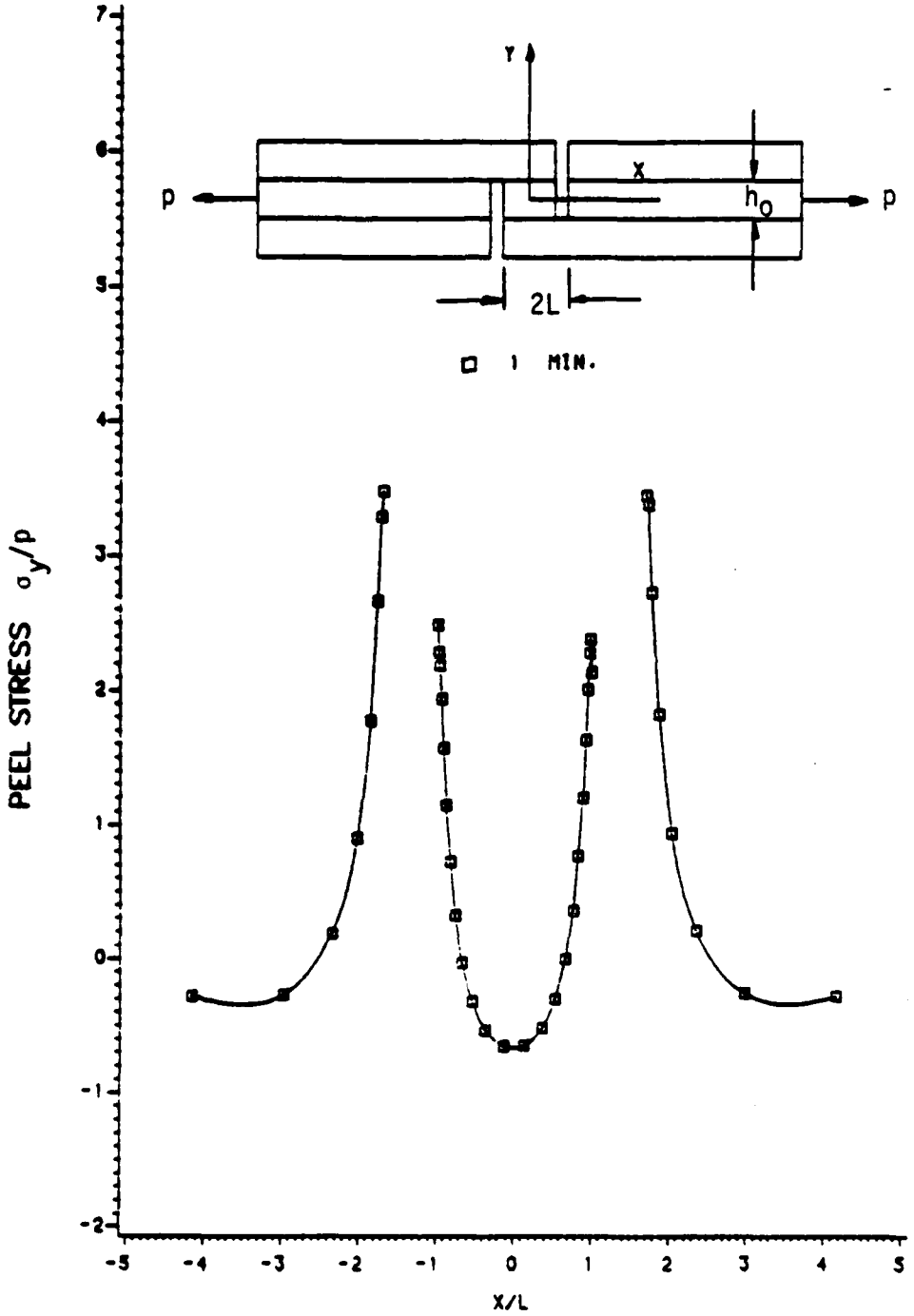

FIGURE 7.15 ADHESIVE PEEL STRESS AT THE INTERFACE ($Y=H_o/2$) OF THE THICK ADHEREND SPECIMEN

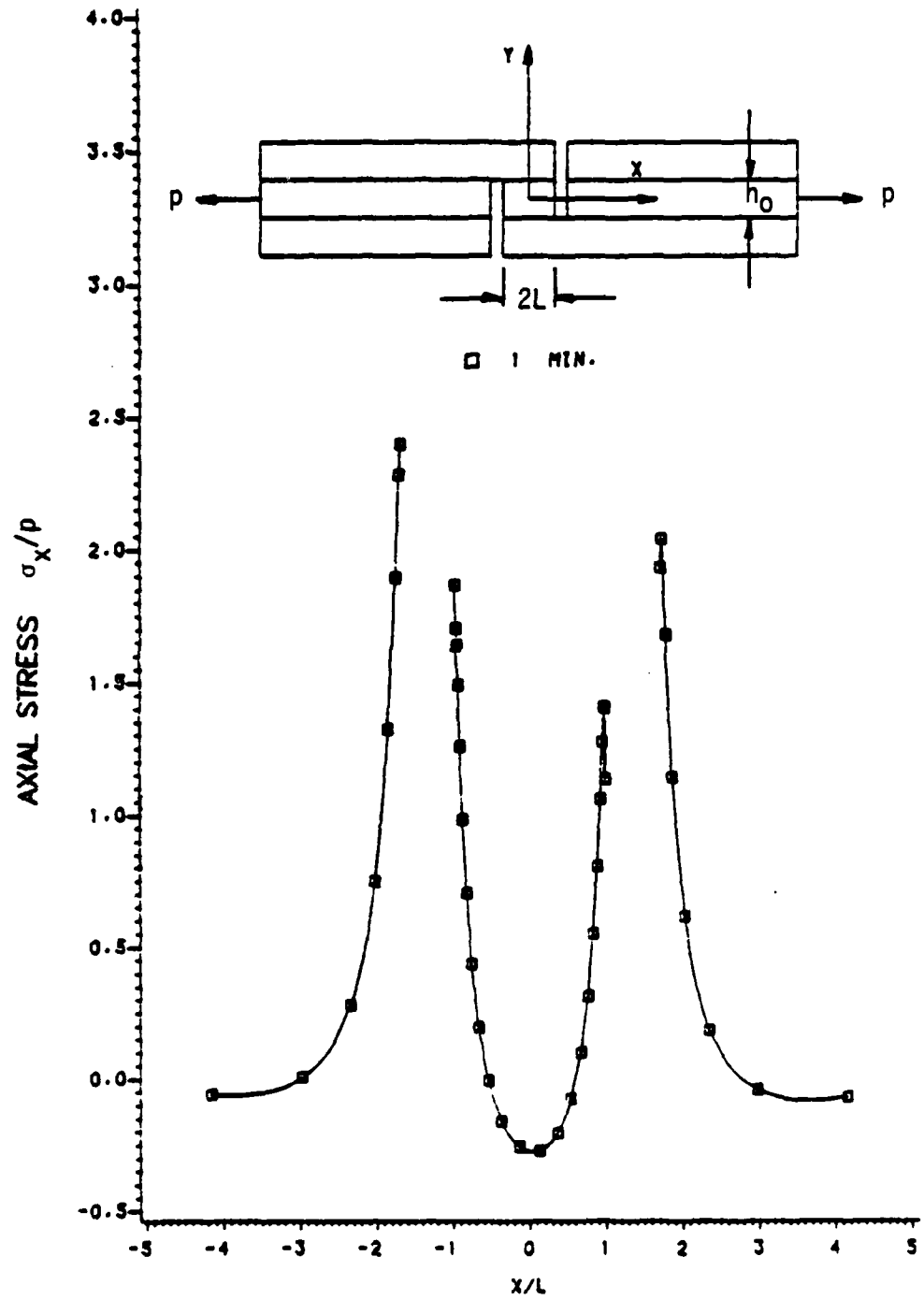

FIGURE 7.16 ADHESIVE AXIAL STRESS AT THE INTERFACE ($Y=H_o/2$) OF THE THICK ADHEREND SPECIMEN

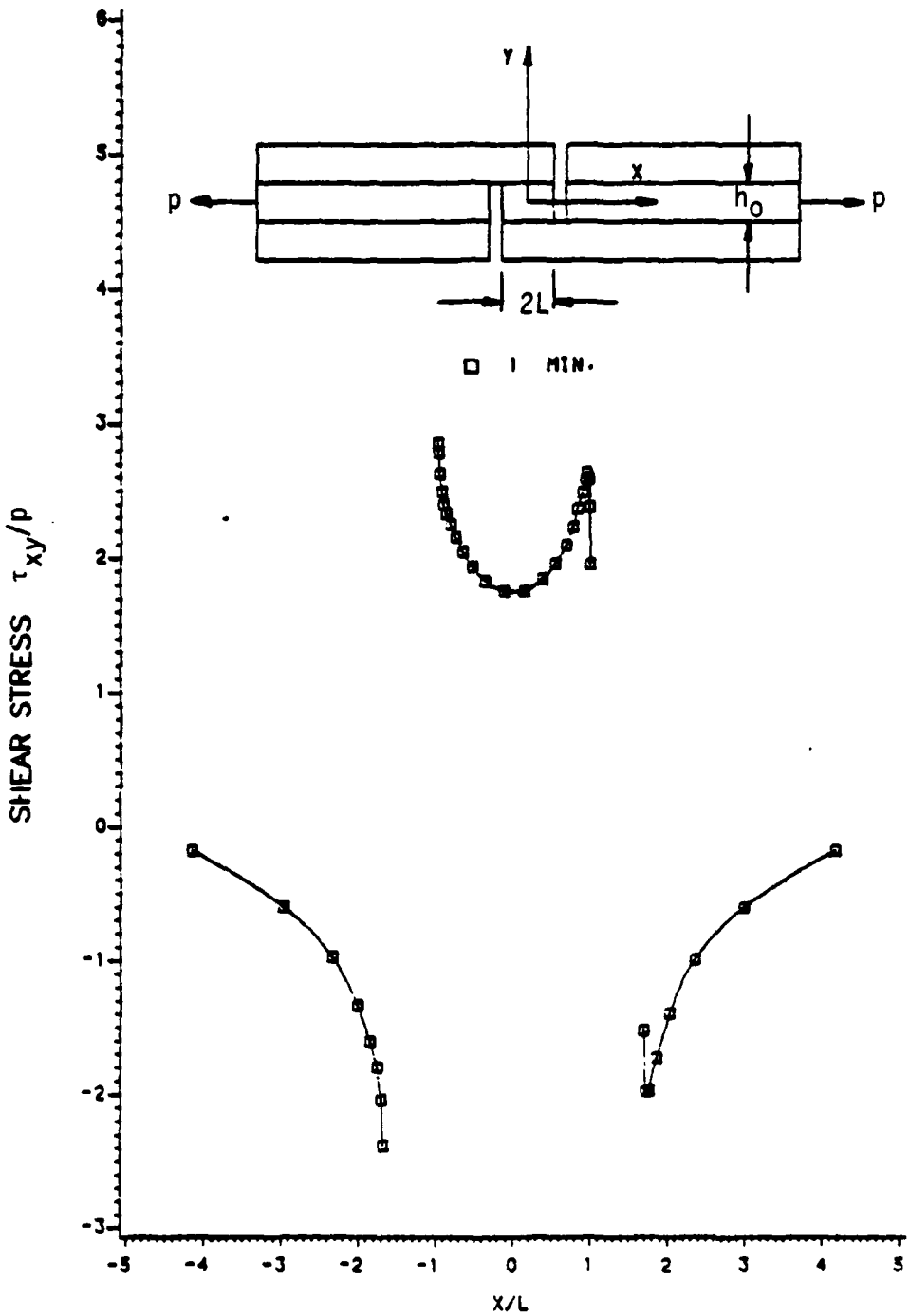

FIGURE 7.17 ADHESIVE SHEAR STRESS AT THE INTERFACE ($Y=H_o/2$) OF THE THICK ADHEREND SPECIMEN

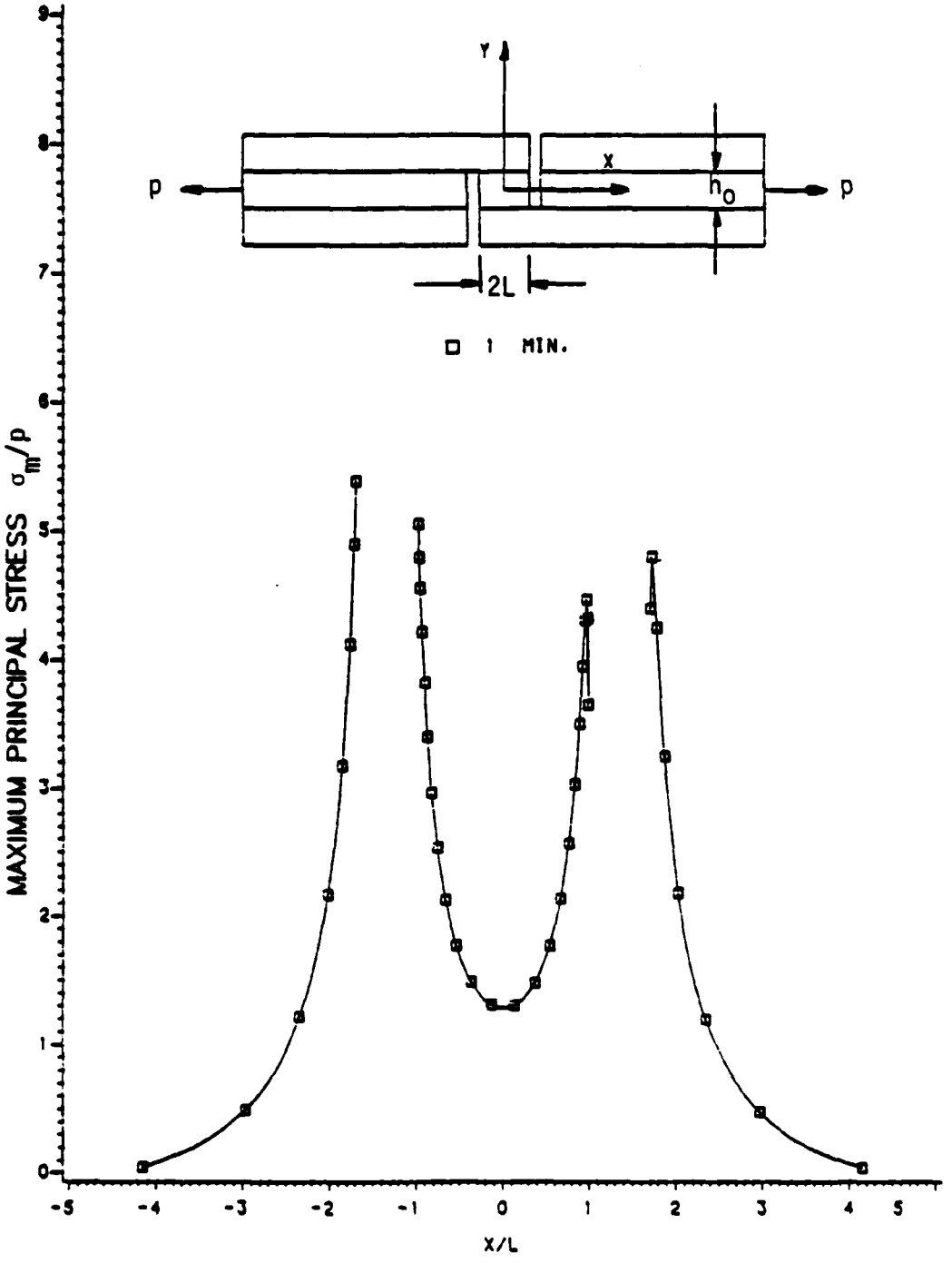

FIGURE 7.18 ADHESIVE MAXIMUM PRINCIPAL STRESS AT THE INTERFACE ($Y=H_o/2$) OF THE THICK ADHEREND SPECIMEN

for example, reaches a peak value of 40% higher than that of the joint. Corresponding values for axial and maximum principal stresses are 30% and 6% higher, respectively. The shear stress (Figure 7.17), however, has a maximum absolute value in the joint section, which is 15% higher than the corresponding peel stress, but 19% lower than the peak peel stress. The peak value of maximum principal stress is seen to be 54% higher than the peak peel stress and 124% higher than both the corresponding axial and absolute shear stresses. Figure 7.17 also shows the shear stress to be far from evenly distributed over the joint region.

The variation of stresses through the adhesive thickness for the time t = 1 minute is shown in Figures 7.19 to 7.22 for peel, axial, shear and maximum principal stresses, respectively. The variation of stresses are shown at three locations outside the joint section, denoted by coordinates x_1 and at four locations in the joint sections, denoted by coordinates x_2. These locations correspond with the third to fifth and third, fifth, seventh and ninth element centroids from the joint edges, $x_1 = 0$ and $x_2 = 0$, respectively.

As was the case with the single lap joint, at first glance, stress gradients through the adhesive thickness do not appear very high. However, on a change in stress per unit distance basis, peak stress gradients through the adhesive thickness are 3.7, 19, 7.7 and 2.0 times higher than those in the axial direction for peel, axial, shear and maximum principal stresses, respectively. The highest stress gradients all occur adjacent to the joint edges. Note from Figures 7.19 to 7.22 that the stress gradients over the adhesive thickness are similar for

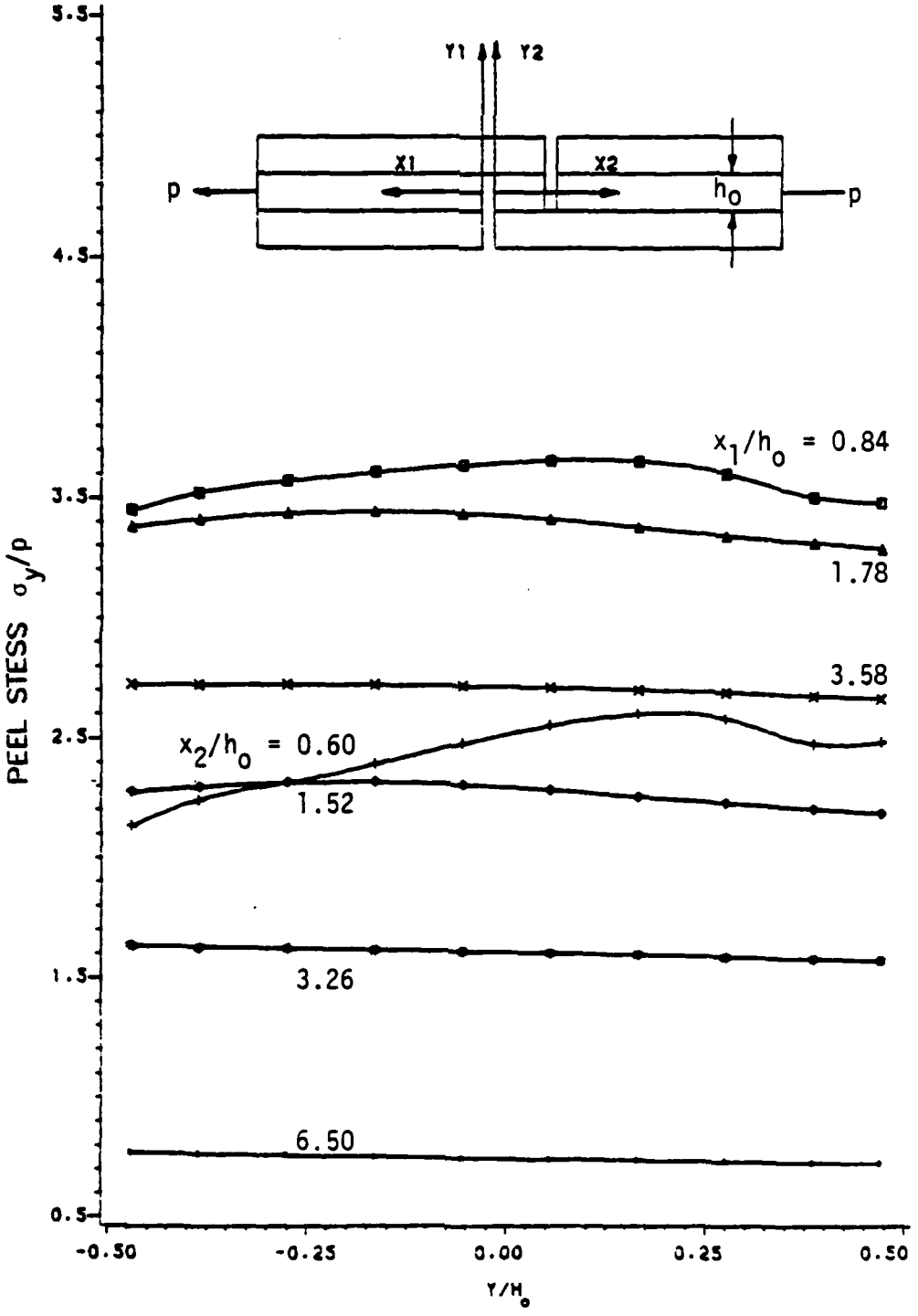

FIGURE 7.19 VARIATION OF ADHESIVE PEEL STRESS THROUGH THE ADHESIVE THICKNESS AS A FUNCTION OF THE AXIAL POSITION IN THE THICK ADHEREND SPECIMEN

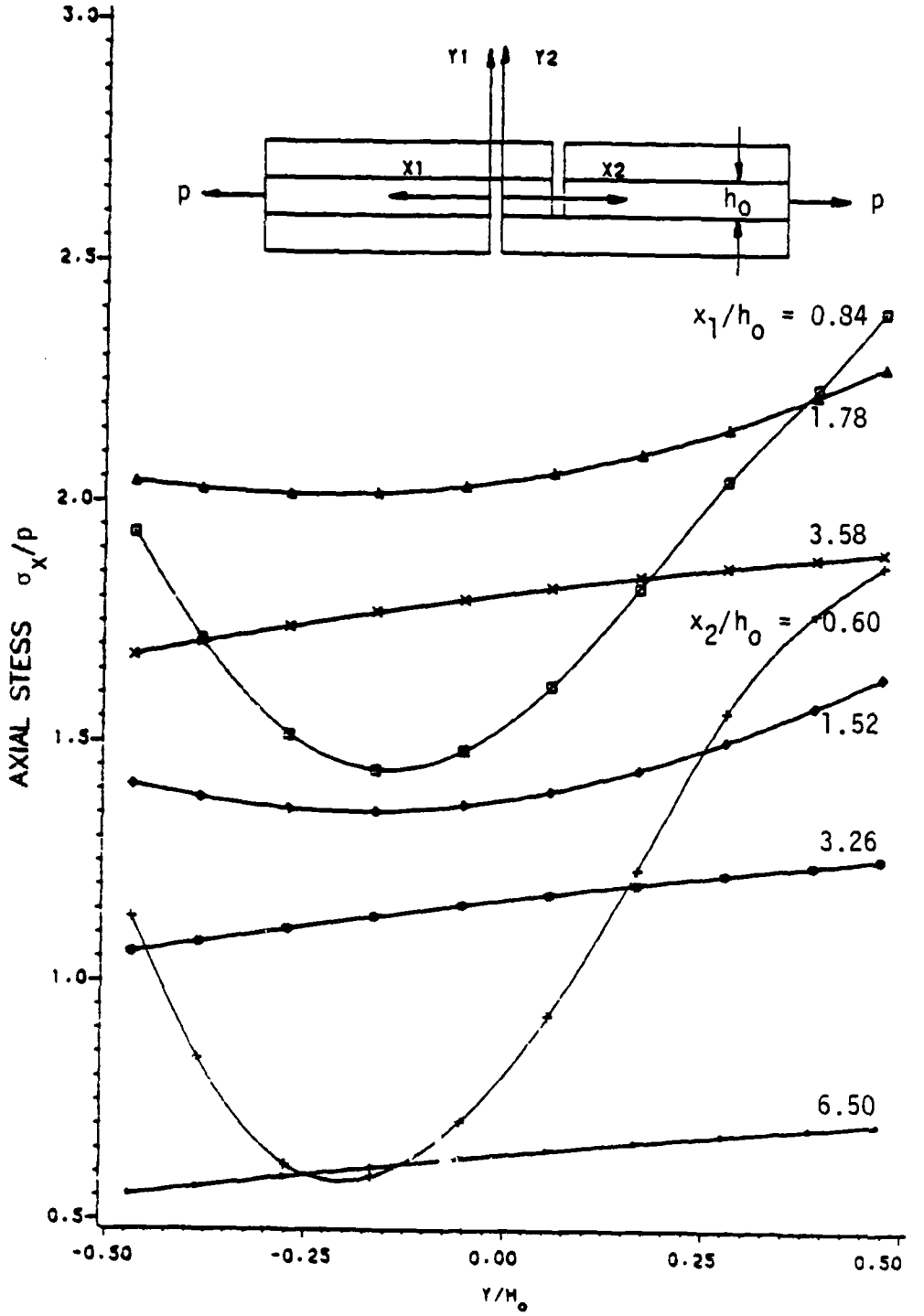

FIGURE 7.20 VARIATION OF ADHESIVE AXIAL STRESS THROUGH THE ADHESIVE THICKNESS AS A FUNCTION OF THE AXIAL POSITION IN THE THICK ADHEREND SPECIMEN

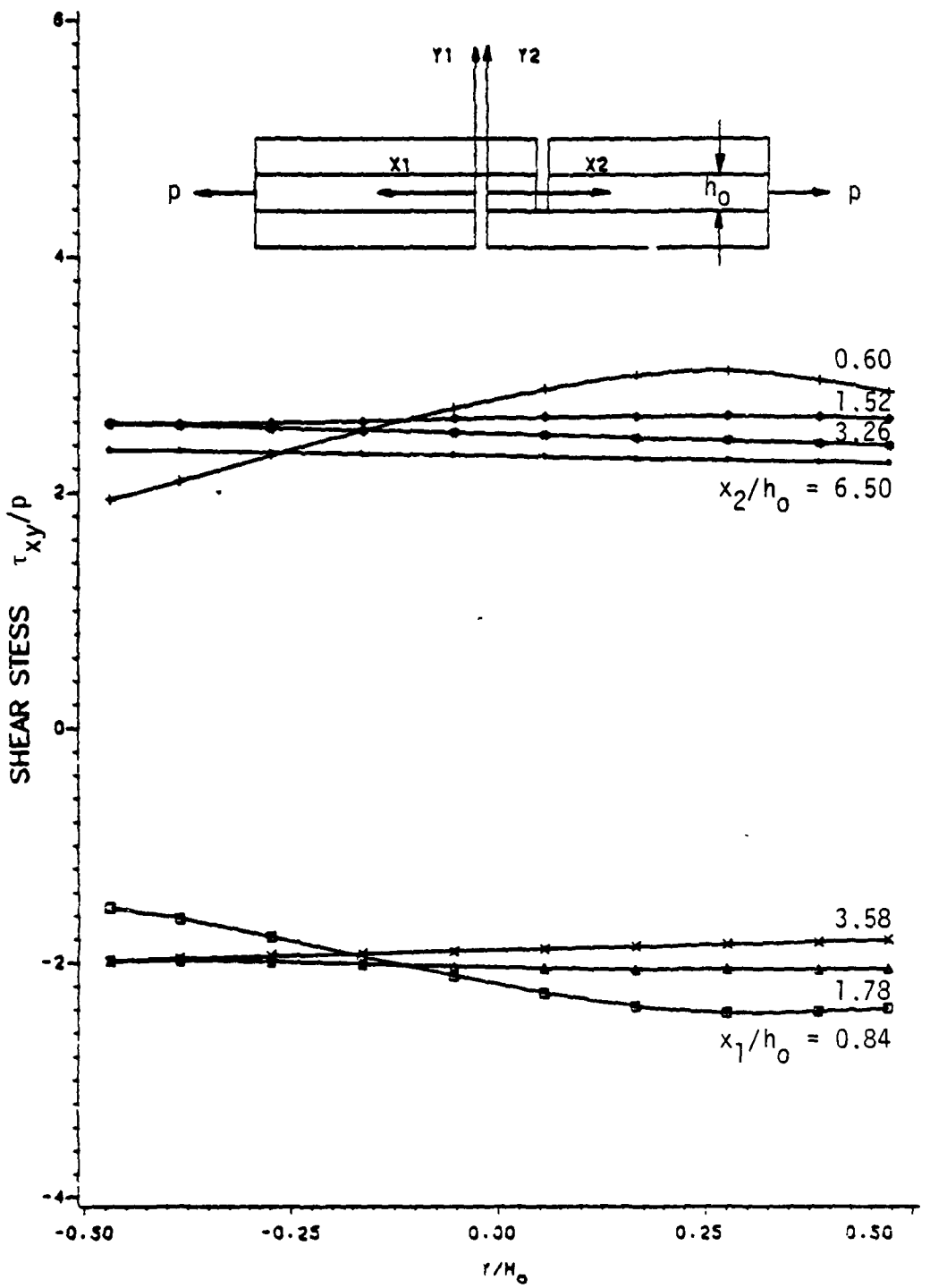

FIGURE 7.21 VARIATION OF ADHESIVE SHEAR STRESS THROUGH THE ADHESIVE THICKNESS AS A FUNCTION OF THE AXIAL POSITION IN THE THICK ADHEREND SPECIMEN

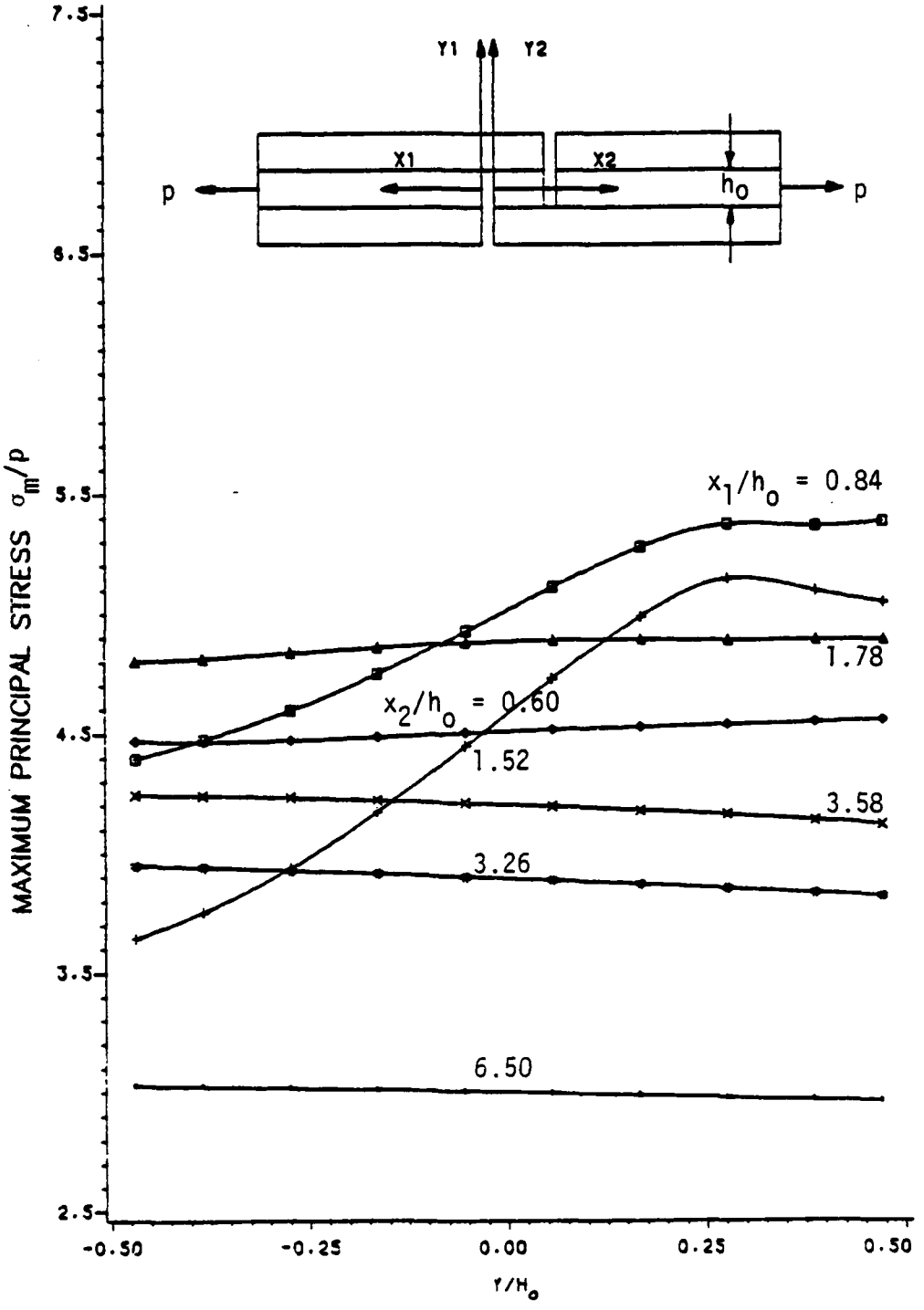

FIGURE 7.22 VARIATION OF ADHESIVE MAXIMUM PRINCIPAL STRESS THROUGH THE ADHESIVE THICKNESS AS A FUNCTION OF AXIAL POSITION IN THE THICK ADHEREND SPECIMEN

both edges, either side of the gap. Only the absolute magnitude of the stresses differ, as was discussed earlier in connection with Figures 7.15 to 7.18. Adjacent to the joint edges, axial and maximum principal stresses have peak values at or close to the interface between the adhesive and the upper adherend (Figures 7.20 and 7.22). Peel and shear stresses, however, have peak values at about one-quarter the adhesive thickness below the upper interface (Figures 7.19 and 7.21). In the latter two cases, the peak value shifts towards the lower interface very rapidly as one moves away from the joint edge. Stress gradients through the adhesive thickness are also seen to decay rapidly away from the joint edges.

7.4 Comparison with Results of Krieger [24]

The method of Krieger to calculate an adhesive shear modulus from experimental results is as follows: First, consider the thick adherend specimen of Figure 7.23 which shows two points in the joint section at a quarter of the overlap length (0.094 inches) from the left-hand joint edge. These two points are those between which the joint deformation at a quarter the overlap length from the joint edge is measured by the so-called KGR-1 gauge. The insert just below the thick adherend specimen in Figure 7.23 is a deformed portion of the joint and $(\Delta L)_{KGR-1}$ is the deformation measured by the KGR-1 gauge. The local experimental adhesive deformation, $(\Delta L)_{exp}$, is calculated from $(\Delta L)_{KGR-1}$ by making a correction for the adherend deformation. The local adhesive shear strain is given by

$$\gamma_{xy} = (\Delta L)_{exp}/h_o \qquad (7.1)$$

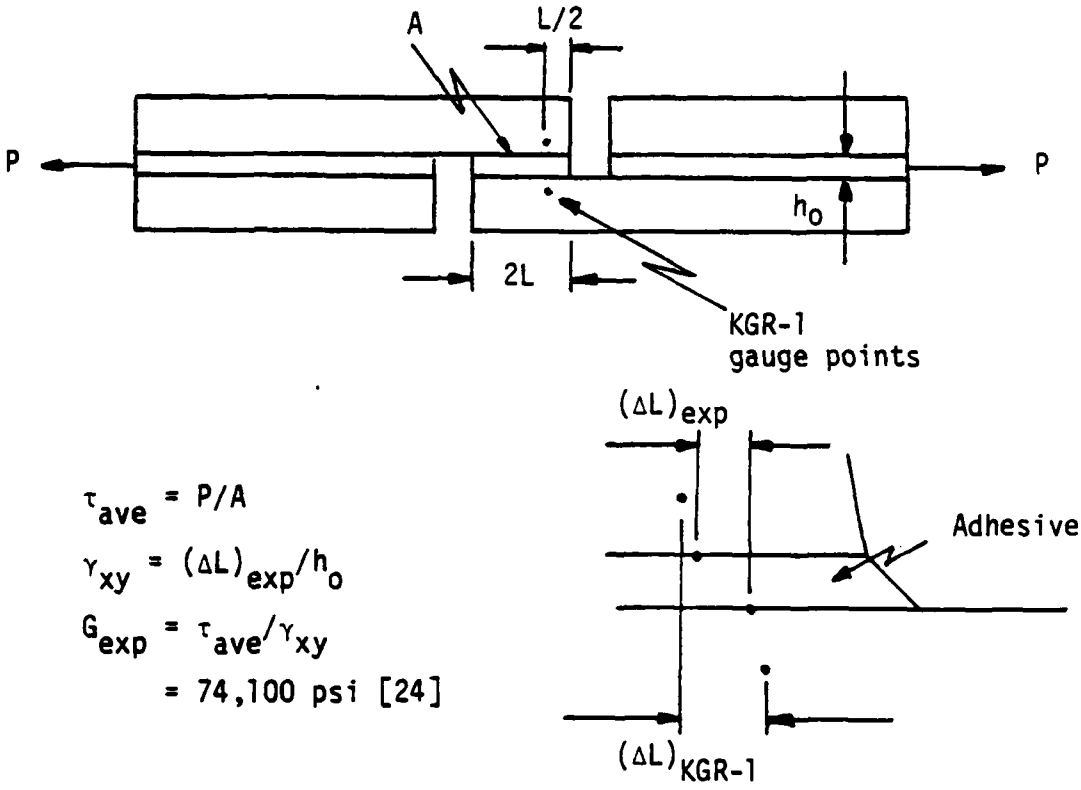

$\tau_{ave} = P/A$

$\gamma_{xy} = (\Delta L)_{exp}/h_o$

$G_{exp} = \tau_{ave}/\gamma_{xy}$

$= 74{,}100$ psi [24]

Figure 7.23 Thick Adherend Specimen and the Experimental Determination of an Adhesive Shear Modulus.

where h_o is the original average adhesive thickness. The average shear stress is given by

$$\tau_{ave} = P/A \tag{7.2}$$

where P is the load applied to the ends of the specimen and A is the total overlap area. The experimental shear modulus of Krieger is now calculated from the above-mentioned average shear stress and local shear strain:

$$G_{exp} = \tau_{ave}/\gamma_{xy} \tag{7.3}$$

The adhesive is assumed to be elastic since no mention is made of the loading rate or the time of measurement after loading. The value for G_{exp} obtained by this method for FM-73 adhesive is 74100 psi [24].

In the finite element analysis, the nodal points did not coincide with the same position as the KGR-1 gauge points between which deformation was measured by Krieger, and, hence, displacements of nodal points, on both sides of the quarter overlap distance from the joint edge, were used to calculate adhesive deformations at 0.073 and at 0.100 inches from the joint edge. The analytical adhesive deformation, ΔL_a, at 0.094 inches (a quarter of the overlap-length) from the joint edge was then calculated from these two deformations by linear interpolation. The calculations were made for times t = 1, 10 and 30 minutes, using the results of the non-linear viscoelastic analysis of Section 7.3. The shear modulus, denoted by G_k, was calculated in the same manner as by Krieger, i.e.,

$$G_k = \tau_{ave}/(\Delta L_a/h_o) \tag{7.4}$$

where τ_{ave}, h_o and ΔL_a were defined above. Values for G_k are provided in Table 7.2 for times t = 1, 10 and 30 minutes.

From the finite element results used to calculate G_k, it was found that the local shear stresses at a quarter of the overlap length away from the joint edge, averaged through the adhesive thickness, were only 4.4%, 4.0% and 3.6% lower than the average shear stress for times t = 1, 10 and 30 minutes, respectively. The local shear strains at the same distance from the joint edge, also averaged through the adhesive thickness, were 6.5%, 7.0% and 5.5% lower than the strains used to calculate G_k from equation (7.4), for times t = 1, 10 and 30 minutes, respectively. The differences in the strains are due to the presence of small peel and axial strains, whereas in Krieger's method for determining, G_k (and G_{exp}) pure shear is assumed, resulting in zero peel and axial stresses. If, at any point in the adhesive, the local shear stress is divided by the local shear strain, the local secant shear modulus results, given by

$$(G_{sec})_{local} = (\tau_{xy})_{local}/(\gamma_{xy})_{local} \tag{7.5}$$

The intersection of $(\tau_{xy})_{local}$ and $(\gamma_{xy})_{local}$ must necessarily lie on the adhesive bi-linear shear stress-strain curve (which is effectively used as input to the finite element program), as shown in Figure 7.24. The local secant shear modulus, $(G_{sec})_{local}$, is therefore different for each point in the adhesive, depending on the level of shear stress. In order to obtain one value for the quarter overlap distance from the joint edge, define

Table 7.2 Experimental and Time Dependent Theoretical Shear Moduli of FM-73 Adhesive

	Shear Modulus		Error
Time (min)	$G_k(t)$ (psi)	$G'_{sec}(t)$ (psi)	$\frac{G'_{sec} - G_k}{G'_{sec}}$
1	115,500	118,500	2.5%
10	102,300	105,900	3.4%
30	97,500	99,500	2.2%

G_{exp} = 74,100 psi [24].

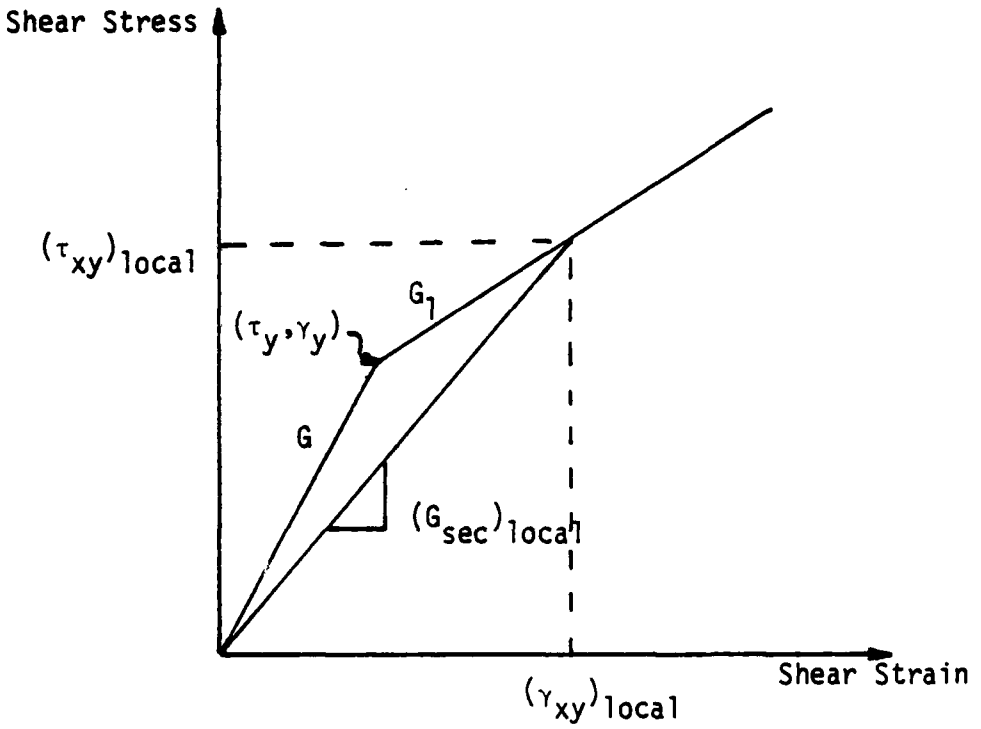

Figure 7.24 Bi-Linear Shear Stress-Strain Curve "Used" as Input to the Finite Element Program

$$G'_{sec} = \frac{\tau'_{xy}}{\gamma'_{xy}} \tag{7.6}$$

where τ'_{xy} and γ'_{xy} are now the shear stress and shear strain, each averaged through the adhesive thickness, at a quarter of the overlap distance from the joint edge. Values of G'_{sec} for times t = 1, 10 and 30 minutes are also given in Table 7.2. G_k is found to be only 2.5%, 3.4% and 2.2% lower than G'_{sec} for times t = 1, 10 and 30 minutes, respectively. Therefore,

$$G_k(t) \approx G'_{sec}(t) \tag{7.7}$$

It has not been determined, however, that equation (7.7) will hold for different levels of loading as well.

For the particular geometry and loading, the small difference between G_k and G'_{sec} (independent of time) indicates that Krieger's method for obtaining G_k is valid for calculating the secant shear modulus at a quarter of the overlap length from the joint edge. The large discrepancy between G_{exp} and G_k is due to two reasons.

(i) The bulk adhesive properties were used as input to the finite element program, from which G_k was calculated. It is well recognized that the adhesive bond properties probably differ greatly from the adhesive bulk properties. The influence of the interface layer and the constraining effect of the adherends are the two most probable reasons for the expected difference between the adhesive bulk and the adhesive bond properties.

(ii) The time effect was not taken into account when G_{exp} was obtained. The moduli G_k and G_{exp} are both related to the adhesive shear strain, and in the previous section (Figure 7.13), the adhesive shear strain was shown to be greatly dependent on time (while the average shear stress in both G_k and G_{exp} is a constant, independent of time).

If true adhesive bond properties were to be used in the finite element program, and the time effect could be taken into account, then

$$G_k(t) \approx G_{exp}(t) \tag{7.8}$$

since the method for obtaining both moduli are based on the same principles (see equations (7.1) to (7.4)). Equation (7.7) was shown to hold for the present analysis, and, therefore, from equations (7.7) and (7.8),

$$G_{exp}(t) \approx G''_{sec}(t) \tag{7.9}$$

where G''_{sec} is now the true local secant shear modulus of the bonded adhesive, a quarter of the overlap length from the joint edge, "averaged" through the adhesive thickness as in equation (7.6). Nothing much can be done with G''_{sec} alone. The elastic Poisson's ratio, ν_e, together with the three variables E, E_1 and σ_y necessary to describe the bi-linear approximation to the non-linear stress-strain curve, are four variables which may be different in the adhesive bond than in the bulk material. If three of these four variables can be predetermined by some other method (which will be the true adhesive bond properties), then the fourth one can be determined by a trial and error process such that

$$G_k(t) = G_{exp}(t) \tag{7.10}$$

If we assume that the discrepancy between G_{exp} and G_k is largely due to the constraining effect of the adherends, then it is possible that the adhesive stress-strain curve is approximately the same for the bulk and the bond adhesive, in which case only the elastic Poisson's ratio differs greatly from the bonded to the bulk adhesive. The elastic Poisson's ratio will vary through the adhesive thickness, but since it is now the only variable, an effective elastic Poisson's ratio $(\nu_e)_{eff}$ can be determined by the trial and error process mentioned above. If, however, the interface layer also influences $G_{exp}(t)$ substantially then the interface layer properties must be predetermined before $(\nu_e)_{eff}$ can be obtained by the trial and error process.

In summary, then, there is really no point in comparing Krieger's value for G_{exp} with the moduli either used in the finite element analysis, or obtained from its results, since G_{exp} is a single value and it is known that the adhesive properties are non-linear. The average shear stress from which G_{exp} is calculated is well into the non-linear range. Furthermore, time was not taken into consideration when G_{exp} was obtained, and the finite element analysis showed a strong dependence of shear strain on time, which was also used to calculate G_{exp}. A third reason why Krieger's G_{exp} should not be compared with the present G_k is the well-recognized difference in bulk adhesive properties, used in the finite element analysis, and the actual adhesive bond properties. If, however, a method or methods can be devised in

which material properties can be found which yield a shear modulus $G_k(t)$, calculated from finite element results, which is a close approximation to $G_{exp}(t)$, then Krieger's method may well be a valuable tool for determining one of the adhesive properties, or for confirming the validation of all predetermined adhesive bond and interface layer properties.

7.5 The Influence of the Interface Layer Stiffness on Adhesive Stresses

In studying the influence of the interface layer stiffness on the adhesive stresses in the thick adherend specimen, a similar procedure was followed as described in Section 6.5 for the same study on the single lap joint. Three non-linear elastic analyses were performed in which E_i had different values, such that E_i/E_a was 0.1, 1.0 and 10.0, respectively, where E_i and E_a are the Young's moduli of the interface layer material and the adhesive, respectively. The same geometry, finite element discretization, and boundary conditions were used as in the analysis of Section 7.3. The analysis in which $E_i/E_a = 1.0$ is the same analysis as that of Section 7.3 for time t = 1 minute, hence, also using the same material properties.

Stresses at the upper interface layer, $y = h_o/2$, are superimposed for the three values of E_i/E_a and shown in Figures 7.25 to 7.28 for peel, axial, shear and maximum principal stresses, respectively. Results in the central overlap region, from $x/L = -1$ to $+1$, are very similar to those given in Section 6.5 for the single lap joint. Stress distributions to the outside of the gaps are seen to be of the same nature as those to the inside of each gap.

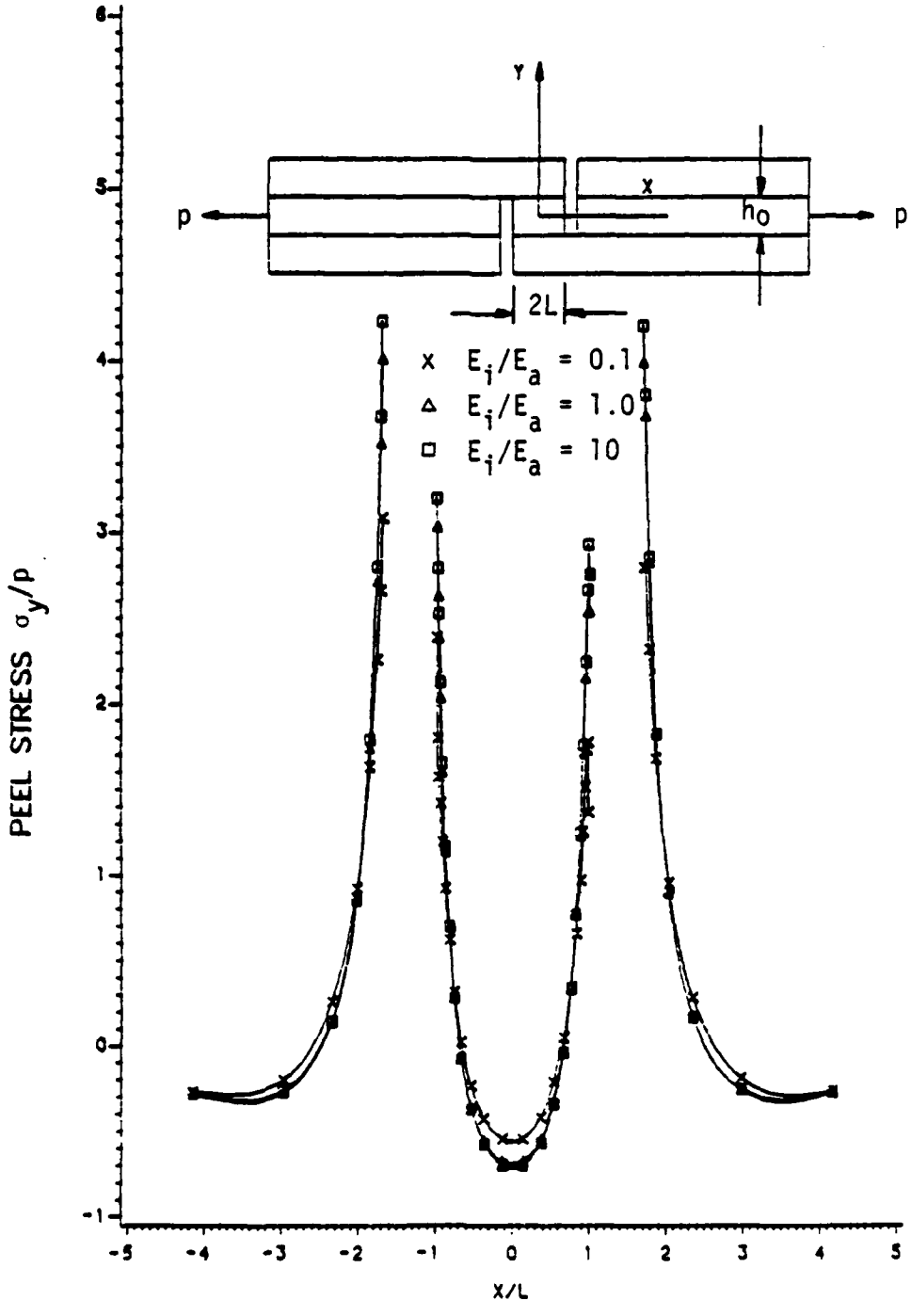

FIGURE 7.25 ADHESIVE PEEL STRESS AT THE INTERFACE ($Y=H_o/2$) OF THE THICK ADHEREND SPECIMEN AS A FUNCTION OF THE INTERFACE LAYER STIFFNESS

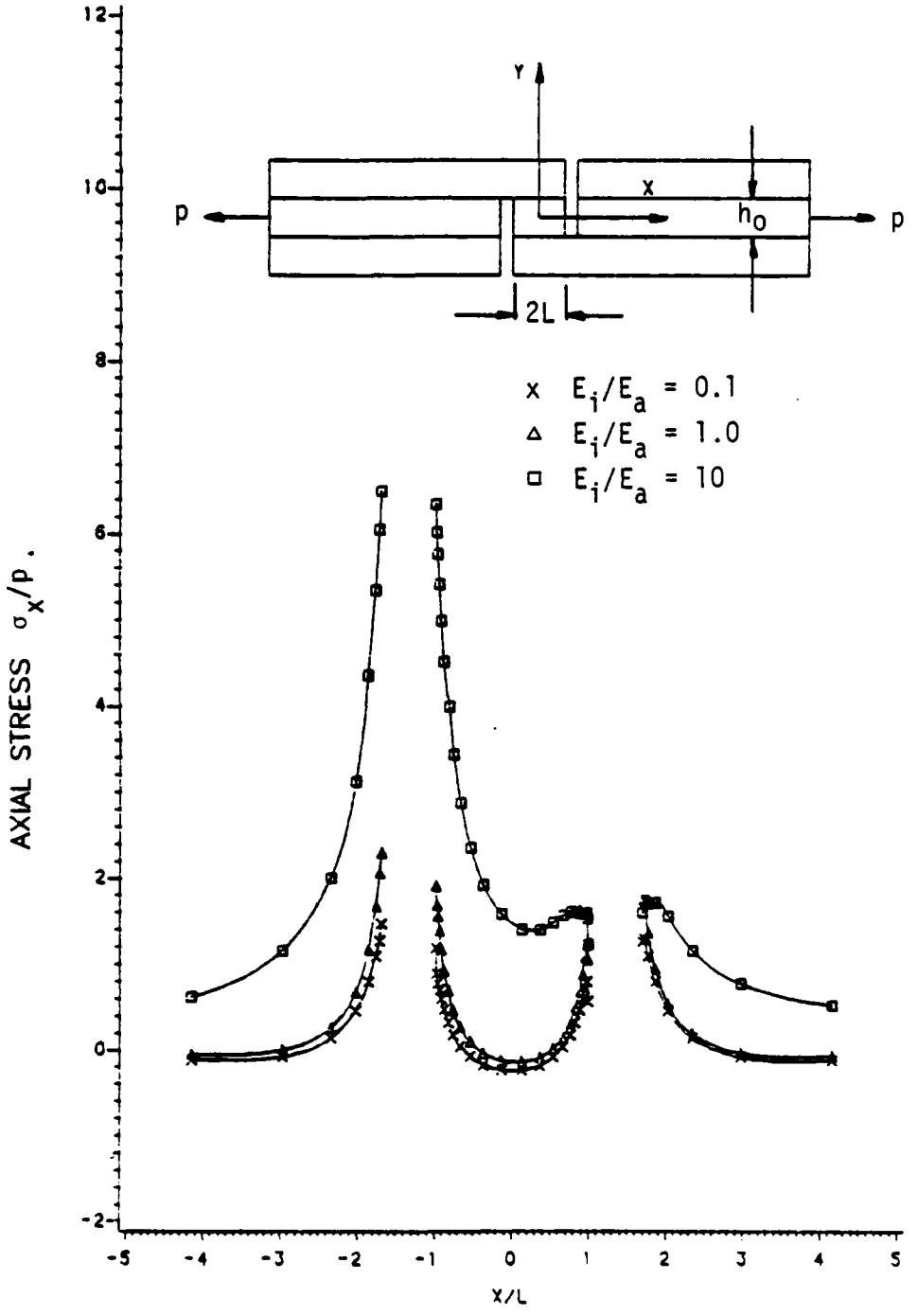

FIGURE 7.26 ADHESIVE AXIAL STRESS AT THE INTERFACE ($Y=H_o/2$) OF THE THICK ADHEREND SPECIMEN AS A FUNCTION OF THE INTERFACE LAYER STIFFNESS

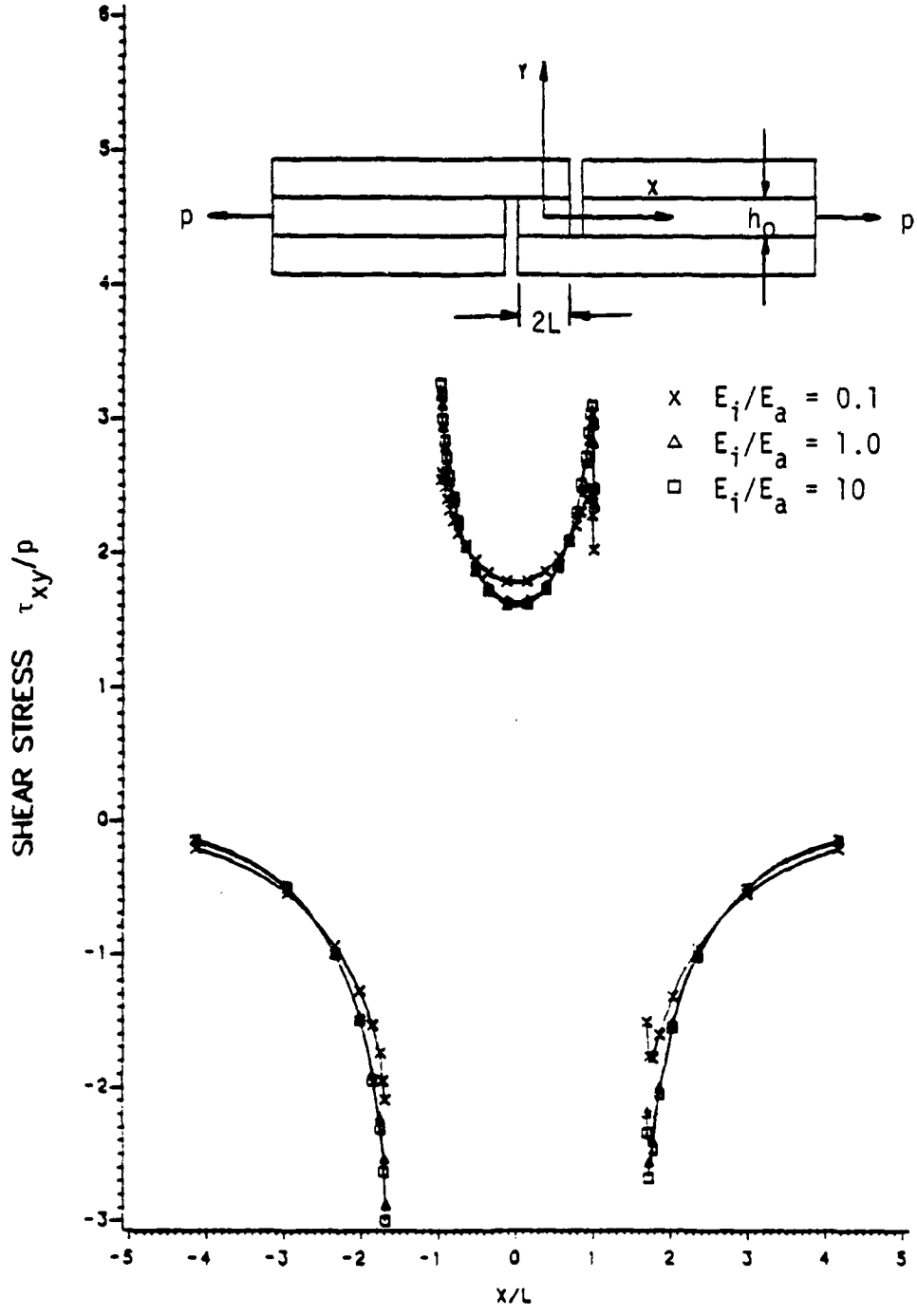

FIGURE 7.27 ADHESIVE SHEAR STRESS AT THE INTERFACE ($Y=H_o/2$) OF THE THICK ADHEREND SPECIMEN AS A FUNCTION OF THE INTERFACE LAYER STIFFNESS

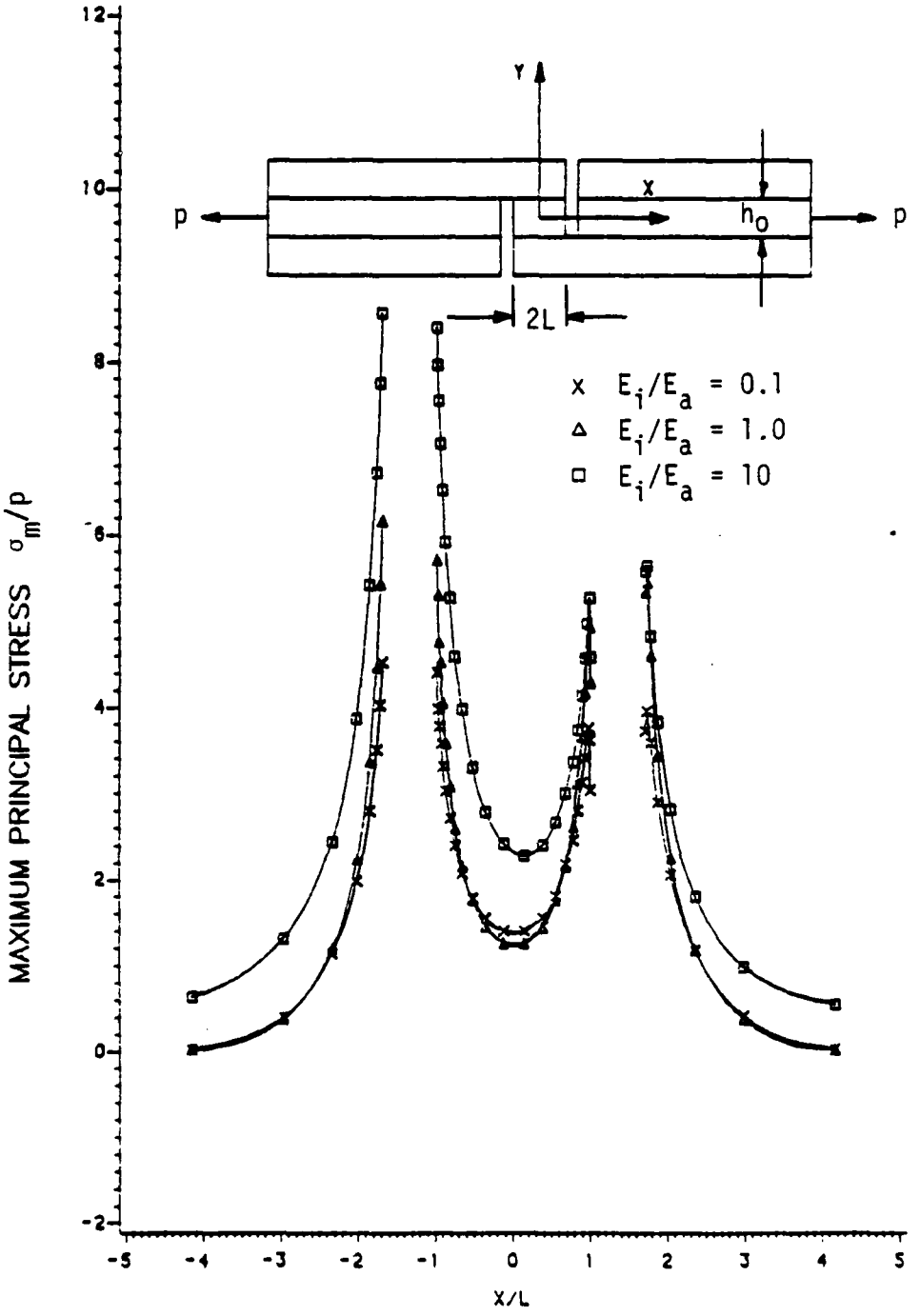

FIGURE 7.28 ADHESIVE MAXIMUM PRINCIPAL STRESS AT THE INTERFACE ($Y=H_o/2$) OF THE THICK ADHEREND SPECIMEN AS A FUNCTION OF THE INTERFACE LAYER STIFFNESS

Raising the interface layer stiffness to an order of magnitude above that of the adhesive has little influence on the overall peel and shear stresses (see Figures 7.25 and 7.27). For example, the peak peel stress is raised by 5.5% and the peak shear stress by just 3.0%. The peak axial stress, however, is increased by 195%, raising it to a value higher than either the peak peel or shear stresses. The same behavior was found in the case of the single lap joint and is explained in Section 6.5. The peak maximum principal stress is raised to values 200% and 260% higher than the peak peel and shear stresses, respectively.

Lowering the interface layer stiffness by an order of magnitude below that of the adhesive, decreases the peak stresses by 23%, 37%, 18% and 26% for peel, axial, shear and maximum principal stresses, respectively. This reduction in peak stresses is not as pronounced for an equivalent lowering in the interface layer stiffness of the single lap joint. In raising the interface layer stiffness, however, it was noted that percentage changes in peak stresses were almost identical to those for the single lap joint. Equivalent changes in peak stresses are not necessarily expected for the two joint configurations due to the overall differences in geometry, loading and material properties.

Chapter 8

CONCLUSIONS AND RECOMMENDATIONS

A relatively efficient method was devised to obtain an efficient finite element mesh for the single lap joint analysis. Equal spacing of the elements through the thickness of the adherends was found to be necessary to represent bending. A surprisingly small amount (5 to 6) of elements in the axial direction of the adherends, outside the joint section of the single lap structure, was found to be sufficient for obtaining accurate results. The single lap joint results were estimated to be within 0.2% accuracy if it is assumed that the present finite element analysis converged to the correct solution. A comparable accuracy for the thick adherend analysis is possibly in the order of 1.0%.

The stress singularities at the joint edges were represented by finite values, and just two to three elements away from the singularities the stress distributions showed a tendency to satisfy the zero stress boundary conditions. In the proximity of the stress singularities, the results were obviously inaccurate, but the distance from the singularities, along which the results were inaccurate, was clearly distinguishable.

For both the single lap joint and the thick adherend specimen, the peak maximum principal stress was found to be considerably higher than the stresses generally considered to be of prime importance, viz., the peel and shear stresses, respectively. If the interface layer

stiffness happens to be higher than the adhesive stiffness by an order of magnitude, then the axial stress also becomes more important than both the peel and the shear stresses. The same rule applies if the entire adhesive layer has a high stiffness, as was found with the Araldite adhesive and aluminum adherend properties used for the viscoelastic analysis of the single lap joint.

The results from the present single lap analysis could not be compared directly with those of Goland and Reissner [2], since the ratios of adhesive moduli to adhesive thickness, and of adherend moduli to adherend thickness, do not satisfy the conditions required by either of the two analyses of Goland and Reissner, but lie somewhere in between. The results of the present analysis, however, do lie in between those of Goland and Reissner's two analyses, and this fact does give a certain degree of confidence in the present results. The comparison of the present results with both the analyses of Humphreys [5] and of Nagaraja and Alwar [17] were unsuccessful since discrepancies were found in both of these analyses. More time was not spent on comparisons but it would have been good to have performed a suitable comparison, especially since it is not known, for sure, how far away from the singularities the results are accurate. From discussions between the author and R. T. Haftka and M. P. Kamat [49], it is believed that the composite type elements used in the SAAS3V programs generally do not give good results where stress gradients are high.

The non-linear viscoelastic analysis on the thick adherend specimen, with FM-73 adhesive properties, shows a very small redistribution of stresses with increasing time and constant load. The shear

strain, however, is greatly dependent on time due to viscoelastic creep in the adhesive. Peel and axial strains change very little with increasing time.

Values of the adhesive shear modulus, calculated from the thick adherend finite element results by Krieger's method, compare well with the local secant shear modulus at a quarter of the overlap length away from the joint edge. These values of shear modulus are greatly dependent on time and should not be compared with the experimental result of Krieger [24]. The reason is two-fold:

1. Bulk adhesive properties were used in the finite element analysis, and it is well-recognized that these properties are probably different from the adhesive properties in a bond.
2. The time effect on the experimentally obtained shear modulus was not taken into account, and it was established that this value should also be highly time-dependent.

In the thick adherend analysis, it was found that the adhesive peel, axial and maximum principal stresses had peak values which were higher at, or close to, the edges outside the gaps than in the overlap or shear area. Unexpected failure in these regions outside the joint may influence experimental results significantly.

In both the single lap and thick adherend analyses, it was found that if the interface layer stiffness was increased by an order of magnitude above that of the adhesive, the peak axial and maximum principal stresses were increased significantly and the peak peel and shear stresses increased just a little. If the interface layer

stiffness was reduced by an order of magnitude below that of the adhesive, the peak peel, shear and maximum principal stresses were reduced significantly and the peak axial stress reduced just moderately for the single lap joint. For the thick adherend specimen, all stresses were reduced just moderately for the same decrease in interface layer stiffness. Whatever the interface layer properties may be, therefore, it is important to distinguish them from those of the adhesive.

Prior to continue using the SAAS3VP program for joint analyses, it is recommended that the results in the present study be compared with results obtained from another finite element program using four- or eight-noded isoparametric elements, since it is believed that these elements generally yield good results where stress gradients are high [49]. Such an element formulation may then have to be implemented in the SAAS3VP program, and subsequent results compared with those of the other program mentioned above.

It is further recommended that the equation

$$G_k(t) \approx G'_{sec}(t) \tag{7.7}$$

be verified for different levels of loading and for different adhesive bond thicknesses. If this equation is valid over a range of load levels and bond thicknesses, then Krieger's method could be a useful tool for determining one material property if the others are predetermined by some other method. A method must then necessarily also be devised for taking the time effect into account when obtaining the experimental shear modulus $G_{exp}(t)$.

It is also recommended to possibly determine the error(s) made by the bi-linear approximation of the non-linear stress-strain curve and by following Schapery's quasi-elastic method of solving the non-linear viscoelastic problem. The necessity for including geometric non-linearities should also be established. A failure criterion should also be developed and incorporated into the finite element program.

SUMMARY

Existing closed form solutions for the stress analysis of the single lap joint were studied intensively, and methods of analysis and assumptions between the analyses of Goland and Reissner, Hart-Smith and Delale and Erdogan were compared. The existing SAAS3V finite element program was modified to accommodate additional mesh generation and plotting capabilities. The modified version, SAAS3VP, was used for performing linear elastic and viscoelastic analyses on the single lap joint, and a non-linear viscoelastic analysis on the thick adherend specimen. Metlbond 1113 and Araldite adhesive properties were used in the linear elastic and viscoelastic analyses, respectively, and results were compared to those of Humphreys, and Nagaraja and Alwar, respectively. FM-73 adhesive properties were used in the non-linear viscoelastic analysis. Time-dependent shear moduli were calculated from the results of the latter analysis and compared with the experimentally obtained shear modulus of Krieger. Interface layers were defined in both the single lap and thick adherend analyses and the influence of changing the interface layer stiffness on adhesive stresses was also investigated.

REFERENCES

1. J. G. Crose and R. M. Jones. "SAAS III: Finite Element Stress Analysis of Axisymmetric and Plane Solids with Different Orthotropic, Temperature-Dependent Material Properties in Tension and Compression." San Bernadino Operations. The Aerospace Corporation, June 1971.

2. M. Goland and E. Reissner. "The Stresses in Cemented Joints." Journal of Applied Mechanics, pp. A17-A27, March 1944.

3. L. J. Hart-Smith. "Adhesive-Bonded Single Lap Joints." Technical Report, Langley Research Center, Hampton, Virginia, January 1973.

4. F. Delale and F. Erdogan. "Viscoelastic Analysis of Adhesively Bonded Joints." NASA NGR 39-007-011, Lehigh University, Bethlehem, Pennsylvania, March 1980.

5. E. A. Humphreys. "Nonlinear Analysis of Bonded Joints with Thermal Effects." Thesis submitted to the Graduate Faculty of the Virginia Polytechnic Institute and State University, Blacksburg, Virginia, May 1977.

6. F. Erdogan and M. Ratwani. "Stress Distributions in Bonded Joints." Journal of Composite Materials, V5, pp. 378-393, July 1971.

7. R. A. Schapery. "Approximate Methods of Transform Inversion for Viscoelastic Stress Analysis." Proceedings of the 4th U.S. National Congress of Applied Mechanics, V2, pp. 1075-1085, 1962.

8. J. K. Sen and R. M. Jones. "Stresses in Double-Lap Joints Bonded with a Viscoelastic Adhesive: Part I. Theory and Experimental Corroboration." AIAA Journal, V18, 10, pp. 1237-1244, October 1980.

9. R. A. Schapery. "A Method of Viscoelastic Stress Analysis Using Elastic Solutions." Journal of the Franklin Institute, V279, pp. 268-289, April 1965.

10. D. J. Allman. "A Theory for Elastic Stresses in Adhesive Bonded Lap Joints." Quarterly Journal of Mechanics and Applied Mathematics, V30, 4, pp. 415-436, November 1977.

11. L. J. Hart-Smith. "Adhesive Bonded Joints for Composites--Phenomenological Considerations." Technology Conference on Advanced Composites Technology, El Segundo, California, March 1978.

12. U. Yuceoglu and D. P. Updike. "Stress Analysis in Bonded Plates and Joints." Journal of the Engineering Mechanics Division, ASCE, V106, pp. 37-56, 1980.

13. F. Delale and F. Erdogan. "Time Temperature Effect in Adhesively Bonded Joints." NASA NGR 39-007-011, Lehigh University, Bethlehem, Pennsylvania, February 1981.

14. J. L. White. "Finite Elements in Linear Viscoelasticity." Report No. AFFDL-TR-68-150. The Boeing Co., 1968.

15. Z. Zudans, M. M. Reddi, H. M. Rishwan and H. C. Tsai. "Elastic-Plastic Creep Analysis of High Temperature Nuclear Reactor Components." Nuclear Engineering and Design, V28, pp. 414-445, 1974.

16. W. E. Haisler and D. R. Sanders. "Elastic-Plastic-Creep-Large Strain Analysis at Elevated Temperature by the Finite Element Method." Computers and Structures, V10, pp. 375-381, 1979.

17. S. Gali and O. Ishai. "Interlaminar Stress Distribution Within an Adhesive Layer in the Non-linear Range." Journal of Adhesion, V9, 4, pp. 253-266, October 1978.

18. Y. R. Nagaraja and R. S. Alwar. "Non-linear Stress Analysis of an Adhesive Tabular Lap Joint." Journal of Adhesion, V10, 2, pp. 97-106, July 1979.

19. Y. R. Nagaraja and R. S. Alwar. "Viscoelastic Analysis of an Adhesive-Bonded Plane Lap Joint." Computers and Structures, V11, 6, pp. 621-627, June 1980.

20. R. D. Adams and N. A. Peppiatt. "Stress Analysis of Adhesively Bonded Lap Joints." Journal of Strain Analysis, V9, 3, 1974.

21. R. W. Bryant and W. A. Dukes. "The Effect of Joint Design and Dimensions on Adhesive Strength." Applied Polymer Symposium, Structural Adhesive Bonding (1965), Interscience Publishers, 1966.

22. S. Amijima, A. Yoshida and T. Fujii. "Strength and Stress Analysis of Adhesive Bonded Joints of Isotropic and Anisotropic Materials." Proceedings of the International Conference on Composite Materials, 2nd, Toronto, Ontario, April 1978, Published AIME, Warrendale, Pennsylvania, pp. 1185-1199, 1978.

23. O. Ishai, D. Peretz and S. Gali. "Direct Determination of Interlaminar Stresses in Polymeric Adhesive Layers." Proceedings of the Society for Experimental Stress Analysis, V34, 2, pp. 265-270, 1977.

24. R. B. Krieger. "Stiffness Characteristics of Structural Adhesives for Stress Analysis in Hostile Environment." American Cyanamid Co., Bloomingdale Plant, Havre de Grace, Maryland.

25. E. Sancaktar and S. C. Schenck. "Material Characterisation of Structural Adhesives in the Lap Shear Mode." Department of Mechanical and Industrial Engineering, Clarkson College, Potsdam, New York, Report No. MIE-89, January 1983.

26. M. P. Renieri. "Rate and Time Dependent Behavior of Structural Adhesives." Thesis submitted to the Graduate Faculty of the Virginia Polytechnic Institute and State University, Blacksburg, Virginia, April 1976.

27. J. Romanko and W. G. Knauss. "On the Time Dependence of the Poisson's Ratio of a Commercial Adhesive Material." Journal of Adhesion, V10, pp. 269-272, October 1980.

28. L. J. Hart-Smith. "Differences Between Adhesive Behavior in Test Coupons and Structural Joints." ASTM Adhesive Committee D-14 Meeting, Phoenix, Arizona, March 1981.

29. D. Peretz and Y. Weitsman. "Nonlinear Viscoelastic Characterization of FM 73 Adhesive." Texas A & M University, College Station, Texas.

30. E. C. Francis, W. L. Hufferd, D. G. Lemini, R. E. Thompson, W. E. Briggs and R. R. Parmerter. "Time Dependent Fracture in Adhesive Bonded Joints." Chemical Systems Division, Sunnyvale, California, Interim Report for the Period 24 April 1981 to 24 October 1982.

31. K. Arin and F. Erdogan. "Penny-Shaped Crack in an Elastic Layer Bonded to Dissimilar Half Spaces." International Journal of Engineering and Science, V9, 1971.

32. P. D. Hilton and G. S. Gupta. "Stress and Fracture Analysis of Adhesive Joints." ASME Paper 73-DE-21, New York, 1973.

33. W. D. Bascom, R. L. Cottington and C. O. Timmons. "Fracture Design Criteria for Structural Adhesive Bonding...Promise and Problems." Naval Engineering Journal, V88, 4, pp. 73-86, August 1976.

34. J. Mijovic. "Morphology and Fracture Properties of Pure and Reinforced Aluminum-Epoxy Adhesives Joints." Journal of Applied Polymer Science, V25, 6, pp. 1179-1193.

35. W. D. Bascom, R. L. Cottington, R. L. Jones and R. Peysor. "The Fracture of Epoxy and Elastomer-Modified Epoxy Polymers in Bulk and as Adhesives." Journal of Applied Polymer Science, V19, pp. 2545-2562, 1975.

36. A. J. Kinloch. "Interfacial Fracture Mechanical Aspects of Adhesive Bonded Joints--A Review." Journal of Adhesion, V10, 3, pp. 193-219, October 1979.

37. G. R. Wooley and D. R. Carver. "Stress Concentration Factors for Bonded Lap Joints." Journal of Aircraft, V8, 10, 1971.

38. G. G. Tratina. "Combined Mode Crack Extensions in Adhesive Joints." Journal of Composite Materials, V6, pp. 371-385, 1972.

39. W. D. Bascom and J. Oroshuk. "Effect of Bond Angle on Mixed Mode Adhesive Fracture." Journal of Materials and Science, V17, 7, July 1978.

40. E. J. Ripling, S. Mostovoy and R. L. Patrick. "Application of Fracture Mechanics for Adhesive Joints." ASTM STP No. 360, Symposium on Recent Developments in Adhesion Science, June 1963.

41. S. Mostovoy and E. J. Ripling. "Fracture Toughness of an Epoxy System." Journal of Applied Polymer Science, V10, p. 1351, 1966.

42. E. J. Ripling, S. Mostovoy and R. L. Patrick. "Measuring Fracture Toughness of Adhesive Joints." Materials Research and Standards, V4, 3, p. 129, March 1964.

43. G. P. Anderson, K. L. de Vries and M. L. Williams. "Finite Element in Adhesion Analysis." International Journal of Fracture, V9, 4, pp. 421-435, 1973.

44. G. C. Sih. "Fracture Mechanics of Adhesive Joints." Polymer Engineering Science, V20, 14, pp. 977-981, September 1980.

45. W. J. Renton. "Structural Properties of Adhesives." Quarterly Progress Report No. 1-7, Vought Corporation, ATC Report No. 13-94400/8CR-26, 1977 to 1978.

46. E. Sancaktar and H. F. Brinson. "The Viscoelastic Shear Behavior of a Structural Adhesive." Adhesion and Adsorption of Polymers, Part A, (L. H. Lee, ed.), Plenum Press, pp. 279-299, N.Y. 1980.

47. S. W. Johnson and R. Everett. Private communication, NASA-Langley, February 1983.

48. H. F. Brinson, C. E. Barker and M. A. Rochefort. "The Viscoelastic Response of FM-73 and FM-300 Adhesive." VPI-Report (in publication).

49. R. T. Haftka and M. P. Kamat. Private discussions, VPI&SU, May 1983.

50. H. F. Brinson, C. T. Herakovich and M. P. Renieri. "Rate and Time Dependent Failure of Structural Adhesives." Fracture Mechanics of Composites, STP 617, American Society for Testing and Materials, Philadelphia, Pa., pp. 177-199, 1975.

51. J. S. Cartner and H. F. Brinson. "The Non-Linear Viscoelastic Behavior of Adhesives and Chopped Fiber Composites." VPI-E-78-21, August 1978.

52. E. Sancaktar, T. Parkingson and H. F. Brinson. "Neutron Radiography for Defect Detection in Adhesively Bonded Joints." Experimental Techniques (in review).

53. D. R. Malville, D. L. Hunsten and P. W. Mast. "Developing Failure Criteria for Adhesive Joints Under Complex Loading." Journal of Materials and Technology, Vol. 100, No. 1, pp. 25-31, January 1978.

54. D. G. O'Connor and H. F. Brinson. "Factors Affecting the Fracture Energy of a Structural Adhesive." VPI-E-79-32, September 1979.

55. D. W. Dwight, M. E. Counts and J. P. Wightman. "Surface Analysis and Adhesive Bonding. II. Polyimides," Colloid and Interface Science, Vol. III, M. Kerker, ed., pp. 143-156, Academic Press, N.Y., 1976.

56. D. W. Dwight, E. Sancaktar and H. F. Brinson. "Failure Characteristics of a Structural Adhesive." Adhesion and Adsorption of Polymers, Part A, L. L. Lee (ed.), Plenum, N.Y., pp. 141-163, 1980.

APPENDICES

The appendices for this document are contained in a separate report, VPI-E-83-17, May 1983 and may be obtained upon request to the authors or the VPI&SU Center for Adhesion Science, 218 Norris Hall, Blacksburg, VA 24061. The appendices contain a documentation and listing of the SAAS finite element computer program.

SECURITY CLASSIFICATION OF THIS PAGE (When Data Entered)

REPORT DOCUMENTATION PAGE		READ INSTRUCTIONS BEFORE COMPLETING FORM
1. REPORT NUMBER VPI-E-83-17	2. GOVT ACCESSION NO.	3. RECIPIENT'S CATALOG NUMBER
4. TITLE (and Subtitle) VISCOELASTIC STRESS ANALYSIS OF ADHESIVELY BONDED JOINTS		5. TYPE OF REPORT & PERIOD COVERED Interim 6. PERFORMING ORG. REPORT NUMBER VPI-E-83-17
7. AUTHOR(s) Louis R. Botha Robert M. Jones H. F. Brinson		8. CONTRACT OR GRANT NUMBER(s) ONR - N00014-82-K-0185 NASA NAG-1-227
9. PERFORMING ORGANIZATION NAME AND ADDRESS Engineering Science and Mechanics 225 Norris VPI&SU, Blacksburg, VA 24061		10. PROGRAM ELEMENT, PROJECT, TASK AREA & WORK UNIT NUMBERS
11. CONTROLLING OFFICE NAME AND ADDRESS ONR, 800 N. Quincy St., Arlington, VA 22217 NASA-Langley, Hampton, VA 23665		12. REPORT DATE May 1983 13. NUMBER OF PAGES
14. MONITORING AGENCY NAME & ADDRESS(if different from Controlling Office) (same as 11)		15. SECURITY CLASS. (of this report) Unclassified 15a. DECLASSIFICATION/DOWNGRADING SCHEDULE

16. DISTRIBUTION STATEMENT (of this Report)

Distribution unlimited

17. DISTRIBUTION STATEMENT (of the abstract entered in Block 20, if different from Report)

Distribution unlimited

18. SUPPLEMENTARY NOTES

19. KEY WORDS (Continue on reverse side if necessary and identify by block number)

Bonded joints, stress analysis, finite element, viscoelasticity

20. ABSTRACT (Continue on reverse side if necessary and identify by block number) Existing closed form solutions for the stress analysis of the single lap joint were studied intensively, and methods of analysis and assumptions between the analyses of Goland and Reissner, Hart-Smith and Delale and Erdogan were compared. The existing SAAS3V finite element program was modified to accommodate additional mesh generation and plotting capabilities. The modified version, SAAS3VP, was used for performing linear elastic and viscoelastic analyses on the single lap joint, and a nonlinear viscoelastic analysis on the thick adherend specimen. Metlbond 1113 and Araldite adhesive properties were used in the linear elastic and (cont.)

DD FORM 1 JAN 73 1473 EDITION OF 1 NOV 65 IS OBSOLETE

SECURITY CLASSIFICATION OF THIS PAGE (When Data Entered)

Item 20 (cont.)

viscoelastic analyses, respectively. FM-73 adhesive properties were used in the non-linear viscoelastic analysis. Time-dependent shear moduli were calculated from the results of the latter analysis and compared with the experimentally obtained shear modulus of Krieger. Interface layers were defined in both the single lap and thick adherend analyses and the influence of changing the interface layer stiffness on adhesive stresses was also investigated.

END

FILMED

1-84

DTIC